SOURCE CONTRIBUTIONS OF VOCs TO OZONE FORMATION IN SOUTHEAST TEXAS USING A SOURCE-ORIENTED AIR QUALITY MODEL

A Thesis

by

ANUPAMA KRISHNAN

Submitted to the Office of Graduate Studies of
Texas A&M University
in partial fulfillment of the requirements for the degree of

MASTER OF SCIENCE

May 2010

Major Subject: Civil Engineering

SOURCE CONTRIBUTIONS OF VOCs TO OZONE FORMATION IN SOUTHEAST TEXAS USING A SOURCE-ORIENTED AIR QUALITY MODEL

A Thesis

by

ANUPAMA KRISHNAN

Submitted to the Office of Graduate Studies of
Texas A&M University
in partial fulfillment of the requirements for the degree of

MASTER OF SCIENCE

Approved by:

Chair of Committee, Qi Ying
Committee Members, Bill Batchelor
Renyi Zhang
Head of Department, John Niedzwecki

May 2010

Major Subject: Civil Engineering

ABSTRACT

Source Contributions of VOCs to Ozone Formation in Southeast Texas Using a Source-oriented Air Quality Model.

(May 2010)

Anupama Krishnan, B.E., Anna University, India

Chair of Advisory Committee Dr. Ying Qi

Houston-Galveston-Brazoria area is in severe non-attainment status for ozone compliance. Source-oriented mechanistic modeling was used to determine the major sources of VOCs that contributes to ozone formation during the Texas Air Quality Study (TexAQS) from August 16, 2000 to September 7, 2000. Environmental Protection Agency (EPA)'s Community Scale Air Quality Model (CMAQ) version 4.6 was used as a host model to include a revised Statewide Air Pollution Research Center (SAPRC99) photochemical mechanism with source-oriented extensions to track the contributions of Volatile Organic Compounds (VOCs) emissions from diesel engines, biogenic sources, highway gasoline vehicles, fuel combustion, off-highway gasoline engines, solvent utilization and petrochemical industries to ozone formation in the atmosphere. Source-oriented emissions needed to drive the model were generated using a revised Sparse Matrix Operator Kernel Emissions (SMOKE) model version 2.4. VOC/NO_x ratios are found to be a critical factor in the formation of ozone. Highest ozone formation rates were observed for ratios from 5-15. The contributions of VOC to ozone formation were estimated based on the linear relationship between the rate of NO to NO_2 conversion due to radicals generated from VOC oxidation and the rate of net ozone formation. Petroleum and other

industrial sources are the largest anthropogenic sources in the urban Houston region and contribute to 45% of the ozone formation in the HGB area. Highway gasoline vehicles make contributions of approximately 28% to ozone formation. Wildfires contribute to as much 11% of ozone formation on days of high wildfire activity. The model results show that biogenic emissions account for a significant amount of ozone formation in the rural areas. Both highway and off-highway vehicles contribute significantly to ozone formation especially in the downwind region. Diesel vehicles do not contribute significantly to ozone formation due to their low VOC emissions.

DEDICATION

I would like to dedicate this work to my mother, father and sister, without whom I would not be here today. They have encouraged me all the way, and have shown me immense faith and support in my pursuit for higher education. I could not have done this without them.

ACKNOWLEDGEMENTS

I would like to express my gratitude to my advisor, Dr. Qi Ying for his valuable input and guidance throughout my research, without which I would not be where I am today. I would also like to thank my committee chair members, Dr. Bill Batchelor and Dr. Renyi Zhang for their support during my graduate studies. I feel honored to have had them on my thesis committee.

Last, but not the least, I would like to extend my warmest regards to my mother, father, sister and my friends who have shown me patience, encouragement and undaunted support in all my endeavors.

TABLE OF CONTENTS

Page

Page

TABLE OF FIGURES

Page

Page

Page

LIST OF TABLES

Page

CHAPTER I

INTRODUCTION

Tropospheric ozone (O_3) is listed by the World Health Organization (WHO) and United States Environmental Protection Agency (EPA) as one of its criteria pollutants. It is an important constituent of photochemical smog, an air pollution event that often occurs in metropolitan cities. O_3 has proved to have adverse effects on human health, especially to the respiratory system (Lippmann, 1993). One in three people in the United States live around areas of unhealthful ozone concentrations (American Lung Association, 2008). It can also adversely affect crops and forest ecosystems (Bascom et al., 1996).

Texas is in non-attainment status for O_3 compliance. O_3 pollution in the Houston area is one of the most notorious concerns facing this fourth most populous city in the country. According to Kleinman et al. (2002), the Houston–Galveston-Brazoria (HGB) and Beaumont-Port Arthur (BPA) areas of southeast Texas experience frequent high O_3 events, with O_3 formation rates rising as high up as 200 ppb hr^{-1}, whereas the maximum rates of O_3 production in most other cities in the United states is less than 40 ppb hr^{-1}.

It is imperative to accurately find the sources contributing to O_3 formation in order to take corrective policy measures and develop cleaner technologies. Source apportionment of O_3 is difficult as it is a secondary pollutant, and is not directly emitted from any source. It is formed as a result of a complex series of photochemical reactions in the troposphere.

This thesis follows the style of Environmental Pollution.

To identify the sources of O_3, it is necessary to understand the nature and sources of O_3 precursors, namely sunlight, VOCs (Volatile Organic Compounds) and NO_x (Oxides of Nitrogen).

1.1 Ozone formation chemistry in troposphere

Tropospheric O_3 is formed mainly due to reactions of anthropogenic VOCs with NO_x emissions in the troposphere. The relation between O_3, VOCs and NO_x has been studied in the past (Sillman, 1999) and it occurs to follow a complex pattern of non-linear photochemistry. The extent of O_3 production differs with respect to the relative concentrations ratios of VOC and NO_x. Depending on whether the O_3 concentration is sensitive to NO_x or VOC emission changes, the O_3 concentration in a given area can be regarded as NO_x-sensitive or VOC sensitive. In NO_x sensitive areas, a change in VOC emissions will only cause a marginal difference in O_3 concentrations while a small change in NO_x emissions will cause a significant variation in O_3 levels. In the VOC sensitive regime, an increase in NO_x shows a decrease in O_3 levels, while increasing VOCs reflect in increased observed O_3 concentrations. Hence, it is important to properly identify the VOC/NO_x ratios in studying the O_3 formation chemistry. An insight into the chemistry of O_3 would give a better understanding of the processes of evolution of O_3 and its precursors.

The first reaction in the troposphere that contributes to O_3 formation is the rapid photolysis of NO_2 in the presence of sunlight. The following reactions have been adapted from Seinfeld and Pandis (1998):

$$NO_2 + h\nu \rightarrow NO + O \qquad \text{(R1. 1)}$$

$$O + O_2 + M \rightarrow O_3 + M \qquad \text{(R1. 2)}$$

The oxygen radical (O) reacts quickly with oxygen molecules in the atmosphere to form O_3.

However, the above two equations will not be able to produce large amounts of O_3 due to the titration reaction of NO with O_3, as shown in reaction (R1.3)

$$O_3 + NO \rightarrow NO_2 + O_2 \qquad \text{(R1. 3)}$$

Thus, it is obvious that additional reactions are needed to convert NO to NO_2 without consuming an O_3 molecule. The radicals formed from VOC reactions with oxidants provide such pathways. The rate of O_3 formation mainly depends on the rate of the reaction of hydrocarbons with the hydroxyl radical (OH) produced by water vapor. (Sillman, 2003)

$$O_3 + h\nu \rightarrow O_2 + O\left(^1D\right) \qquad \text{(R1. 4)}$$

$$O\left(^1D\right) + H_2O \rightarrow 2OH^{\cdot} \qquad \text{(R1. 5)}$$

$$RH + OH^{\cdot} \xrightarrow{O_2} RO_2^{\cdot} + H_2O \qquad \text{(R1. 6)}$$

The free radicals of VOCs (RO_2) react with NO and form aldehydes and other secondary hydrocarbons, in the process regenerating NO_2 and $OH^{\cdot}$

$$RO_2^{\cdot} + NO \rightarrow NO_2 + RO^{\cdot} \qquad \text{(R1. 7)}$$

$$RO^{\cdot} + O_2 \rightarrow R'O_2^{\cdot} + HO_2^{\cdot} \qquad \text{(R1. 8)}$$

$$HO_2^{\cdot} + NO \rightarrow NO_2 + OH^{\cdot} \qquad \text{(R1. 9)}$$

The free radicals are terminated when OH reacts with NO to form nitric acid.

$$OH + NO \rightarrow HNO_3 \qquad \text{(R1. 10)}$$

Other termination reactions among HOx and NOx radicals are

$$HO^{\cdot} + HO^{\cdot} \rightarrow H_2O + O_2 \qquad \text{(R1. 11)}$$

$$HO^{\cdot} + HO_2^{\cdot} \rightarrow H_2O + O \qquad \text{(R1. 12)}$$

$$HO_2^{\cdot} + HO_2^{\cdot} \rightarrow H_2O_2 + O_2 \qquad \text{(R1. 13)}$$

Acyl radicals in the troposphere react with O_2 by addition to form acyl peroxy radical.

$$RCO + O_2 + M \rightarrow RC(O)OO^{\cdot} \qquad \text{(R1. 14)}$$

where, R = alkyl group

These acyl peroxy radicals in the troposphere react with NO, NO_2 and HO_2, forming Peroxy Acetyl Nitrate (PAN) among other products.

$$RC(O)OO^{\cdot} + NO_2 \rightarrow RC(O)OONO_2 \quad (PAN) \qquad \text{(R1. 15)}$$

These termination reactions remove NO_x and radicals from the system and thus inhibit O_3 formation.

1.2 Ozone studies done in Texas

The Houston-Galveston-Brazoria area is home to the largest petrochemical industrial complex in the world. Texas possesses unique meteorology, namely high temperatures, intense sunlight and a land-sea wind circulation that combine to cause consistently high O_3 concentrations in many parts of southeast Texas (Bao et al., 2005). Numerous ozone studies were carried out in Texas, especially the HGB and BPA areas which are in severe and moderate non-attainment status for

O_3 compliance as per NAAQS (National Ambient Air Quality Standards). In an effort to better understand the atmospheric processes and its mechanisms, Texas carried out two intensive air quality studies in the years 2000 and 2006. The data gained during these study episodes have supported numerous research efforts in understanding the effects of emissions, meteorology and free radical chemistry on O_3 formation in Texas. The TexAQS 2000 and 2006 experiments helped cover the huge gap that existed in estimating the major sources whose emissions lead to O_3 formation in the Texas area.

Not all VOCs result in formation of O_3. There is a group of Highly Reactive VOCs (HRVOCs) that are found to play a major role in O_3 formation in Texas. Studies from the intense field campaign, as will be further discussed, showed that plumes of HRVOCs like ethene and propene released from petrochemical facilities could rapidly and efficiently produce huge quantities of O_3 downwind of Houston (Berkowitz et al., 2005; Ryerson et al., 2003). The local character of these events, termed Rapid Ozone Formation Events (ROFE) combined with the typically short duration of very high ozone concentrations is suggestive that the origin of O_3 is from a geographically constrained region of sources that emit high-reactivity hydrocarbons, most likely those surrounding the Houston Ship Channel (Kleinman et al., 2002; Ryerson et al., 2003). The data collected by aircraft during the TexAQS 2000 experiments revealed high concentrations of VOCs downwind of industrial areas. The releases were found to be sporadic in nature.

Research on TexAQS 2000 also showed that the emissions of these reactive VOCs were severely underestimated in the emission inventories used in Houston by 1-2 orders of magnitude (Gilman et al., 2009; Ryerson et al., 2003). A significant revelation of the TexAQS II study is that the underestimate of emission fluxes of HRVOC from petrochemical facilities that had been

established by the TexAQS 2000 studies have not yet been fully integrated into inventories developed since that study (Parrish, 2009).

Despite the several experimental and modeling efforts to determine the influence of industrial emissions in Texas, there still lay uncertainties regarding the quantification and magnitude of these influences. O_3 formation was examined under flow conditions where plumes from the major source regions in the region could be studied separately (Ryerson et al., 2003; Wert et al., 2003). The chemical composition of the plume observed from an industrial source differs significantly from that usually observed in other urban areas, in that they contain unusually high concentrations of hydrocarbon oxidation products such as formaldehyde and photochemical product species like peroxides. Back trajectories from the locations where these high O_3 plumes were observed passed over, or in close proximity to, revealed sources of NO_x and hydrocarbons surrounding the Houston Ship Channel (Daum, 2004).

By looking at the efficiencies and instantaneous rates of ozone formation, Daum et al. (2004) showed that ozone formation over and around the Houston Ship Channel could be very rapid and very efficient. High concentrations of reactive hydrocarbons and NOx emitted by industries in this area appeared to be the cause of these high rates and efficiencies. Emissions from the Houston Ship Channel were found to have VOC/NO_2 reactivity ratios that were many times higher than urban Houston, conditions which promoted the rapid and efficient formation of high concentrations of O_3. In the Wert et al. (2003) study, the combined Houston urban and Ship Channel emissions rapidly and efficiently produced plumes of O_3 concentrations higher than 200 ppb. It was, thus concluded that the measured high concentrations of ethene and propene emitted from the Ship Channel could alone account for the high O_3 concentrations that were observed (Daum, 2003).

Using the data from the 2000 field studies, periodic VOC measurements and source apportionment studies for VOC observations were performed (Buzcu and Fraser, 2006; Wittig and Allen, 2008; Zhao et al., 2004). These studies have verified that the observed HRVOC are strongly associated with industrial emissions, and have identified specific sources for highest HRVOC emissions.

There have been attempts to measure emission fluxes from industrial point sources in small areas and short time frames (Parrish, 2009). Two independent techniques were deployed during TexAQS 2006 to quantify fluxes of ethene from industrial sources near Houston, Texas: one, a laser photoacoustic spectroscopy (LPAS) instrument on board an aircraft and the other, a solar occultation flux (SOF) instrument operated in a mobile laboratory. Both instruments repeatedly quantified ethene fluxes from the Mont Belvieu chemical complex to the northeast of Houston, which is one of the largest emission sources in the Houston area (Parrish, 2009). These flux studies verified that industrial point source emissions for the study areas were underreported by an order of magnitude.

In another study by Gilman et al. (2009) in assessing the impact of industrial VOC sources, VOC measurements made during the TexAQS 2006 study were used to calculate VOC mixing ratios. These ratios were compared between Houston and other urban settings. Anthropogenic VOC mixing ratios were highest from industrial sources including chemical plants and petroleum refineries. The impact and variability of industrial sources were evidenced by very high maximum mixing ratios (>50 ppbv) of a variety of VOCs.

There have been several modeling studies on ozone formation to determine the importance of industrial sources on ozone formation. Vizuete et al. (2008) studied the contribution of industrial

emissions to O_3 formation in Houston during August 25 and 26, 2000. The simulations showed that industrial emissions were major sources of Highly Reactive VOCs (HRVOCs), especially propene, ethene, butene and 1,3 butadiene. It was found that O_3 production was directly related to the amount of hydroxyl radicals produced as a result of the photolysis of formaldehyde and other aldehydes. O_3 production was found to be sensitive to these hydroxyl radical sources, and this sensitivity existed regardless of whether the plume from the industrial emission event encountered high sources of NO_x.

An analysis of the conditions under which ROFEs occurred in the Houston-Galveston area was done by Murphy and Allen (2005). It was found that the frequency of the HRVOC releases, along with the location and magnitude of the release were all important factors in determining the occurrence of an ROFE. If the combination of these and other factors like meteorology become conducive to O_3 formation, then large spikes in O levels are experienced in the HGB area. Lin et al. (2005) found that point source emissions of VOC and NO_x made the highest contribution to peak O_3 values in the ROFEs of the urban-industrial regions of southeast Texas. Modeling in the absence of VOC and NO_x point sources in the emission inventory showed that ozone peaks reduced by 128 and 70 ppb respectively. During the ROFE analysis, based on August 25, 2000, VOC reductions caused greater reductions in peak O_3 than NO_x reductions in southeast Texas. An extended version of the Statewide Air Pollution Research Center (SAPRC99) chemical mechanism was used by Czader et al. (2008) in the CMAQ model during August 23-30 of the TexAQS 2000 study period in the Houston-Galveston area. Not all the VOCs contribute equally to the formation of ozone. The reactivities of VOCs were found to vary with the air composition of the urban and industrial region as well as meteorology. The most

reactive compounds considering the impact on O_3 formation were ethene, propene and formaldehyde.

A photochemical modeling study in Houston determined the effect of NO_x and VOCs on O_3 formation during the TexAQS 2000 study period. Initially, O_3 levels were being under-predicted. Upon increasing the propene and ethene concentrations by a factor of 10, O_3 predictions were more accurate in comparison to observed data (Jiang and Fast, 2004). Jobson et al. (2004) measured C1 to C10 hydrocarbon concentrations at La Porte, Texas. After comparing the measurements with emission signatures of roadway vehicles and industrial emissions, they determined that short chain hydrocarbons from industrial emissions dominate the air mass reactivity and ozone formation in Houston. However, detailed source contributions to VOC or air mass reactivity were not quantified in that study.

Other sources also have an important influence on the formation of ozone, and several studies have been carried out in this regard. Industrial sources, though predominant, are not the only sources influencing ozone formation in southeast Texas. Biogenic emissions, mainly isoprene, are a significant part of the VOC emission inventory in Texas and can cause significant increase in O_3 concentrations in the larger part of southeast Texas, although they are generally considered not directly responsible for O_3 non-attainment in the urban areas. Biogenic emissions in the ozone non-attainment area of Houston-Galveston from August 22 - September 1, 2000 were studied in detail by Byun et al. (2005) using the Land use-Land cover data from satellites. Uncertainties in biogenic emission estimates were found to exist, which caused O_3 concentrations to vary based on location, and in some cases going up as much as 10 ppb. The spatial distribution of the ozone concentrations depended on the location of biogenic emissions with respect to the sources of NO_x and VOCs. Song et al. (2008) compared model predictions with observation

datasets for isoprene during the TexAQS study period. Two different vertical schemes were used in the model simulations, causing differences in isoprene concentrations by as much as 270%. The diurnal variations in surface isoprene concentrations were well-predicted by the model. However, concentrations in the rural areas were over-predicted by a factor of two in the rural areas.

The effect of wildfires on ozone formation in Southeast Texas during TexAQS 2000 was studied by Junquera et al. (2005). An important conclusion drawn from the study was that for fires larger than 10,000 acres, greatest increases in O_3 formation were observed within 10-100 km of the fires. Background sources have also known to contribute significantly to ozone formation in Houston through regional transport. During TexAQS and TexAQS II, background sources were found to lead to 50% and 66% of the total ozone on days of 8-h ozone exceedances respectively. This calls for a more regional perspective on ozone precursor controls (Kemball-Cook et al., 2009). It was also found that in the TexAQS 2006, 84% of daily 8-h maximum ozone concentrations from 30 stations in the Houston area was attributed to the regional background (Langford et al., 2009).

The TexAQS experiments were also helpful in understanding new chemical pathways in the formation of ozone in Texas. Chemical characterization of O_3 formation was done by Lei et al. (2004) for the TexAQS 2000 period. It was found that NO_x oxidation during the midday hours had an O_3 production efficiency of 3-8 molecules of O_3 per NO_x molecule oxidized. More than 70% of the RO_2 radical in the nighttime occurs due to alkene-NO_3 reactions. O_3 production accelerates by about an hour due to the heterogeneous conversion of NO_2 to HONO that occurs on the surfaces of soot aerosol in the morning and leads to a noticeable increase of 7 ppb on average in the daytime O_3 level.

Chang and Allen (2005) studied the impacts of chorine free radical chemistry on tropospheric O_3 formation in southeast Texas from August to September 2000. The analysis concluded that chorine emissions can enhance O_3 concentrations in localized areas by up to 70 ppb in the mornings. Its impact on O_3 levels is not as pronounced (up to 10 ppb) in larger areas and during peak hours of O_3 concentrations. Simon et al. (2009) carried out a photochemical modeling study to gain an insight into the physical and chemical processes leading to O_3 formation in urban areas. The effect of nitryl chloride ($ClNO_2$) was analyzed on the formation of O_3 in Houston area over the period from August 30 to September 9, 2006. $ClNO_2$ is expected to affect O_3 formation as its photolysis products include NO_2 and chlorine atoms. The results showed that the changes in O_3 concentrations due to $ClNO_2$ were modest, of the order of 1.5 ppb at the highest.

In other regions, the influence of different sources and meteorology are different from that in the areas of southeast Texas. In a comparative study of five cities with regard to VOC reactivity, Kleinman et al. (2002) found that the industrial component was highest for Houston. In Philadelphia, the contribution of industrial and biogenic sources to VOC reactivity was found to be the same. Biogenic also dominated the VOC reactivity in Tennessee, and was prominent in New York as well. In Phoenix, the industrial component was higher than other sources, but their contribution was nearly 8 times lesser than that for Houston. In a study by Shi et al. (2009) of the U.S-Mexico border region from June 1-4, 2006 using back trajectories, the main sources to O_3 episodes were found to be local photochemical production and regional transport. In San Diego, fumigation and transport at high-altitudes were the main contributors to O_3.

There are numerous publications that describe methods for adjusting measured ozone for the effects of meteorology (Camalier et al., 2007; Davis et al., 1998). Zhang et al. (2007) studied the impacts of uncertainties in meteorology on the model prediction of O_3 concentrations in Houston

on August 30, 2000. Inaccurate meteorological parameters were found to be significantly affect the accuracy of O_3 predictions. Small uncertainties in wind and temperature caused large uncertainties in the O_3 predictions in and around Houston.

In a study by Bao et al. (2005), to evaluate the performance of a forecasting weather-chemistry model, the meteorological simulations over Houston were compared to data obtained from the TexAQS observations for August 25-30, 2000. It was found that the wind predictions had a consistent easterly bias, while the low-level temperature predictions had a cold bias. Small errors in low moisture levels, when coupled with a cold bias caused large over-predictions in the relative humidity. Vertical diffusion and the chemical composition of the local environment were seen to have an effect on the O_3 mixing ratios. For example, Vizuete et al. (2008) found that the composition of an industrial release affects the areas downwind where the greatest increase in peak O_3 occurs. This implies that a personal exposure to ozone would vary based on emission composition. Thus, the composition of the release and the chemical environment in which these plumes enter are important factors in O_3 production. In layers above the surface layer, O_3 formation contributes to the surface O_3 concentration through rapid vertical turbulent diffusion within the mixing layer (Byun et al., 2007).

1.3 Methods of determining sources that contributes to ozone formation

There are a number of receptor oriented models that have been used in air pollution source apportionment studies. Several of these techniques include Chemical Mass Balance (CMB) (Watson, 1990) and Positive Matrix Factorization (PMF) (Paatero and Tapper, 1994).

The CMB is based on a set of mass-balance equations that relate the relative contributions of resolved sources, the emission chemical signatures (source profiles) of these sources and the

measured concentrations of chemicals at receptor locations. The inputs to the CMB receptor model were profiles of the emission sources and measured pollutant concentrations at receptor locations. The mass-balance equations of various chemical species are solved to determine the contribution of each source to the observed pollutant concentrations (Fujita, 2001). PMF is also based on the basic mass-balance equations described above but it uses a different technique that determines site-specific source profiles and source contributions as a function of time based on the existing time series of measured pollutant concentrations.

A 1996 Paso del Norte (PdN) ozone study (Fujita, 2001) carried out source contribution of VOCs in El Paso, Texas and Chihuahua, Mexico using the CMB receptor-oriented modeling approach from August 9 – September 30, 1996. The results show that on-road mobile sources are the main source of NMHCs, and gasoline vehicle exhausts make up two-thirds of NMHCs in El Paso in the morning and afternoon commuting hours. Abu-Allaban et al. (2002) used a chemical mass balance (CMB) model to study source contributions to the observed VOC concentrations at several sites in Cairo, Egypt, and determined that mobile emissions, lead smelting, and liquefied petroleum gas were the major sources.

In an effort to identify source contributors of VOCs, Zhao et al. (2004) augmented the CMB model with equations accounting for wind profiles, temperature and weekend/weekday effects. The model was applied in La Porte site in Houston during the TexAQS 2000 experimental period. The model results were favorable, providing a reliable approach to resolve source contribution in complex VOC systems. Propene was estimated to be emitted by the refineries along the ship channel. The contribution of biogenic isoprene was found to be small in the immediate proximity of the La Porte, Texas.

To find the relative anthropogenic source contribution of VOCs in southern Taiwan, an air trajectory statistical analysis was conducted to identify the locations of major pollutant sources from 1994-1998. The results showed that the relative contribution of point, line and area sources were in the ratio 5:2:3. The highest contributing districts in Taiwan were also identified (Lin and Chang, 2002). Another statistical approach that carried out source apportionment of VOCs, (Non-Methane Hydrocarbons) NMHC from industries and traffic in particular is the study by Chang et al. (2009). Along with a vehicular indicator, the study involved using Principal Component Analysis (PCA) to differentiate the influence of different sources in urban-industrial complexes in Taiwan from 2002 to 2004. The ambient NMHC concentrations were resolved into four major sources: traffic, household fuel leakage, industrial, and biogenic.

An ozone study in Houston carried out VOC source apportionment using PMF method (Buzcu and Fraser, 2006). The study was done for the period between June and October 2003. The key findings of the study were that the major source emissions were consistent with the chemical profiles of petrochemical, refinery and evaporative emissions. Miller et al. (2002) compared the source contributions of VOC exposures by evaluating four receptor-oriented source apportionment models, namely chemical mass balance, principal component analysis/absolute principal component scores, PMF and graphical ratio analysis. The data used was from an EPA study carried out from 1984-1990. All models simulated only the major contributors to total exposure concentrations. None could distinguish between sources having similar chemical profiles, or source contributions less than 5%.

In a study using PMF, Elbir et al. (2007) carried out the source characterization of VOCs in Izmir, Turkey in 2003 and 2004. It was found that the air in suburban areas contained 40.6% toluene, while urban areas contained 30.5%, during the summer. The source factors identified

from suburban sites are diesel (40%), gasoline and paint applications. The major source factors from urban areas are gasoline vehicle exhaust, diesel vehicle exhaust, paint, degreasing and dry cleaning. In another similar study by Yuan et al. (2009) in Beijing, China, the PMF method was used to identify the source contributors of VOCs in a rural and urban areas from August-September, 2006. Vehicle activities were found to contribute to 60% of VOC loading. Liquefied petroleum gas, coal and biogenic emissions were among the other sources. This source-apportionment analysis tends to underestimate the VOCs from distant sources, as it does not account for VOCs consumed during transport towards formation of secondary pollutants like ozone.

One of the many limitations of CMB is that it is not predictive; rather it helps understand the reason for the existing emission concentrations (Miller et al., 2002). It also assumes a linear relationship between the receptor species, devoid of any chemical reactions. In addition, source contributions are resolved only at receptor locations. Large scale receptor oriented modeling studies that covers a wide area requires intensive field sampling and high operational costs. Due to these reasons, the receptor models can only determine source contributions in very limited areas and source contribution information in a regional scale cannot be easily obtained. Due to its linear approach, only primary PM and night time VOCs can be apportioned. Wittig and Allen (2008) explored the possibility of using modified source profiles for VOC source apportionment of daytime samples but reported poor CMB model performance when aged source profiles were used.

Source oriented mechanistic air quality models overcome the many limitations of a receptor oriented model in carrying out a regional source apportionment. Source oriented models can give the source contributions to primary and secondary pollutant concentrations at not only the

receptor locations but also at any other points in the study domain. In the source oriented model, the emissions primary pollutants and precursors of secondary pollutant precursors from different sources are tracked individually in the model simulation of the emission, transport, physical and chemical transformation and removal processes (Kleeman and Cass, 2001). The source-oriented modeling technique has been previously used by Ying et al. (2007) to find source attributions of primary and secondary airborne particulate matter in California (Ying and Kleeman, 2006). It is natural that this technique can be applied to study source contribution to O_3 formation.

1.4 Objectives

The objectives of this study are to 1) develop a source-oriented model to determine the contributions of VOCs from major emission sources to regional O_3 formation and 2) apply the model in Southeast Texas to determine source contributions to O_3 formation during a severe O_3 air pollution episode. This is the first time regional source contributions of VOCs to O_3 formation have been quantified using a three-dimensional source-oriented air quality model.

CHAPTER II

MODEL DESCRIPTION

The model used in this study is the US Environmental Protection Agency's Community Multiscale Air Quality Modeling system (CMAQ), version 4.6 (CMAS Center, 2009a). CMAQ is a multi-pollutant, multi-scale air quality model that contains state-of-the-science capabilities to simulate all atmospheric and land processes that impact the regional and urban scale transport, transformation, and deposition of atmospheric pollutants and/or their precursors. This three-dimensional Eulerian atmospheric and chemistry transport model is designed to approach air quality with a "one atmosphere" approach by incorporating advanced techniques to handle important air quality issues like ozone formation, acid deposition, visibility and particulate matter formation in the troposphere.

2.1 CMAQ Base-case model

The CMAQ modeling system consists of three primary components (meteorology, emissions, and a chemical transport model) and several interface processors. In our study, the Fifth Generation Penn State University/ National Center for Atmospheric Research Mesoscale Model (MM5) (2008) is the model used to generate the meteorology fields and the Sparse Matrix Operator Kernel Emissions Model (SMOKEv.2.4) is the model used to produce the emissions. The CMAQ system uses interface processors to incorporate the output data from these two models into the CMAQ Chemical Transport Model (CCTM), along with input information of initial and boundary conditions and photolysis rates generated by other processors (Byun and Schere, 2006). Figure 2.1 illustrates the CMAQ modeling system framework.

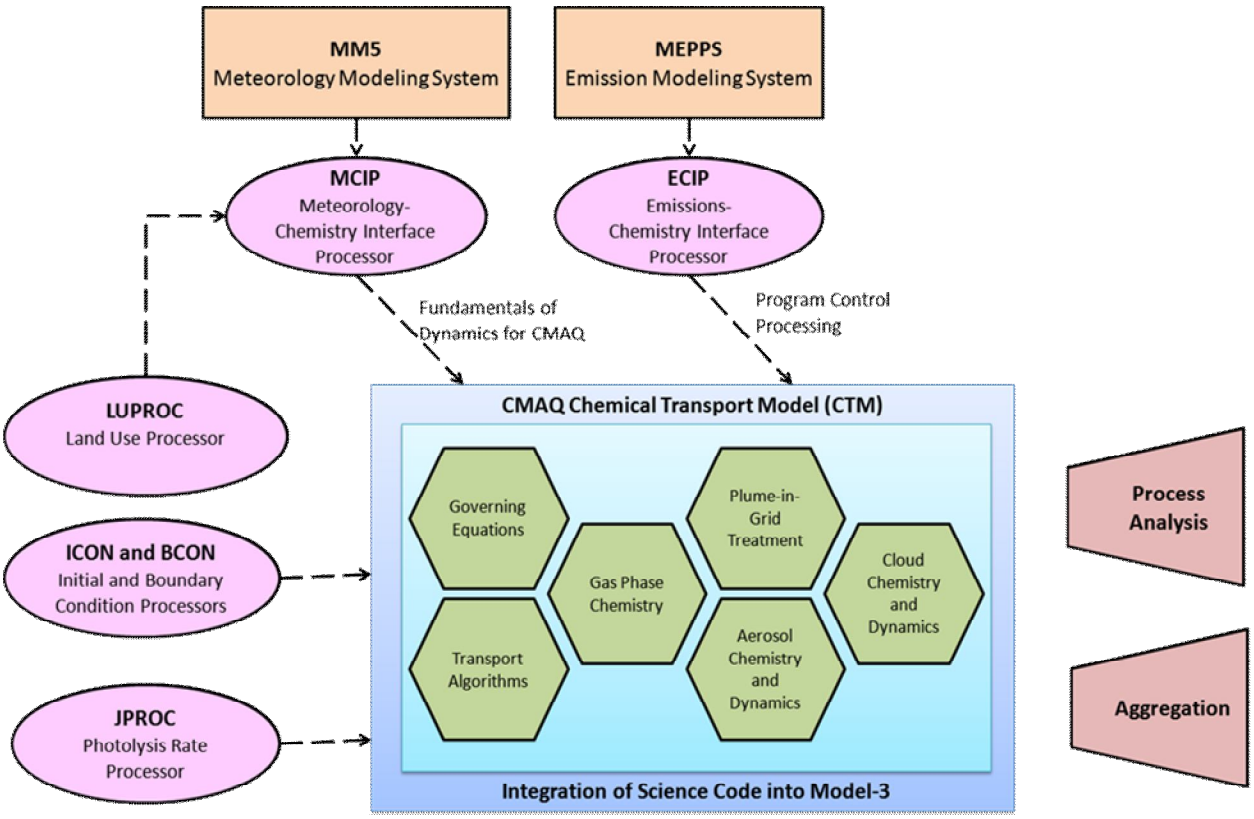

Figure 2.1 CMAQ Modeling System Framework, Chapter 1.1 (Byun and Schere, 2006).

The concept behind CMAQ is that it performs a mass balance within each cell of the modeling domain to determine the transport across cell boundaries and chemical transformations within a cell at a given time period. The model solves sets of ordinary differential equation to simulate atmospheric processes to calculate the concentration changes in each grid cell of the modeling domain. The processes considered in the model are emissions from sources, horizontal advection and diffusion, vertical advection and diffusion, chemical transformation and deposition.

Mathematically, it is represented by a simplified continuity equation listed below:

$$\frac{\partial C_i}{\partial t} = -\frac{\partial (UC_i)}{\partial x} - \frac{\partial (VC_i)}{\partial y} - \frac{\partial (WC_i)}{\partial z} + \frac{\partial}{\partial x}\left(K_{xx}\frac{\partial C_i}{\partial x}\right) + \frac{\partial}{\partial y}\left(K_{yy}\frac{\partial C_i}{\partial y}\right) + \frac{\partial}{\partial z}\left(K_{zz}\frac{\partial C_i}{\partial z}\right) + R_i + L_i + S \quad (2.1)$$

where U, V, W indicate wind speed in x, y and z directions respectively; C denotes concentration of species 'i', K_{xx}, K_{yy} and K_{zz} are the turbulent diffusivities in x, y and z planes; R and L denote the rate of production and loss due to chemical reactions respectively; and S is the emission rate of the species 'i'.

The meteorological data for this study was obtained from the Texas Commission on Environmental Quality (TCEQ) and processed using the Meteorology-Chemistry Interface Processor (MCIP) package. The MCIP translates and processes model outputs from the meteorology model for the CCTM. MCIP interpolates the meteorological data if needed, converts between coordinate systems, computes cloud parameters, and computes surface and planetary boundary layer (PBL) parameters for the CCTM. MCIP uses land-use information from the land-use processor (LUPROC) to calculate the PBL and surface parameters (Byun and Schere, 2006; U.S.EPA, 1999).

The emission files were generated using the pre-processing Sparse Matrix Operator Kernel Emissions (SMOKEv2.4) model (Houyoux, 2000). SMOKE is used for the preparation of area, mobile, point, and biogenic emission data ready for CMAQ model input. The input files needed for SMOKE are meteorology, chemical speciation, temporal and spatial allocation, mobile, biogenic and point emission files. SMOKE not only deals with individual chemical species but also accommodates lumped (grouped) species consistent with the gas phase chemical mechanisms contained in the CMAQ model. As an output, SMOKE provides gridded,

temporalized (usually hourly), and speciated emission data for criteria, particulate, and toxic pollutants.

2.2 Enhancement of CMAQ for source-apportionment

The SAPRC99 photochemical mechanism is revised with source-oriented extensions to track the contribution of different emissions to VOC concentrations in the atmosphere. In the original form of the source-oriented method, emissions from all resolved sources are tracked simultaneously in the model. For example, if A and B represent two sources, then the reaction of a general alkane (RH) with OH that generates a peroxy radical (RO_2) can be written as:

$$\begin{aligned} RH^{A} + OH &\rightarrow RO_2^{A} + H_2O \\ RH^{B} + OH &\rightarrow RO_2^{B} + H_2O \end{aligned} \qquad \text{(R2. 1)}$$

However, to explicitly include reactions for all the sources that need to be tracked in the model will increase the number of reactions and the number of chemical species significantly due to the large number of reactions that includes two or more typed species in the reactants. A simplification to the source-oriented mechanism is to use only two source types in the mechanism: one type represents a source that needs to be tracked explicitly and the other type represents all the remaining sources, as shown in the reactions below:

$$\begin{aligned} RH^{X} + OH &\rightarrow RO_2^{X} + H_2O \\ RH^{O} + OH &\rightarrow RO_2^{O} + H_2O \end{aligned} \qquad \text{(R2. 2)}$$

where, X represents VOC emissions and oxidation products from an explicit source X (for example, gasoline powered vehicles) whose contribution is to be resolved in a model simulation and superscript O represents lumped emissions and oxidation products from all other VOC sources. In this way, the number of reactions and species in the expanded mechanism is reduced significantly. An obvious drawback of this method is that only one source can be resolved for

each model run. In each model simulation, VOC contribution to O_3 formation from one explicit source will be determined. During the emission processing stage, emissions from different sources have been saved in different emission files. Each simulation uses all the emission files but designates a different explicit source than previous simulations. For example, if the current simulation is to determine the source contribution of diesel vehicles, the VOCs from diesel vehicles will be represented with the 'X'-tagged species. Emissions of VOCs from other sources will be lumped into the 'O'-tagged species. Processing the results associated with the 'X'-tagged species will allow us to determine the contribution from diesel vehicles. The simulations are repeated with a different explicit source each time until the contributions from all the sources are determined.

The SAPRC99 chemical mechanism was manually updated to include the above tagged chemistry. A detailed description of the SAPRC-99 VOC species is included on Table 2.1 (Carter, 2000). The Process Analysis tool in CMAQ is used to determine the net ozone formation rate and the contribution of each of the reactions in the chemical mechanism to the conversion of NO to NO_2.

Table 2.1 Description of VOC species in the SAPRC99 chemical mechanism

Species	Description
ALK1	Alkanes and other non-aromatic compounds that react only with OH, and have kOH < 5x 10^2 ppm-1 min-1. (Primarily ethane)
ALK2	Alkanes and other non-aromatic compounds that react only with OH, and have kOH between 5 x 10^2 and 2.5 x 10^3 ppm-1 min-1. (Primarily propane and acetylene)
ALK3	Alkanes and other non-aromatic compounds that react only with OH, and have kOH between 2.5 x 10^3 and 5 x 10^3 ppm-1 min-1.
ALK4	Alkanes and other non-aromatic compounds that react only with OH, and have kOH between 5 x 10^3 and 1 x 10^4 ppm-1 min-1.
ALK5	Alkanes and other non-aromatic compounds that react only with OH, and have kOH greater than 1 x 10^4 ppm-1 min-1.

Table 2.1 Continued

Species	Description
PROD2	Ketones and other non-aldehyde oxygenated products which react with OH radicals faster than 5 x 10^{-12} cm3 molec-2 sec-1.
ARO2	Aromatics with kOH > $2x10^4$ ppm-1 min-1.
OLE1	Alkenes (other than ethene) with kOH < $7x10^4$ ppm-1 min-1.
OLE2	Alkenes with kOH > $7x10^4$ ppm-1 min-1.
TERP	Terpenes
BALD	Aromatic aldehydes (e.g., benzaldehyde)
CCHO	Acetaldehyde
ACET	Acetone
CRES	Cresols
GLY	Glyoxal
HCHO	Formaldehyde
ISO-PROD	Lumped isoprene product species
MEOH	Methanol
PHEN	Phenol
RCHO	Lumped C3+ Aldehydes
CCO-OH	Acetic Acid
HCOOH	Formic Acid
RCO-OH	Higher organic acids
MEK	Ketones and other non-aldehyde oxygenated products which react with OH radicals slower than 5 x 10^{-12} cm3 molec-2 sec-1.

2.3 SMOKE and its modification to generate typed emissions

Source-oriented emissions needed to drive the model are generated using a revised SMOKE model version 2.4 (CMAS Center, 2009b; Houyoux, 2000). The SMOKE program is modified to include a Source Classification Code (SCC) filter so that only emissions from a set of predefined SCC codes will be processed. The source categories chosen are all the major contributors to VOC releases in the atmosphere. The nine sources are biogenic, fuel combustion, highway gasoline, off-highway gas, diesel vehicles, petroleum-related processes, solvent utilization, wildfires and other sources. These typed emissions are processed to generate CMAQ-ready files

that contain emissions from the particular source as well as total emissions of all sources. This can be helpful in analyzing the relative contribution of each source to ozone formation with respect to the total emission concentrations.

CHAPTER III

MODEL APPLICATION

3.1 Description of simulated episode

The study episode chosen for the simulation was August 16, 2000 to September 7, 2000. The period chosen has air quality data available due to the TexAQS carried out during the same time. The study episode for this project was part of the TexAQS study experiment period (August 15 – September 15, 2000) that witnessed a 9-day period of 1-hour National Ambient Air Quality Standard (NAAQS) surface O_3 exceedances in the metropolitan areas of Houston according to Bao et al. (2005) and the weather conditions during this period were characterized by high temperatures and less precipitation (Bao et al., 2005). Maximum observed hourly averaged surface O_3 concentrations during some of the high O_3 days in the study episode were 185 ppb on August 25, 119 ppb on August 26, 146 ppb on August 29, and 199 ppb on August 30, 2000 (Bao et al., 2005).

High O_3 episodes are a result of a combination of variable factors, such as the time of release of its precursors, meteorology and NO_x availability during that period (Bao et al., 2005; 2006). Meteorology plays an important role in ozone concentrations in a region. Each meteorological parameter has its own unique effect on O_3 trends. Temperature, for example is directly proportional to O_3 while increase in wind speed is associated with decreasing O_3 due to the dilution effect (Camalier et al., 2007).

Five days of the episode experienced veering winds associated with flow reversal and high O_3 in the HBG area. Light easterly winds on August 25 led to maximum O_3 levels in Crawford, center of Houston, and southeasterly winds on August 26 carried the O_3 peaks to Conroe, 40 miles

north of Houston. The next two days witnessed southeasterly sea breeze winds that transported the diluted O_3 plume from Crawford to Conroe, resulting in low O_3 concentrations in Crawford. From August 29-31, light westerly winds followed by afternoon sea breezes place the high O_3 parcel on the east side at La Porte, Deer Park and Mt. Belvieu (Byun et al., 2007).

Occurrence of strong sea breeze also influences the concentrations of surface O_3 in the Houston area. Before the onset of a sea breeze, the O_3 levels and its precursors remain localized. Without any transport, O_3 levels only rise due to the accumulation of fresh O_3 formed during the next day. The onset of a breeze in the Houston area causes the recirculation of O_3 and NO_x to a convergence zone which experiences high O_3 exceedances (Bao et al., 2005).

The HGB area contains large concentration of petroleum refineries and chemical manufacturing facilities. The observations taken at the TexAQS experimental study showed that O_3 concentrations as high as 200 ppb form inside the plumes of these industrial facilities (Nam et al., 2006). The months of August and September, 2000, also witnessed intense drought and subsequent wildfire activity. Days that experienced most severe wildfire activity were August 23, August 30-September 6, 2000 (Junquera et al., 2005). Approximately 95,000 acres were reported to have burned in wildfires in the HGB and BPA regions during that period. Estimated emissions on some days were as high as 3700 tons of CO, 250 tons of VOCs, 340 tons PM2.5 and 50 tons of NO_x (Junquera et al., 2005). Although the impacts of each fire are different, for wildfires less than 10,000 acres O_3 concentrations can be increased by 60 ppb within 10 km of the wildfire.

3.2 Domain setup

The areas around Houston-Galveston-Brazoria (HGB) and Beaumont-Port Arthur (BPA) were used as the finest domain with a grid size of 4 km. This domain was nested inside a coarser

domain with a grid size of 12 km. Both these domains were further nested in the coarsest modeling domain of 36 km grid size that covers all of eastern U.S and south-eastern parts of Canada. The initial and boundary conditions for the 36 km domain were based on default clean boundary profiles. The Eastern US domain contains 67x62 grid cells, each cell measuring 36x36 km^2. The East Texas 12 km domain contains 89x89 cells in the horizontal direction, while the 4 km modeling domain contains 83x65 cells in the horizontal direction. All three domains contain 14 vertical layers. The thickness of each layer is given in Table 3.1:

Table 3.1 Thickness of each layer in the CMAQ simulation

Layer	Thickness (m)
1	42.41
2	42.54
3	85.64
4	173.43
5	176.37
6	270.31
7	467.09
8	589.61
9	627.29
10	1019.2
11	1270.74
12	2286.4
13	4334.49
14	9426.72

The CMAQ modeling system (version 4.6) (CMAS Center, 2009a) was the host air quality model applied in this study. CMAQ is a comprehensive Eulerian air quality grid model designed for assessments of multiple atmospheric pollutants, including O_3 and other oxidants, aerosols, air toxics and mercury species on urban to continental scale domains. CMAQ is composed of state-

of-science algorithms designed to solve the relevant dynamic, chemical, and atmospheric removal processes.

3.3 Configuration of the CMAQ model

In this study, the CMAQ model was configured to use the Statewide Air Pollution Research Center (SAPRC-99) photochemical mechanism (Carter, 2000). The SAPRC-99 is one of the most common chemical mechanisms used to describe urban atmospheric chemistry. It has been specifically designed for volatile organic compound (VOC) reactivity assessment and has been employed to generate VOC reactivity scales used in regulatory applications. This mechanism uses the lumped molecule approach in condensing VOCs in which lumped or surrogate species are used to represent organic compounds with similar structures and OH reactivities.

For the purpose of this study, the default SAPRC99 mechanism was modified to calculate source contributions of VOCs to ozone formation. Section 2.2 describes how the chemical mechanism was revised to incorporate the source tags in reactions that contribute towards NO to NO_2 conversion, and thereby to ozone formation. Each reaction was tagged once with the source, say A, and once with the remaining sources lumped together, as “Other”.

An example of a sample reaction that represents the reaction of a peroxy radical with NO_2 in the tagged version of the reaction system is given below:

$$\begin{aligned} RO_2^A + NO &\rightarrow RO^A + NO_2 \\ RO_2^{other} + NO &\rightarrow RO^{other} + NO_2 \end{aligned} \qquad \text{(R2. 3)}$$

As discussed in Section 2.2, the Process Analysis tool in CMAQ was activated to determine the reaction rates in the conversion of NO to NO_2.

3.4 Input data

3.4.1 Meteorology

The Pennsylvania State University (PSU)/National Center for Atmospheric Research (NCAR) Mesoscale Modeling System (MM5) (Grell, 1994) is used to provide the meteorology input data to the air quality simulations. MM5 is a limited-area, non-hydrostatic, terrain-following sigma-coordinate model designed to simulate or predict mesoscale and regional-scale atmospheric circulation. The meteorological fields of wind speed and direction, temperature, water vapor mixing ratio are generated using this MM5 model (Shrestha et al., 2009).

3.4.2 Emission and incorporation of wildfires

The Clean Air Interstate Rule (CAIR) 2001 emission inventory of U.S. EPA (EPA) (CMAS Center, 2009a) was used to generate model ready emission files. The original emission inventory data were categorized into the following types: area, on-road, off-road and point sources. The emission data were processed using the SMOKE model (CMAS Center, 2009b; Houyoux, 2000) to generate temporally resolved, spatially distributed and speciated model-ready emissions data for CMAQ. The plume rise of pollutants from point sources was calculated off-line within SMOKE using the stack parameters and meteorological fields in order to vertically allocate point source emissions into model layers. Emissions from natural sources (biogenic and soil) were computed by the Biogenic Emissions Inventory System (BEIS) version 3.13 (CMAS Center, 2009c) incorporated within the SMOKE model.

Based on the EPA emission inventory used in this study, the major sources of VOCs are industrial processes, on-road vehicles and solvent use. In addition, non-road equipment and

miscellaneous, wild fires, waste disposal, fossil fuel combustion, and residential wood combustion are also important.

Wildfires contribute to ozone formation by emitting large amounts of NO_x and VOCs. The 22 day study period saw events of wildfires that contributed to elevated pollutant concentrations downwind (Junquera, 2004). At least 20 major wildfire events occurred during that period (Junquera, 2004). Hence, a wildfire inventory is acquired from Dr. David Allen and added to the overall emissions inventory for improved model accuracy and performance.

The emission inventory is split into nine sources that were identified as major sources of VOC emissions. It is informative to show the contribution of each source to the emission of total VOCs. The emissions were summed over the entire model domain for August 31st, a day that not only experienced a high ozone event, but was also accurately predicted by the CMAQ model during the base-case run (see section 4.1.1). A list of emissions of different VOCs emitted from each source type is given in Table 3.2. This table contains emissions averaged over 24 hours for the model domain during August 31, 2000.

Table 3.2 Emission of different SAPRC-99 VOCs from each source for the 4 km domain on August 31, 2000

Species (kmol/day)	Petroleum	Solvent	Highway	Wildfire	Fuel	Off-highway	Other	Diesel	Biogenic
ACET	18.10	12.71	11.85	0.00	1.44	0.00	41.56	0.00	1608.13
ALK1	410.00	23.55	100.28	473.23	212.77	39.75	757.70	0.00	544.48
ALK2	455.99	11.52	168.30	449.21	53.35	40.33	414.07	0.00	727.58
ALK3	325.37	86.72	742.31	8.18	46.92	186.39	532.49	0.00	2412.20
ALK4	469.36	101.65	679.22	16.74	34.89	201.45	622.23	0.00	0.00
ALK5	284.55	774.58	196.54	0.00	2.52	97.90	1142.67	0.00	0.00
ARO1	125.21	170.67	296.27	0.00	9.08	69.94	388.72	0.00	0.00
ARO2	111.28	61.48	198.81	0.00	10.52	103.55	294.76	0.00	0.00
BALD	0.00	0.00	0.00	0.00	0.00	0.00	0.00	0.00	0.00
CCHO	18.22	0.00	16.62	0.00	0.36	5.24	28.40	13.73	1069.98
CCOOH	12.09	0.00	0.00	0.00	0.00	0.00	10.49	0.00	544.48
CRES	0.60	0.06	0.00	0.00	0.00	0.00	5.93	0.00	0.00
ETHENE	567.62	0.00	273.97	925.95	23.83	123.91	316.03	145.14	2412.20
GLY	0.01	0.00	0.00	0.00	0.01	0.00	0.29	0.00	0.00
HCHO	151.30	1.46	53.62	0.00	200.26	20.31	166.63	59.58	2139.96
HCOOH	2.16	0.00	0.00	0.00	0.00	0.00	7.66	0.00	1088.96
IPROD	0.14	0.00	0.84	0.00	0.00	0.24	1.65	2.99	0.00
ISOPRENE	0.94	0.00	3.59	0.00	0.00	0.94	5.88	0.00	29943.87
MACR	13.20	0.00	1.57	0.00	0.01	0.88	12.81	0.00	0.00
MEK	7.87	2.52	2.07	0.00	0.00	0.00	12.23	0.00	0.00
MEOH	52.80	0.00	53.41	0.00	0.00	0.00	39.55	0.00	9724.87
MGLY	0.01	0.00	0.00	0.00	0.00	0.00	0.23	0.00	0.00
OLE1	150.22	1.56	212.31	149.85	26.61	46.69	176.79	0.00	4377.00
OLE2	72.10	2.61	214.19	35.35	3.82	84.04	143.90	0.00	1118.82
PHEN	11.24	0.00	0.00	0.00	0.66	0.00	5.86	0.00	0.00
PROD2	1.28	6.66	0.00	0.00	0.00	0.00	13.04	0.00	0.00
RCHO	5.10	0.00	5.53	0.00	0.63	0.28	27.94	6.50	356.66
RCOOH	5.90	0.00	0.00	0.00	0.00	0.00	13.05	0.00	0.00
TRP1	0.10	0.01	0.00	0.00	0.00	0.00	63.16	0.00	5029.57

Figure 3.1 summarizes the contributions to total VOC emissions from different source categories.

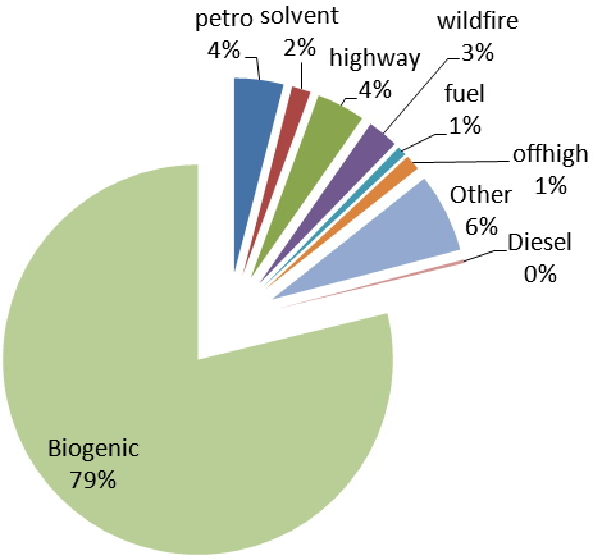

Figure 3.1 Contribution to VOC emissions from each source on August 31, 2000.

Biogenic sources were found to be the major contributors of VOC emissions, making up for 79% of total VOC emissions. Isoprene is the most prominent VOC species emitted from biogenic sources. High emission rates of isoprene are especially observed in rural areas. The next highest contributor to VOCs were the other sources, that are a combination of several smaller sources that do not fall under any of the eight named sources. Other sources account for 6% of total VOCs. The major VOC species in this category are the highest reactive alkanes, and less reactive aromatics. Highway gasoline and petroleum related processes make an equal contribution to VOCs of 4% each. The predominant VOC species in highway gasoline are olefins, lesser reactive aromatics and moderately reactive alkanes. In petroleum processes, ethene is the dominant VOC released, followed by higher reactive alkanes.

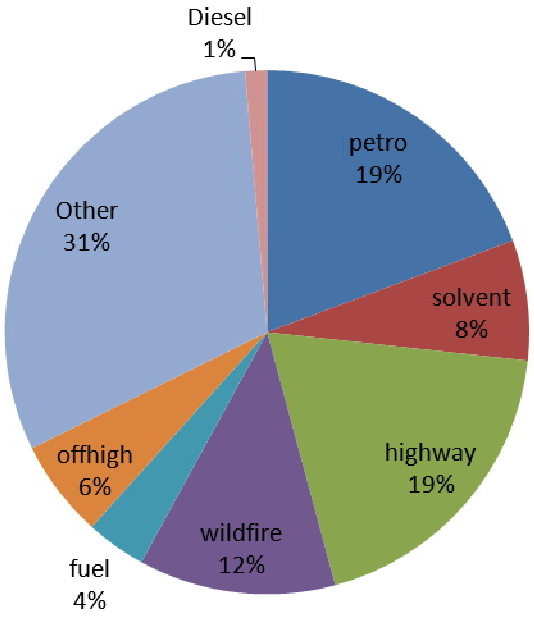

Figure 3.2 Anthropogenic source contributions to daily VOC emissions on August 31, 2000.

Figure 3.2 shows that while considering only anthropogenic sources of VOCs, approximately 19% is from highway gasoline and petroleum processes each. Solvent utilization and off-highway gasoline make up 8% and 6% respectively of anthropogenic VOCs. Wildfires emit more VOCs (12%) than fuel combustion that accounts for 4% of total VOCs from anthropogenic sources. Diesel vehicles emit the least amounts of VOCs (1%), predominantly ethene and formaldehyde. The low VOC emissions from diesel engines are consistent with literature reported diesel emission characteristics (Watson et al., 1991).

Figure 3.3 shows the regional distribution of VOC emissions processed by SMOKE for the 4km domain. The plot contains daily emission rates of highly reactive VOCs, like ethene, alkenes, alkanes and aromatics for August 31, 2000.

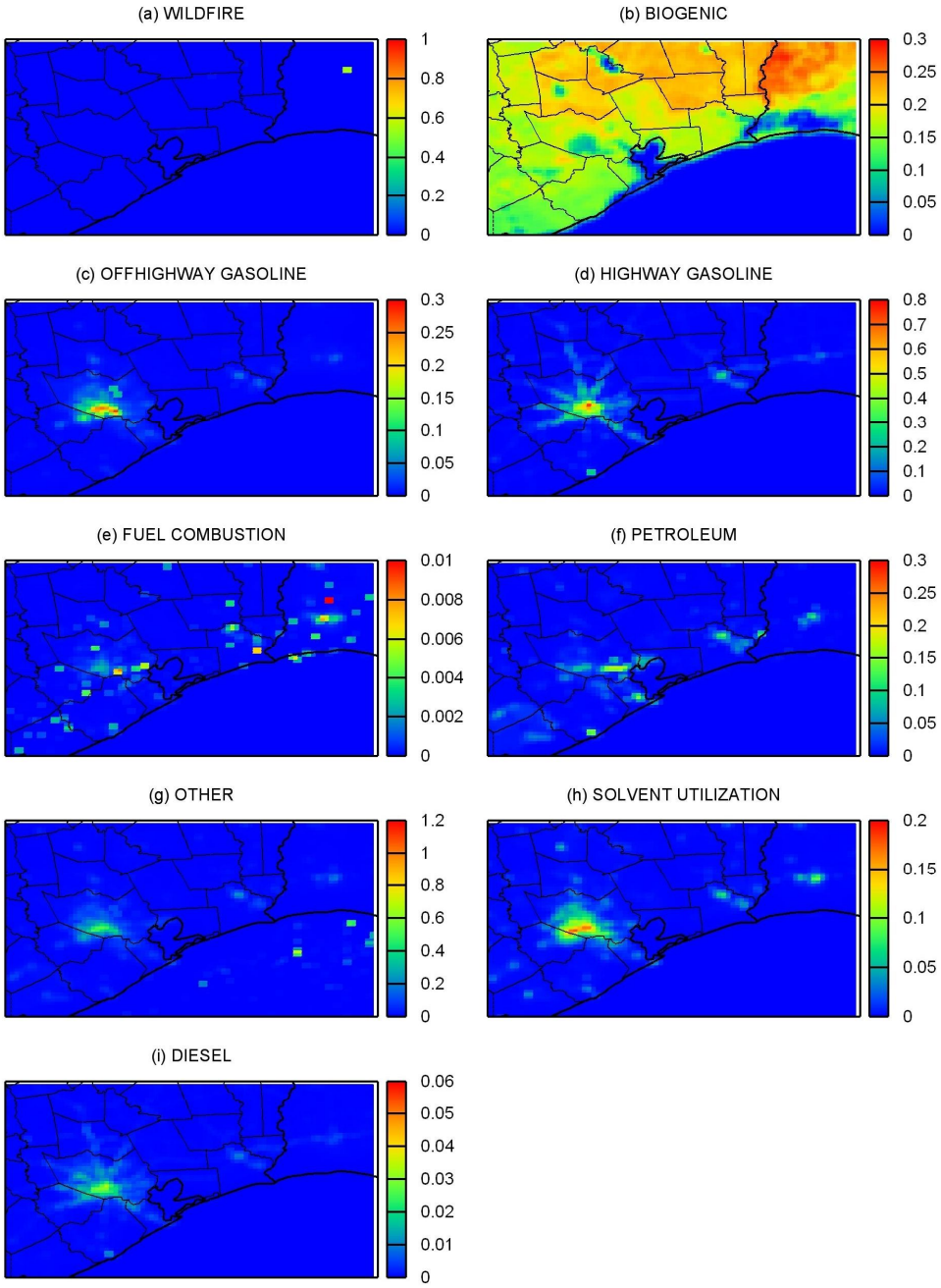

Figure 3.3 Regional distribution of SMOKE processed VOC emissions on a high O_3 day at CST 1200-1300 (August 31, 2000) in the 4km HGB modeling domain. Units are mol sec^{-1} grid $cell^{-1}$. Isoprene emissions are large and are not included in this figure so that the distribution and emission rates of other biogenic emissions can be illustrated.

CHAPTER IV

RESULTS AND DISCUSSION

4.1 Evaluation of base-case results

The CMAQ modeled concentrations are compared to the observed data sets to evaluate the model performance as well as the accuracy of the emissions input into the model. This process was done for the 36 km and 4km grid size domain. For the 36 km domain covering the eastern U.S, two stations for each State were chosen from the EPA's Aerometric Information Retrieval System (AIRS) database (U.S.EPA, 2009), one representing a rural site and the other representing an urban site. Table 4.1 lists the stations that are used to validate the 36 km model results. The AIRS code, the name of the stations and their latitude/longitude are included in the Table. For the finest domain, all sites available in the AIRS database were chosen for a detailed statistical model performance analysis. The AIRS sites in the 4km domain for detailed model performance analysis are plotted as shown in Figure 4.1.

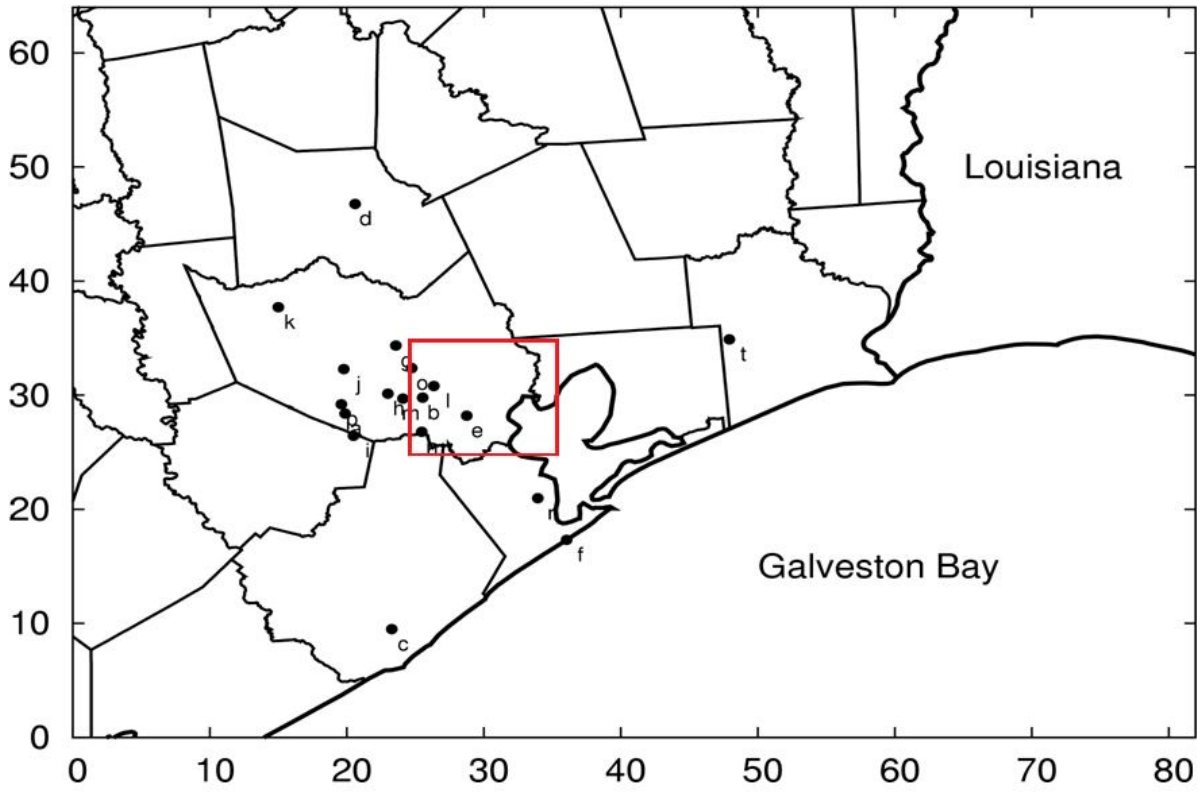

Figure 4.1 The 4 km grid resolution model domain and the locations of AIRS stations used in the model performance evaluation.

Table 4.1 Description of the AIRS sites in the HBG area

Site Name	Site Code	Longitude	Latitude	Site Type
BAYP(a)	482010055	-95.499	29.696	Residential Urban
C35C(b)	482011035	-95.258	29.734	Industrial Suburban
CLTA(c)	480391003	-95.398	29.011	Commercial Suburban
CONR(d)	483390089	-95.422	30.354	Commercial Urban
DRPK(e)	482011039	-95.129	29.670	Residential Suburban
GALC(f)	481670014	-94.857	29.263	Commercial Urban
HALC(g)	482010024	-95.326	29.901	Residential Suburban
HCFA(h)	482011037	-95.361	29.751	Commercial Urban
HCQA(i)	482010051	-95.474	29.624	Residential Suburban

Table 4.1 Continued

Site Name	Site Code	Longitude	Latitude	Site Type
HLAA(j)	482010047	-95.489	29.835	Residential Suburban
HNWA(k)	482010029	-95.675	30.039	Residential Urban
HOEA(l)	482011034	-95.221	29.768	Commercial Urban
HROC(m)	482010070	-95.316	29.735	Residential Suburban
HSMA(n)	482010062	-95.2675	29.6258	Residential Suburban
HWAA(o)	482010046	-95.284	29.827	Residential Suburban
SHWH(p)	482010066	-95.504	29.725	Industrial Urban
TLMC(q)	481671002	-94.933	29.399	Residential Suburban
JEFC(t)	482450022	-94.318	29.864	Residential Suburban

The performance analysis was done for gaseous species of O_3, CO, and NO_x as well as particulate matter (PM) species, including elemental carbon (EC), organic carbon (OC), sulfate and PM2.5 (particulate matter with aerodynamic diameter less than 2.5 μm).

4.1.1 Gas phase pollutants (O_3, NO_x, CO)

Figure 4.2 shows the CMAQ model simulation of O_3 in the 36km modeling domain covering eastern U.S. A detailed description of the AIRS stations used in this analysis is included in Table 4.2. This table lists the locations in the time-series analysis for 1-hour O_3 of the 36 km domain. The model does a good job of predicting the peak O_3 concentrations in the ten different sites under analysis. In Georgia (Cobb), for example, the high O_3 days from August 23 to August 31, 2000 are all predicted well by the CMAQ model. However, the decreased O_3 concentrations during the nighttime are not as accurately predicted. The slight over-prediction at night is due to a slightly large minimum vertical diffusivity (k_{zz}=0.5) used in the study. However, this minimum k_{zz} is necessary to improve O_3 performance during the day. The good model performance during

the day gives confidence that the boundary conditions provided by the 36 km resolution simulation are reasonable. Although no 12 km results are shown here, it is expected that the 12 km simulation also performs well.

Table 4.2 Description of the AIRS sites in the 36 km domain

Site Name	Site Code	Longitude	Latitude	Site Type
New Jersey (Morris)	340273001	-74.676	40.788	Agricultural Rural
Georgia (Cobb)	130670003	-84.607	34.015	Commercial Suburban
Florida (Pinellas)	121030004	-82.732	27.946	Commercial Suburban
South Carolina (Richland)	450790007	-80.962	34.094	Commercial Suburban
Arkansas (Pulasky)	051191002	-92.260	34.836	Forest Rural
Missouri (Greene)	290770026	-93.263	37.123	Residential Suburban
Oklahoma (Love)	400850300	-97.276	33.881	Agricultural Rural
Kansas (Sedgewick)	201730010	-97.314	37.701	Residential Urban
Louisiana (East Baton Rouge)	220330003	-91.183	30.419	Residential Urban
Tennessee (Montgomery)	471251010	-87.169	36.625	Agricultural Rural

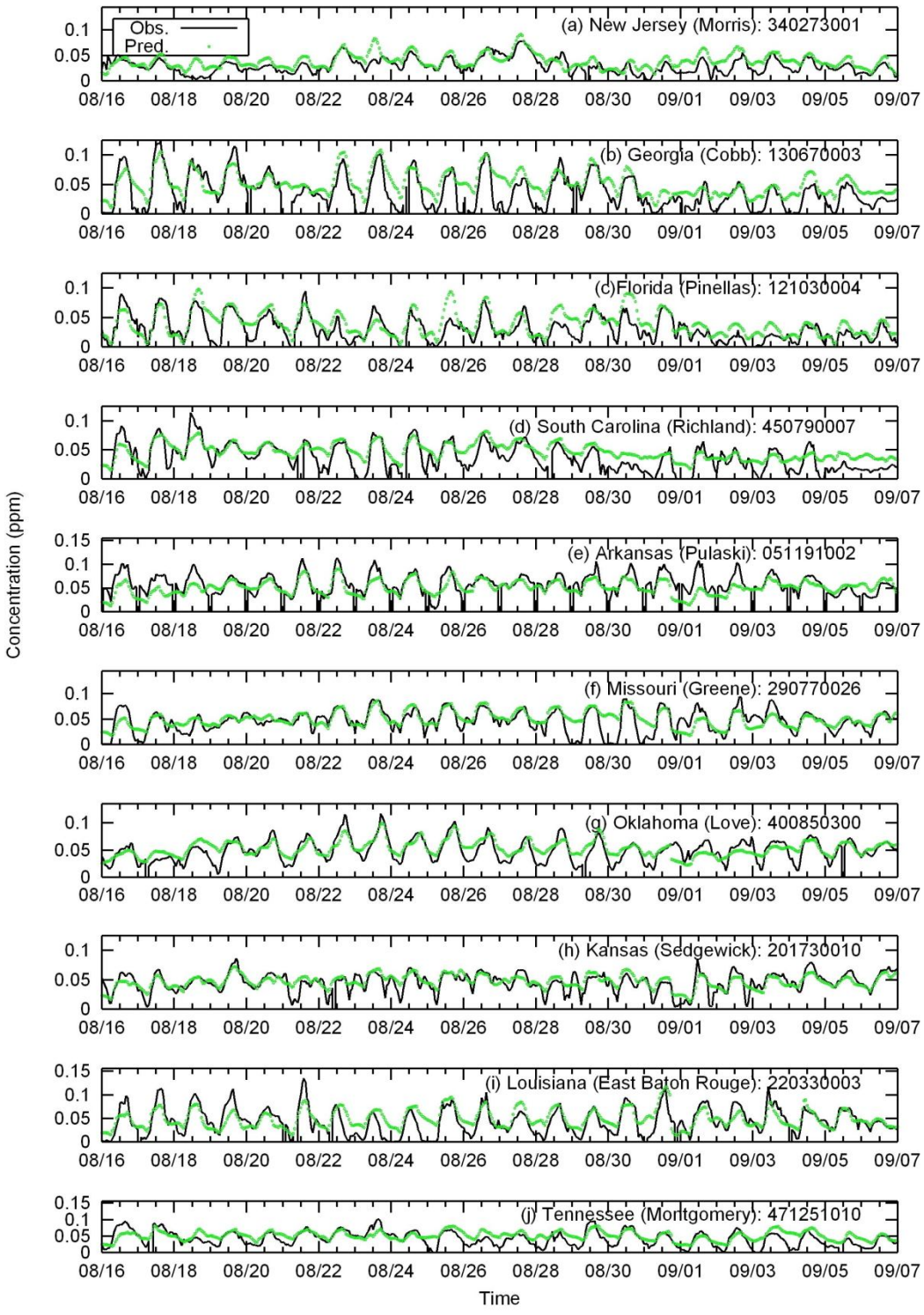

Figure 4.2 Time series of observed and predicted 1-hour O_3 concentrations based on the 36 km results from August 16, 2000 to September 7, 2000.

Figure 4.3 shows the model simulated versus observed 1-hour ozone in all the AIRS sites within the 4 km modeling domain between August 16, 2000 and September 7, 2000. It is evident from these figures that peak O_3 days were experienced at most stations on August 21, 22, 25,26, 30, 31, 2000 and at several stations on September 2, 3, 4 and 5, 2000. The predicted peak concentrations are generally under-predicted on these high ozone days. Most of the under-predictions are due to an under-prediction of the emissions from industrial sources in the Houston Ship Channel areas (Jiang and Fast, 2004; Vizuete et al., 2008). On some other days, the under-predicted is thought due to imperfect meteorology fields predicted by the MM5 model, especially the wind direction under low wind conditions. No efforts have been made in this study to correct the under-prediction of the emissions. Of the these high O_3 concentration days, modeled values accurately reflects peak observed values on September 2, 2000, and for this reason this day is used to carry out further analysis related to high ozone days. Of the remaining moderate and low O_3days, model performance is good.

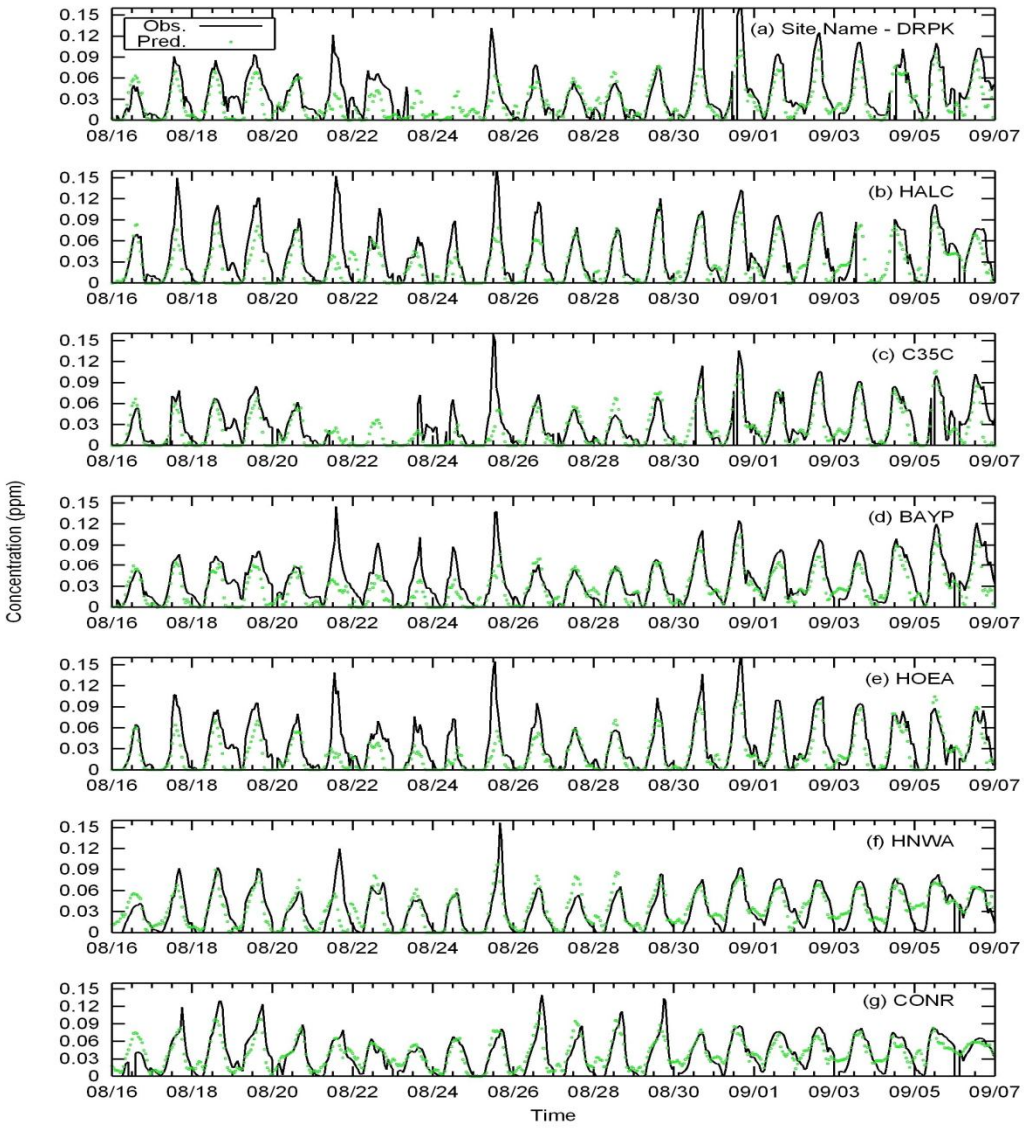

Figure 4.3 Time series of observed and predicted 1-hour O_3 concentrations in the 4 km domain from August 16, 2000 to September 7, 2000.

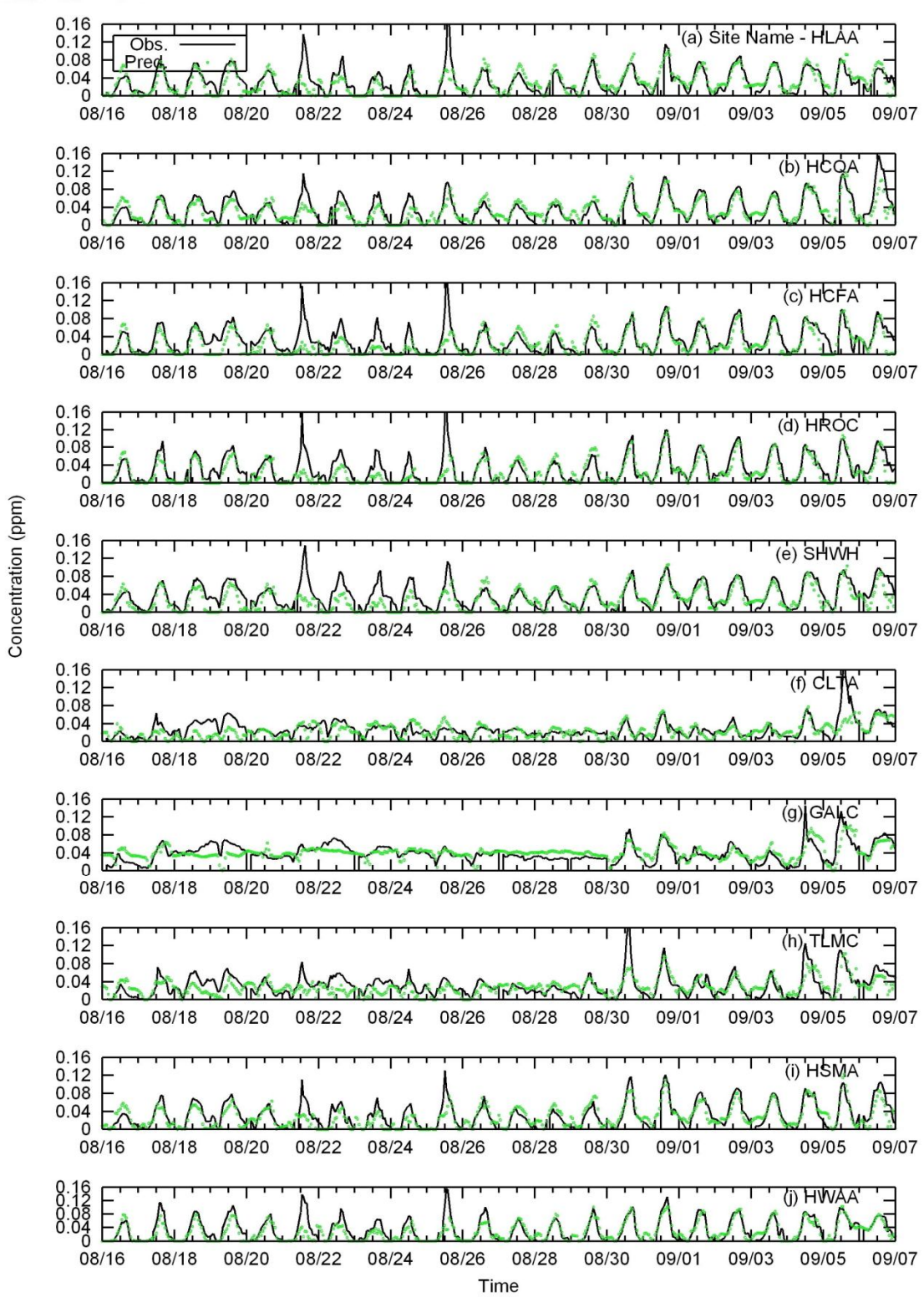

Figure 4.3: (cont.)

The model performance of CO simulation in the 4km domain is fairly decent, as seen in Figure 4.4. The observed concentrations are generally on the order of 0.5 at all stations, which are correctly predicted by the model simulation. The peak values usually occur in the early morning traffic times and are mostly well-predicted. The day-to-day variations are also accurately predicted by the model. For example, in HCFA and HLAA sites, CO concentrations are higher during the days in August than the days in September. This variation is correctly captured by the model, though there are over-predictions during the earlier days of the episode. Concentrations at C35C reached 1.5 ppm on August 24-27, 2000 and the simulation did not capture this change. A possible explanation could be that sudden releases from nearby industrial facilities occurred during that period, and were not recorded by the CO emissions inventory. It is also possible that an instrument malfunction occurred on August 24 and went undetected until August 27, 2000.

Figure 4.5 indicates that NO_2 concentrations are slightly over-predicted overall. All sites under analysis, both urban and industrial, experience over-predictions of NO_2. C35C is an industrial site that experiences over-prediction of NO_x. No particular trend appears from the figure, as the model performs well in HCFA and HLAA, and over-predicts in DRPK and BAYP, though all of these are urban sites. It also appears that the model predictions improve during the latter part of the simulation. Figure 4.6 compares model predictions and observations of NO_x in the same sites as for NO_2. The model performance for NO_x is better than that for NO. The predictions agree with observations very well from August 25, 2000, although the concentrations are still generally over-predicted during August 16-24, 2000 at most stations. This suggests that NO_x emissions are likely over-estimated before August 24, 2000. However, it is difficult to explain why the emissions of NO_x should differ significantly. This seems to suggest that meteorology model performance is not as good in those days and leads to over-prediction of the NO_x concentrations.

A closer look at the meteorology model performance should be able to determine this. However, this is out of the scope of the current study.

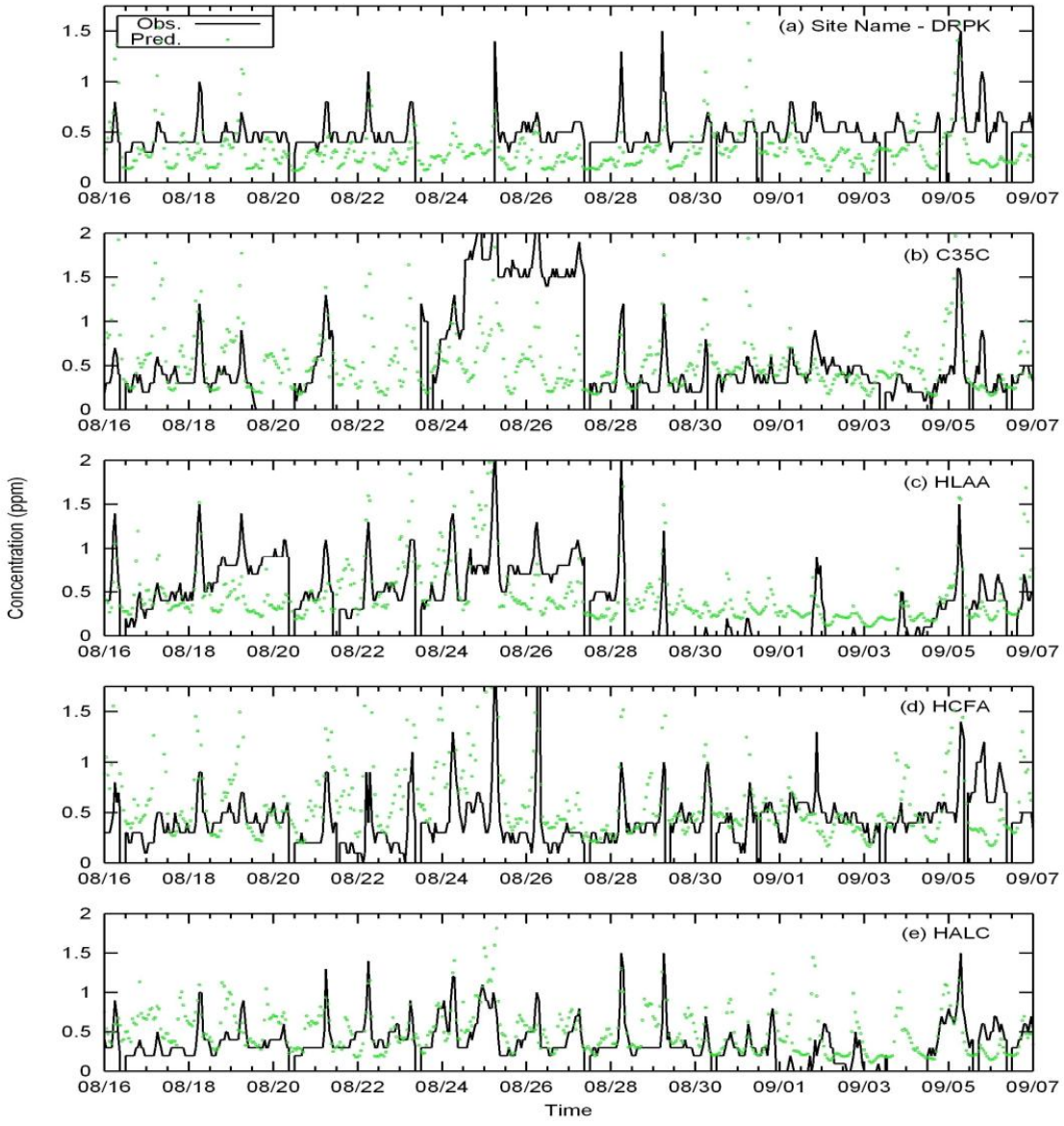

Figure 4.4 Time series of observed and predicted hourly CO concentrations in the 4 km domain from August 16, 2000 to September 7, 2000.

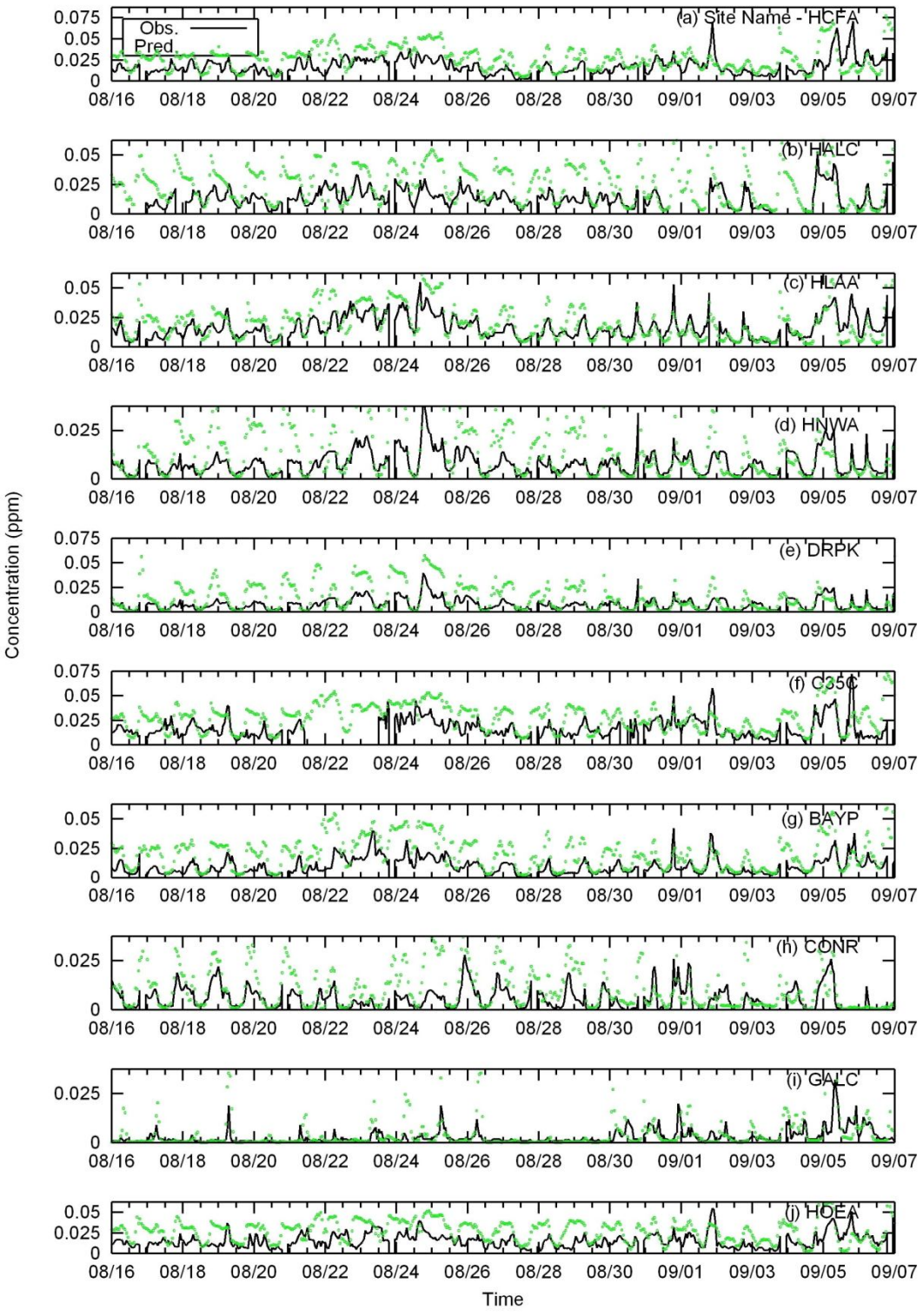

Figure 4.5 Time series of observed and predicted 1-hour NO_2 concentrations in the 4 km domain from August 16 – September 7, 2000.

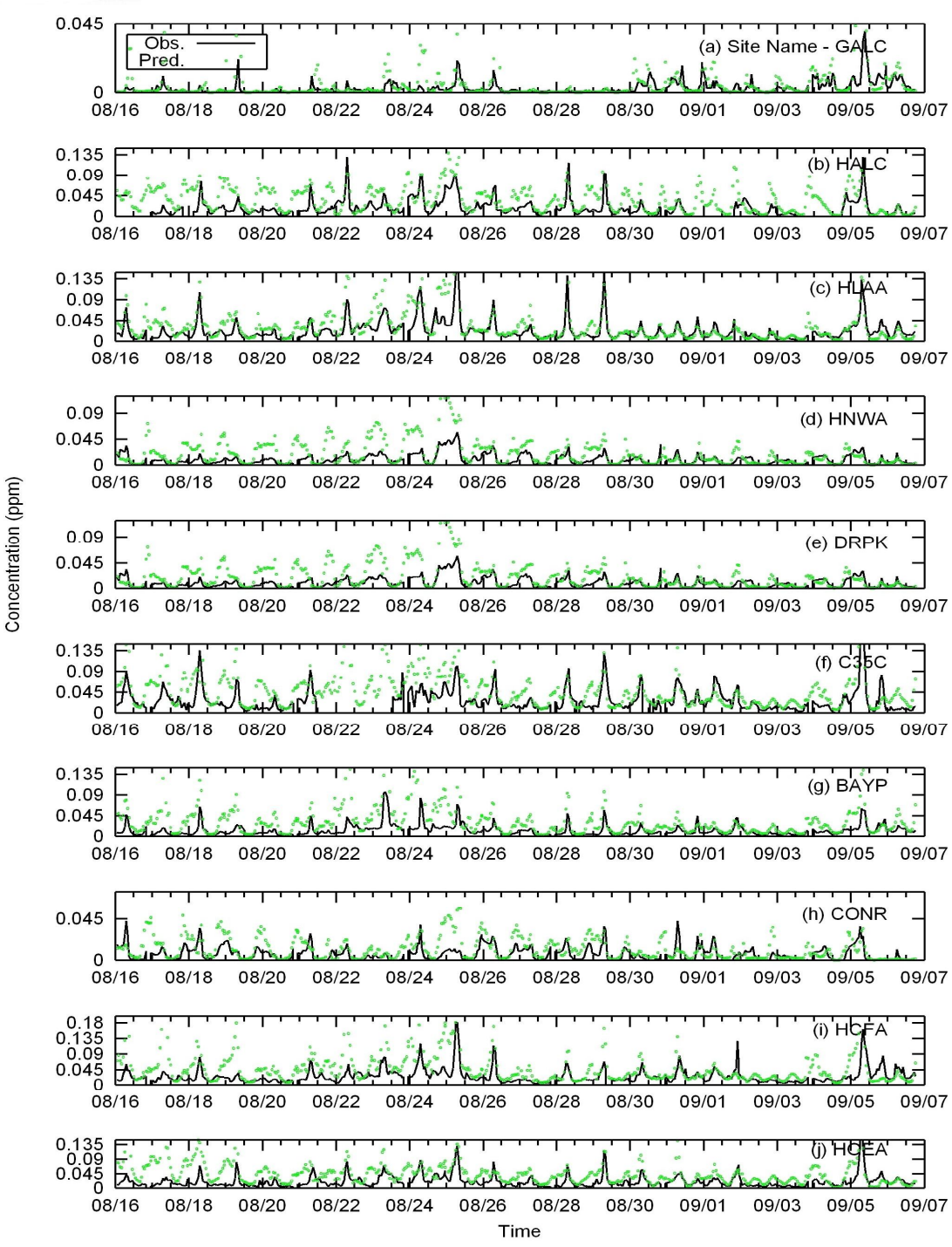

Figure 4.6 Time series of observed and predicted 1-hour NO_x concentrations in the 4 km domain from August 16 – September 7, 2000.

4.1.2 Particulate matter (EC, OC, Sulfate and PM2.5)

Although PM results are not directly used in the O_3 source apportionment calculations, it is still useful to compare the predicted concentrations against observation. A good agreement between observations and predictions will provide more confidence in the emission and meteorology input data and thus the overall source apportionment results. Unlike gas phase observations, which are typically reported at 1-hour resolution, the PM measurements are typically reported as daily averaged values.

Figure 4.7 shows the simulated vs. observed total PM2.5 sulfate in the 36km model domain over the 22 day study episode at a few stations. The observations were only available every 3 days so there are only a few data points available for comparison. Generally speaking, model performance is fairly good at all stations. The observed concentrations are generally within 5-15 $\mu g\ m^{-3}$ and the predicted concentrations are also within this range. The day-to-day variation of the PM2.5 sulfate is also captured by the simulation. In Illinois (Cook), for example, a decent estimate of sulfate is made, with a slight over-prediction on August 28, 2000 and a subsequent under-prediction on August 31, 2000. Since most of the sulfur is secondary in nature, this suggests that the emissions of SO_2 and the subsequent photochemistry that converts SO_2 to sulfate are properly captured in the model.

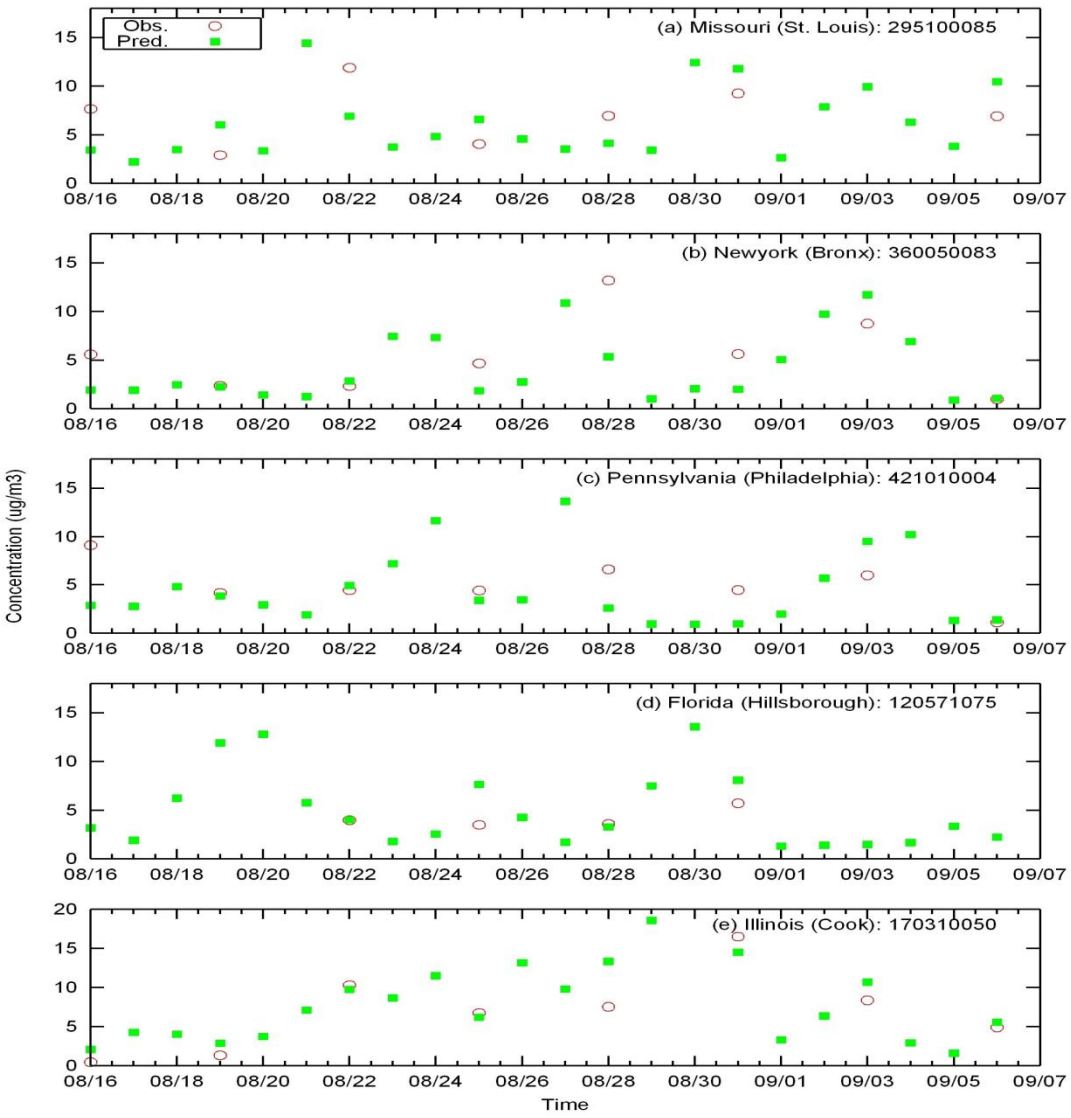

Figure 4.7 Time series of observed and predicted 24-hour averaged PM2.5 sulfate concentrations in the 36 km domain from August 16, 2000 to September 7, 2000. The observations are available every three days.

In the 4km model domain, model performance was studied for EC, OC and sulfate and PM2.5. Figure 4.8 indicates that the model properly predicted the EC concentrations at GALC and JEFC, where the overall concentration is low. The model slightly over-predicts the EC concentrations at urban and industrial sites such as HALC and DRPK. The over-predictions suggest that the diesel

emissions might be over-estimated because EC is mostly emitted from diesel vehicles. It is also possible that EC fractions in the diesel and gasoline vehicle profiles used to speciate PM2.5 to EC during the emission processing are over-estimated. This seems to be more likely because the CO concentrations are well predicted at all stations. Inaccuracy in the meteorology is not likely the cause of this over-prediction as the over-predictions persist during the latter modeling days. The day-to-day variations of EC are properly captured. For example, both observation and prediction show an increase in the EC concentrations in early September.

Figure 4.9 shows that model performance for OC is good, especially at urban and industrial impacted locations such as DRPK and HALC, where primary emitted OC dominate the measured OC concentrations. OC in sites like GALC and JEFC are however, under-predicted by the model. This under-prediction is likely due to an underestimation of secondary organic aerosol formation at downwind locations.

Time series of PM2.5 mass in the 4km domain are plotted in Figure 4.10. It can be seen that the predictions agree well with observations. The time series analysis for model performance for sulfate concentrations in the 4km domain is shown in Figure 4.11. It can be seen that sulfate concentrations are well predicted by the model on all the sites. The temporal variations are also fairly well captured, during days of high and low concentrations. The model properly predicted the significant increase in PM2.5 mass and PM2.5 sulfate concentrations on September. However, in all the locations of analysis, the model makes under-predictions only on days from August 17- August 23, 2000. The timing of this over-estimation agrees very well to that of NO_x, which further suggests possible problem in the meteorology inputs during that period.

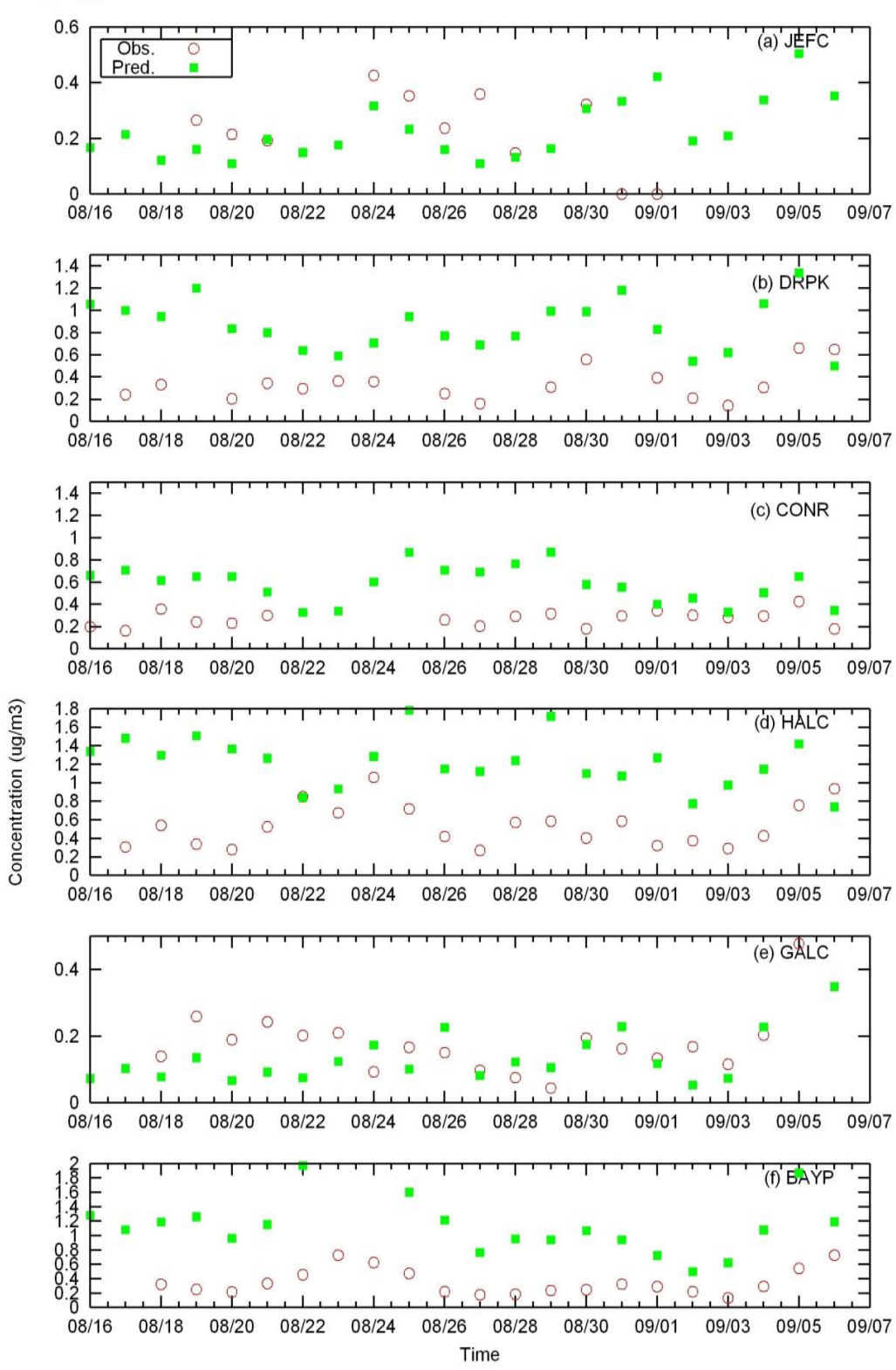

Figure 4.8 Time series of observed and predicted 24-hour averaged elemental carbon (EC) concentrations in the 4 km domain from August 16, 2000 to September 6, 2000.

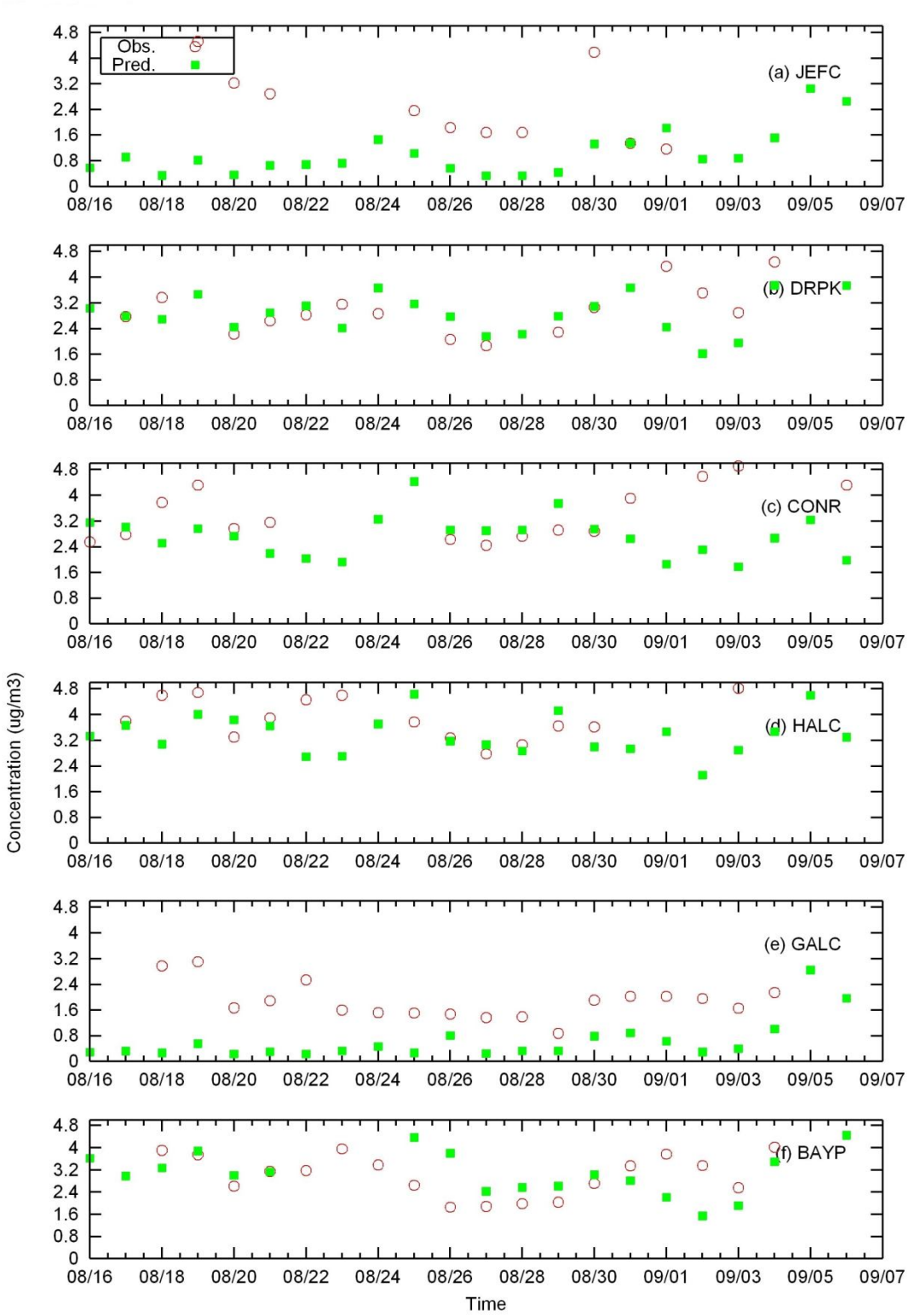

Figure 4.9 Time series of observed and predicted 24-hour averaged OC concentrations in the 4 km domain from August 16 – September 7, 2000.

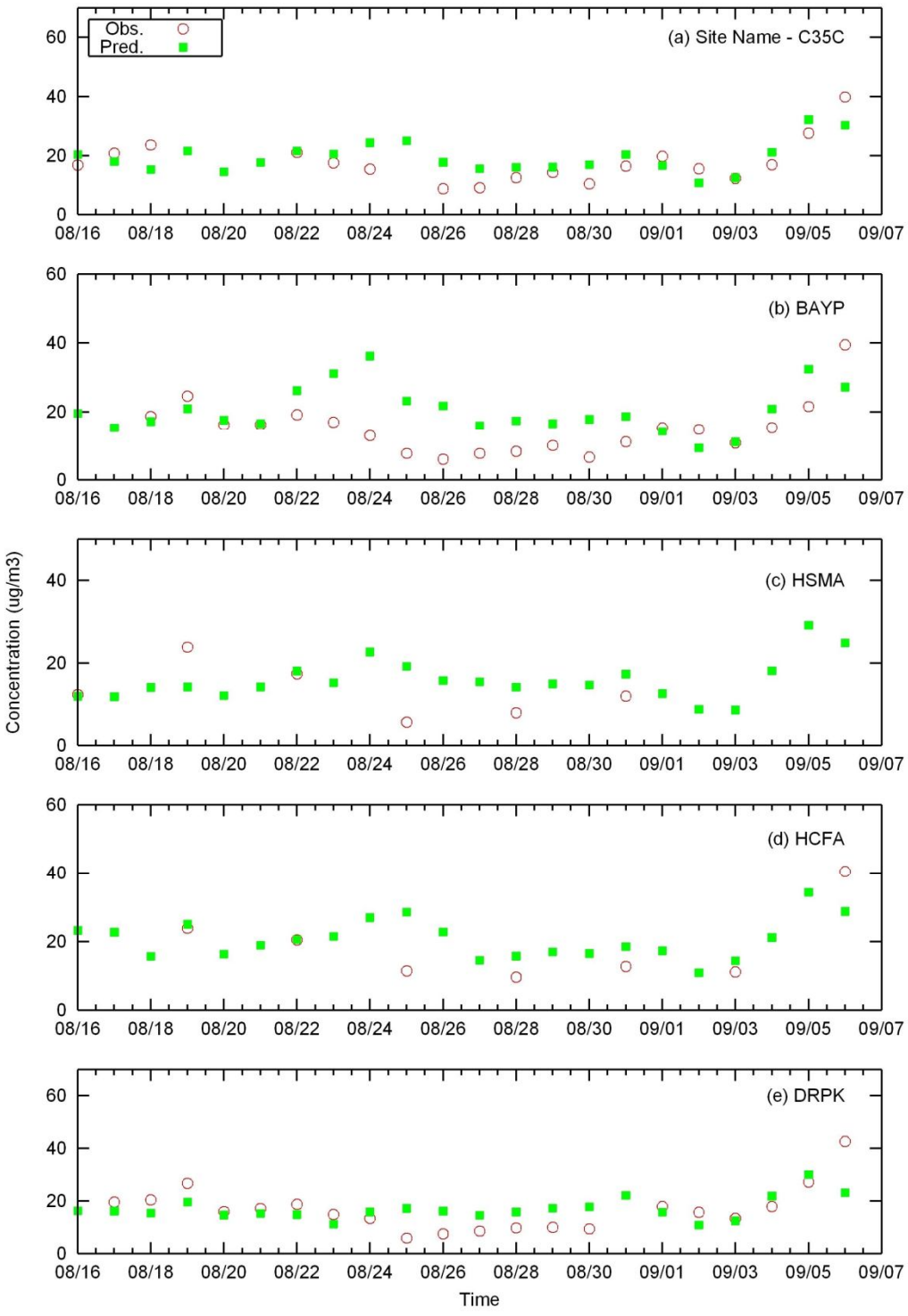

Figure 4.10 Time series of observed and predicted 24-hour averaged PM2.5 concentrations in the 4 km domain from August 16 – September 7, 2000.

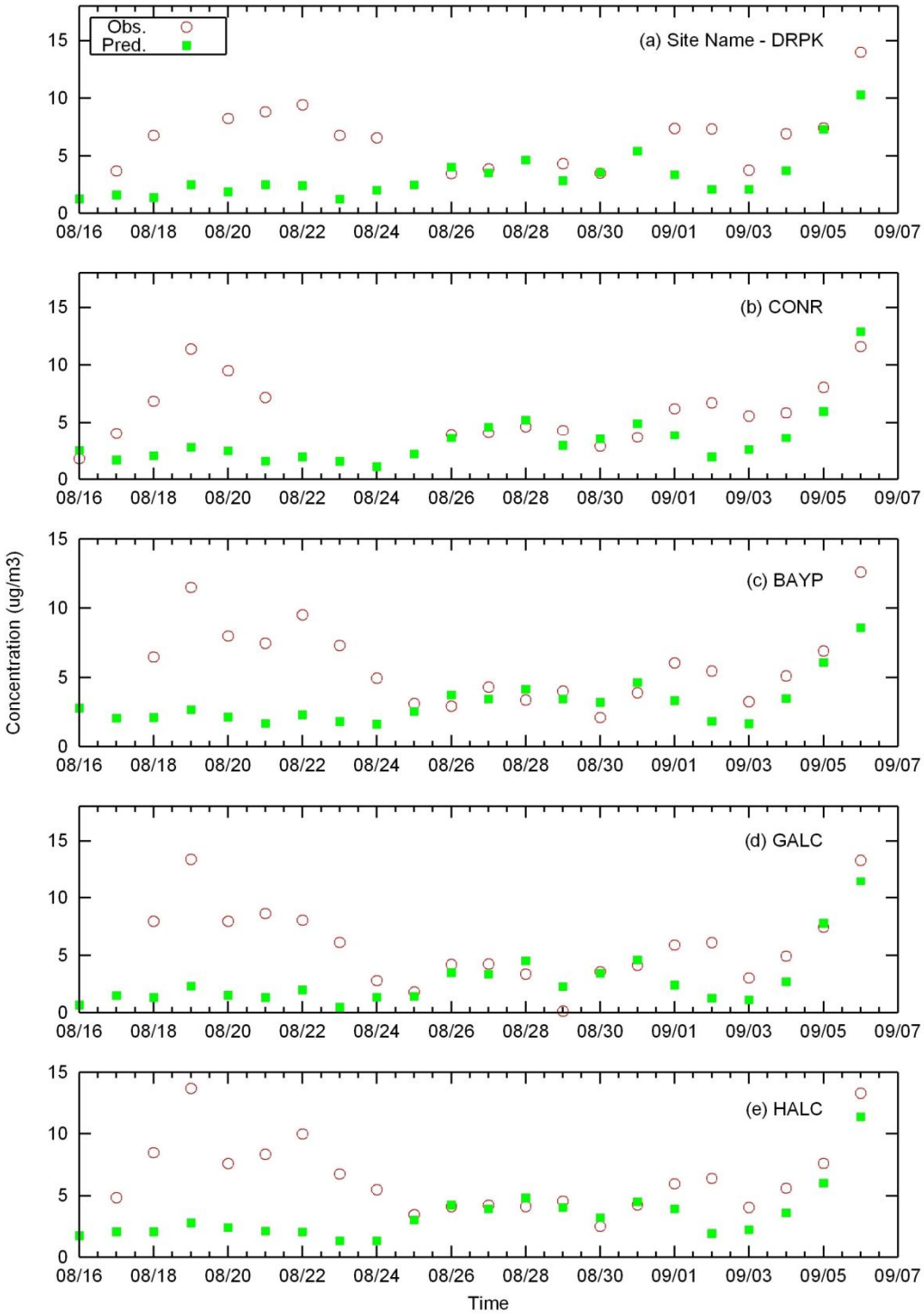

Figure 4.11 Time series of observed and predicted 24-hour averaged PM2.5 Sulfate concentrations in the 4 km HGB domain from August 16 – September 7, 2000.

4.1.3. Statistical model performance analysis

In order to evaluate the simulation of O_3 and PM2.5 air quality in the MM5-CMAQ system, several quantitative statistical performance measures were used collectively in the assessment. The statistical parameters were calculated using all the available data in the HGB and BPA areas between August 16 and September 6, 2000. O_3 performance statistical parameters used in this analysis are mean fractional bias (MFB), mean fractional error (MFE), mean normalized bias (MNB), accuracy of pair peak (APP), accuracy of unpaired peak (AUP), absolute accuracy of paired peak (AAPP) and absolute accuracy of unpaired peak (AAUP). These parameters are defined by Table 4.3.

Table 4.3 Definitions of statistical performance indicators (Ying et al., 2007)

Statistical Parameter	**Equation**
Mean Fractional Error	$\mathrm{MFE} = \frac{2}{N}\sum_{i=1}^{N}\frac{\lvert (C_{p,i} - C_{o,i})\rvert}{C_{p,i} + C_{o,i}}$
Mean Fractional Bias	$\mathrm{MFB} = \frac{2}{N}\sum_{i=1}^{N}\frac{(C_{p,i} - C_{o,i})}{(C_{p,i} + C_{o,i})}$
Mean Normalized Bias	$\mathrm{MNB} = \frac{1}{N}\sum_{i=1}^{N}\frac{C_{p,i} - C_{o,i}}{C_{o,i}}$
Mean Normalized Error	$\mathrm{MNE} = \frac{1}{N}\sum_{i=1}^{N}\frac{\lvert C_{p,i} - C_{o,i}\rvert}{C_{o,i}}$
Accuracy of Pair Peak	$\mathrm{APP} = \frac{C_{p,o\_peak} - C_{o,o\_peak}}{C_{o,o\_peak}}$

Table 4.3 Continued

Statistical Parameter	Equation
Accuracy of Unpaired Peak	$AUP = \frac{C_{p,p\_peak} - C_{o,o\_peak}}{C_{o,p\_peak}}$
Absolute Accuracy of Paired Peak	$AAPP = \left\| \frac{C_{p,o\_peak} - C_{o,o\_peak}}{C_{o,o\_peak}} \right\|$
Absolute Accuracy of Unpaired Peak	$AAUP = \left\| \frac{C_{p,p\_peak} - C_{o,o\_peak}}{C_{o,p\_peak}} \right\|$

In the above equations, N is number of data points. C_p and C_o represent the predicted and observed concentrations, respectively. Subscripts o_peak and p_peak indicate the hours when the observed and predicted concentrations are in their peak values, respectively.

4.1.3.1 Statistical analysis of model ozone performance

For O_3 performance, an observation-based minimum threshold concentration of 60 ppb was set and only those values above it were considered in the statistical analysis. Data points with missing observation data were also excluded from the analysis. EPA recommends using these metric in conjunction with an observation-based minimum threshold for the reason that excluding lower O_3 concentrations is reasonable as the NAAQS deals with only peak O_3 concentrations (EPA, 1991).

The MNB metric considers the observation to be the absolute truth. It also is unfairly biased, as over-predictions are weighted more than under-predictions. On the other hand, the MFB

performance metric is symmetrical and bounded. Same weight is given for over-prediction and under-predictions. This metric is used while studying PM performance as they are many species of PM that are present in very low concentrations, which makes it difficult to introduce an observation-based threshold without washing out most of the data points. MFB and MFE normalize the difference between the modeled and observed concentrations and do not let a few data points dominate the metric. The values are dimensionless and can be applied to any performance study irrespective of their units of measurement (Boylan and Russell, 2006).

Table 4.4 1-hour O_3 performance statistics in the 4 km HGB domain using data between August 16, 2000 and September 6, 2000

SNo.	Site	MFB	MFE	MNB	MNE	APP	AUP	AAUP	AAPP	Points
1	HLAA	-0.19	0.26	-0.13	0.20	-0.14	-0.24	0.37	0.24	86
2	HCQA	-0.29	0.31	-0.22	0.25	-0.24	-0.27	0.29	0.26	103
3	HCFA	-0.33	0.35	-0.23	0.26	-0.28	-0.34	0.38	0.31	92
4	HROC	-0.37	0.38	-0.28	0.29	-0.31	-1.03	1.04	0.32	131
5	SHWH	-0.39	0.41	-0.28	0.30	-0.28	-0.31	0.33	0.29	116
6	CLTA	-0.42	0.43	-0.30	0.32	-0.30	-0.48	0.49	0.31	30
7	GALC	-0.29	0.35	-0.22	0.29	-0.30	-0.32	0.32	0.30	79
8	TLMC	-0.41	0.43	-0.30	0.33	-0.39	-0.42	0.42	0.39	54
9	HSMA	-0.24	0.27	-0.19	0.22	-0.23	-0.22	0.25	0.26	87
10	HWAA	-0.28	0.31	-0.20	0.24	-0.24	-0.47	0.51	0.26	122
11	DRPK	-0.41	0.41	-0.31	0.32	-0.35	-0.32	0.32	0.35	108
12	HALC	-0.37	0.38	-0.28	0.29	-0.31	-1.03	1.04	0.32	131
13	C35C	-0.31	0.34	-0.23	0.25	-0.28	-0.37	0.39	0.29	85
14	BAYP	-0.38	0.39	-0.29	0.30	-0.32	-0.32	0.34	0.34	121
15	HOEA	-0.39	0.41	-0.29	0.31	-0.35	-0.49	0.51	0.37	115
16	HNWA	-0.20	0.24	-0.15	0.19	-0.21	-0.11	0.20	0.23	105
17	CONR	-0.18	0.23	-0.14	0.20	-0.22	-0.15	0.16	0.23	149

Table 4.5 1-hour O_3 performance statistics in the 4 km HGB domain using data between August 25, 2000 and September 6, 2000

Site	MFB	MFE	MNB	MNE	APP	AUP	AAUP	AAPP	Points
HLAA	-0.07	0.17	0.05	0.15	-0.17	-0.15	0.20	0.22	59
HCQA	-0.21	0.25	0.16	0.20	-0.14	-0.10	0.14	0.17	68
HCFA	-0.20	0.24	0.15	0.19	-0.04	-0.08	0.28	0.19	62
HROC	-0.25	0.26	0.21	0.21	-0.14	-0.15	0.20	0.18	81
SHWH	-0.25	0.28	0.19	0.22	-0.23	-0.17	0.17	0.23	75
CLTA	-0.36	0.38	0.26	0.28	-0.17	-0.10	0.13	0.18	26
GALC	-0.14	0.24	0.10	0.22	-0.19	-0.39	0.40	0.20	46
TLMC	-0.32	0.35	0.24	0.28	-0.25	-0.26	0.26	0.25	41
HSMA	-0.18	0.22	0.14	0.19	-0.30	-0.25	0.25	0.30	66
HWAA	-0.15	0.20	0.12	0.17	-0.14	-0.11	0.14	0.17	81
DRPK	-0.38	0.39	0.30	0.31	-0.31	-0.30	0.30	0.31	72
HALC	-0.25	0.26	0.21	0.21	-0.23	-0.17	0.17	0.23	81
C35C	-0.28	0.31	0.21	0.24	-0.20	-0.22	0.25	0.22	65
BAYP	-0.30	0.31	0.24	0.25	-0.22	-0.19	0.23	0.24	80
HOEA	-0.28	0.31	0.22	0.25	-0.28	-0.23	0.27	0.31	76
HNWA	-0.11	0.16	0.09	0.14	-0.14	-0.06	0.16	0.16	73
CONR	-0.16	0.23	0.13	0.20	-0.17	-0.11	0.14	0.17	102

The performance goal for a model was set to the level of accuracy that is considered to be close to the best a model can be expected to achieve. The performance criteria for a model was set to the level of accuracy considered acceptable for regulatory applications (Boylan and Russell, 2006). Table 4.4 and Table 4.5 show the calculated O_3 performance statistics using the predicted and observed 1-hour O_3 concentrations from August 16 to September 6, 2000 and from August 25 to September 6, 2000, respectively. The additional ozone performance statistics shown in Table 4.5 better represents the performance of the model by ignoring the days with poor

meteorology. The model did a good job of predicting O_3 in the HGB modeling domain through the entire study episode lasting 22 days. Of the 17 stations analyzed, all stations had a mean normalized O_3 bias of less than 0.30, and the lowest value of all the stations was found as -0.31 (-0.30). There is an overall under-prediction of O_3 concentrations at all the monitoring sites and that is reflected by the negative normalized bias for all the stations. The AAUP and AAPP values indicate an under-prediction of peak 1-hour O_3 by approximately 30% (23%). The under-prediction of ozone in these sites is attributed to problems in the emissions inventory.

Considerable research has been conducted to identify the uncertainties in the emissions inventory and their effects on the simulation of O_3 in the HGB area. Ryerson et al. (2003) found that, since NO_x emissions are fairly constant with time, and are well-represented by the emissions inventory, it implies that the uncertainties are more likely in the estimation of VOCs. Wert et al. (2003) concluded that large discrepancies between measurements and the emissions database were due to consistent and substantial underestimation of alkene emissions, especially from petrochemical facilities. Byun et al. (2007) carried out a series of sensitivity simulations to test the effect of enhanced HRVOC (Highly Reactive Volatile Organic Compounds) emissions towards ozone formation. The imputed inventory did result in CMAQ predicting more O_3 peaks than with the base-case inventory. It however, failed to capture the ambient O_3 concentrations near the Ship Channel and downwind of the region where HRVOC emissions are high. In another study by Jiang and Fast (2004), when the point source emission rates of propylene and ethylene were enhanced by a factor of 10, the model predicted ozone values were more accurate than before. Other sources of emission variability like episodic releases of large concentrations of HRVOCs from industrial plumes that go undetected by sampling stations can cause significant increase in O_3 levels near and downwind of the plume (Allen et al., 2004).

This underestimation of VOCs from industrial sources in the emissions inventory is likely to underestimate the net O_3 concentrations, particularly in sites near the industrial zone and other areas that are downwind of those industrial facilities. Specific to this study, the contribution of petroleum-related processes towards net ozone formation would expect to be underestimated.

4.1.3.2 Statistical analysis of model PM2.5 performance

Table 4.6 shows the model performance statistics for PM2.5. For PM2.5 mass, the performance goal is set at MFE $\leq$ 50% and MFB $\leq \pm$ 30%. An air quality model is considered to meet the performance criteria if MFE $\leq$ 75% and MFB $\leq \pm$ 60% (Boylan and Russell, 2006). Considering these criteria, PM2.5 performance is also very good, as all 5 stations met the model performance criteria and only 1 of 5 stations did not meet the model performance goals with an MFB of 35%.

Table 4.6 1-hour PM2.5 performance statistics in the 4 km HGB domain using data between August 16, 2000 and September 6, 2000

Site	**MFB**	**MFE**
C35C	0.11	0.27
BAYP	0.35	0.46
HSMA	0.25	0.43
HCFA	0.24	0.33
DRPK	0.08	0.35

The highest MFE in all the stations was 46%, less than the performance goal value of 50%. There is a tendency toward overall over-prediction of PM2.5 in the MM5-CMAQ system used in this research, as can be seen from the positive results of the MFB. Overall, a very good model

performance was observed for PM2.5. Promising model performance builds confidence on the further source-apportionment results to be predicted by the model.

4.2 Relationship between NO to NO_2 conversion rate due to VOCs and O_3 formation

To measure the contribution of each VOC source towards O_3 formation, it is critical to establish a relationship between VOC and O_3 production. The amount of O_3 formed in the photochemical reactions in general determines the observed O_3 concentration in the atmosphere. Net O_3 formation can be attributed to responsible VOC sources based on the contributions of the VOCs and their intermediate oxidation products to the NO to NO_2 conversion process. Figure 4.12 shows the major photochemical cycles of NO_x and HO_x, the oxidation of VOCs and the formation of the peroxy (RO_2) and alkoxy (RO) radicals that lead to net O_3 formation to better illustrate this concept. Each NO_2 formed from the reaction of NO with RO_2 can lead to the net formation of an O_3 molecule. The RO_2 radicals are generated from VOC reactions with oxidants, mostly with the OH radical. In addition, each hydroperoxyl radical (HO_2) formed from the reaction of RO with O_2 can convert another NO to NO_2, which has the potential of forming an additional O_3 molecule. Thus, the rate of net photochemical O_3 formation should be proportional to the rate of NO to NO_2 conversion due to RO_2 and HO_2.

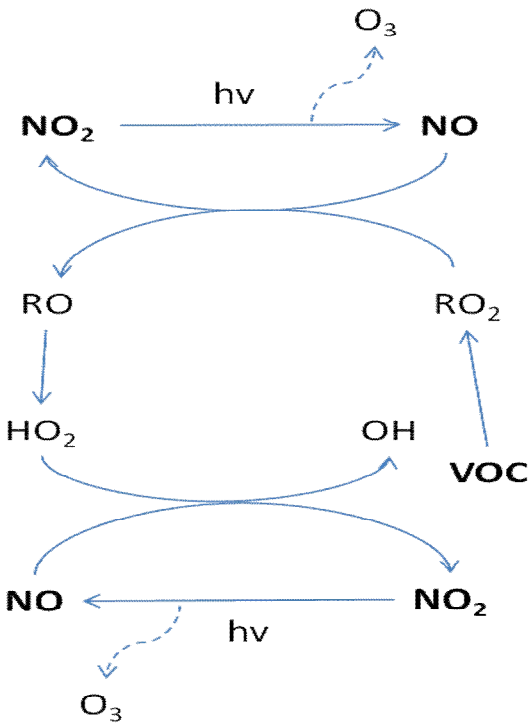

Figure 4.12 Photochemical cycling of NOx and HOx and ozone formation in the polluted atmosphere. Note that the hydroxyl radical source and termination pathways are not illustrated on the figure.

Figure 4.13 shows the NO_2 formation rate due to RO_2/HO_2 radicals versus net O_3 formation rate for each daytime hours of August 17, 2000 in the surface layer. The data points are color coded by the VOC/NO_x ratio.

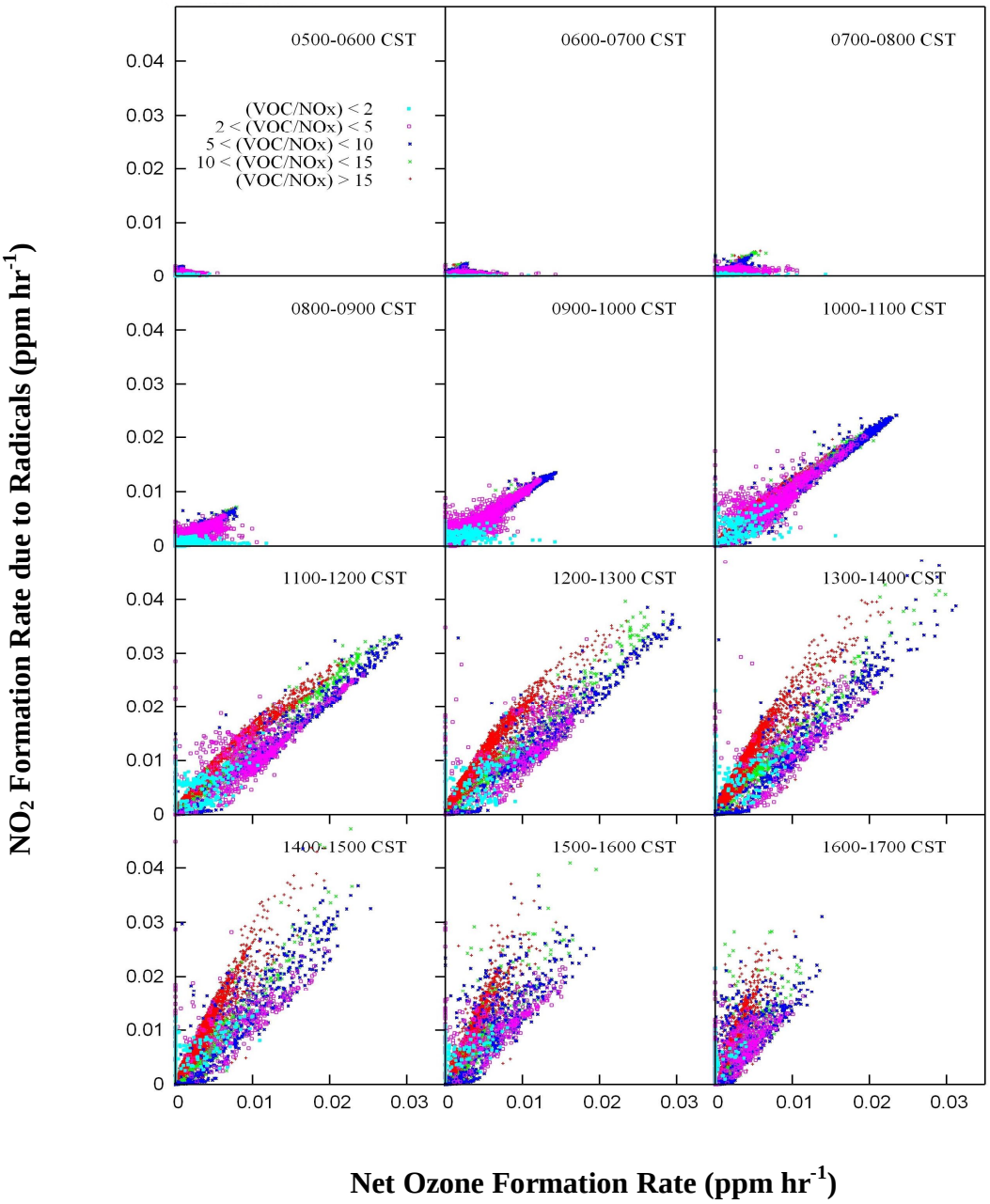

Figure 4.13 Relationship of NO_2 formation rate due to RO_2 radicals and net O_3 formation rate for different VOC/NOx ratios.

Different VOC/NOx ratios appear to have slight different slope in the linear relationship. In addition, the linearity varies for different VOC/NO_x ratios. It is more linear for points with VOC/NO_x ratios greater than 5. It is evident that for VOC/NO_x ratios less than 2, the relationship

between the production rates is more scattered. However, there are very few points in the modeling domain that have VOC/NO_x ratios less than 2 (light blue dots) and the overall ozone formation rates are generally low under this condition, thus these points do not contribute much to the overall ozone formation in the domain and thus do not significantly affect our source apportionment calculations. Majority of the points have VOC/NO_x ratios greater than 5. Best linearity is observed from 1000-1300 CDT (1600-1900 GMT), which corresponds to the hours with highest O_3 formation rates. It is obvious that there is a strong link between the NO_2 produced from radicals generated by the oxidation of VOCs and the net O_3 formation. This result forms the basis to calculate net ozone formation from each source based on the total NO_2 production in that point.

In order to more quantitatively determine which VOC/NO_x ratio leads to the highest ozone formation rates in the domain, average ozone formation rate for each VOC/NO_x ratio bin is calculated. Figure 4.14 shows that the net ozone formation for different VOC/NO_x ratios in the 4km HGB modeling domain. The values were averaged over all the days of the episode and normalized by the number of grid cells in each VOC/NO_x bin. The net O_3 formation rate is lowest for VOC/NO_x ratios lower than 2 in the order of E-10 ppm, and accordingly increases as the ratio increases. It reaches a high at ratios 5-10, before it starts receding again with increasing VOC/NO_x ratio. When the VOC/NO_x ratio in the ambient air is relatively low as in the case of VOC/NO_x less than 2 (NO_x is plentiful relative to VOC), NO_x tends to inhibit O_3 formation. The reason is that NO_2 react with the OH radicals in the troposphere to form HNO_3, reducing the OH radical concentrations and thereby preventing the formation of O_3. For VOC/NO_x ratios higher than 15, the higher concentrations of VOCs react with the OH radical produced by photolysis of

other VOCs, making the VOC-OH formation more pre-dominant than O_3 formation (N., 1998; Phillips, 2001).

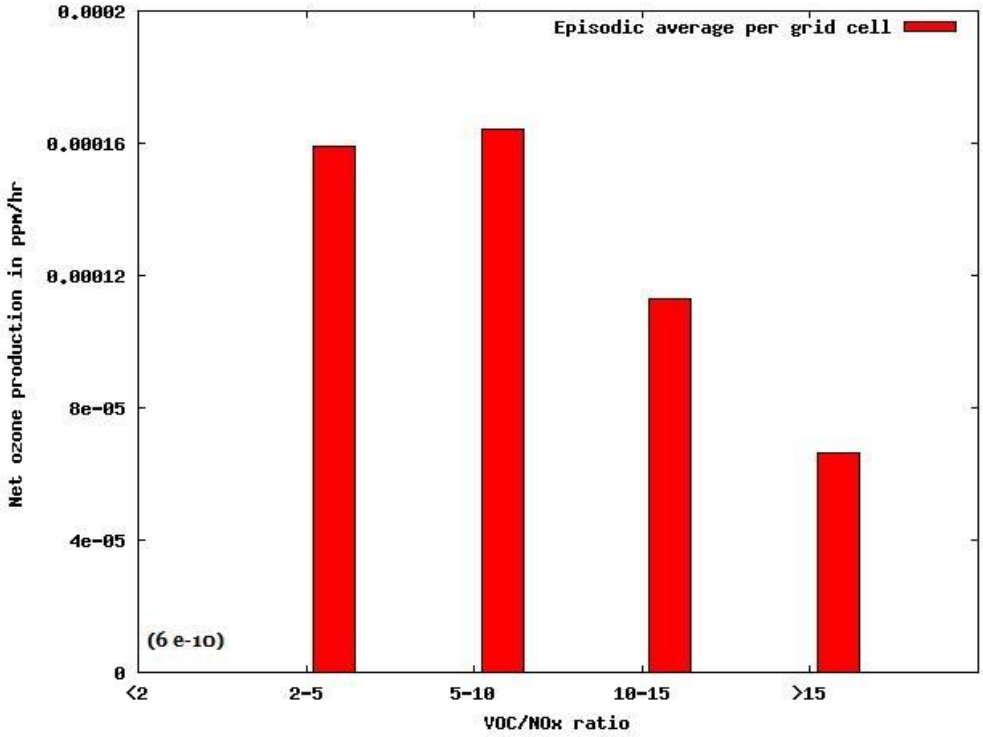

Figure 4.14 Episodic total of net O_3 formation per grid cell for different VOC/NO_x ratios.

4.3 Source apportionment results

4.3.1 Regional source contribution to VOC concentrations

Figure 4.15 shows the regional source contribution of anthropogenic VOC concentrations predicted by the CMAQ model in the surface model layer at 1200-1300 CST averaged over the entire model episode. The VOCs considered are high reactive VOCs like ethene, formaldehyde, alkenes, alkanes and aromatic compounds in order to get a better idea of the spatial distribution of non-biogenic VOCs. Isoprene is not considered in this plot. It is clear from the figure that these VOC species from biogenic sources are widely distributed in the model domain, except in the urban Houston-Galveston-Brazoria area where the vegetation cover faction is low. As mentioned earlier, a few days in the episode witnessed wildfire events on the northeast corner of the domain. On days of intense wildfire activity, the total VOC concentrations due to this wildfire dominate those from the other sources in localized areas, indicating that wildfire could significantly affect ozone in nearby locations.

VOCs from highway gasoline and off-highway gasoline sources are predominantly seen in the urban areas. Petroleum-related processes contribute to VOCs primarily near the Houston Ship Channel, while VOCs from solvent use are prominently found in the urban areas. Diesel vehicles make only small contribution to VOC emissions.

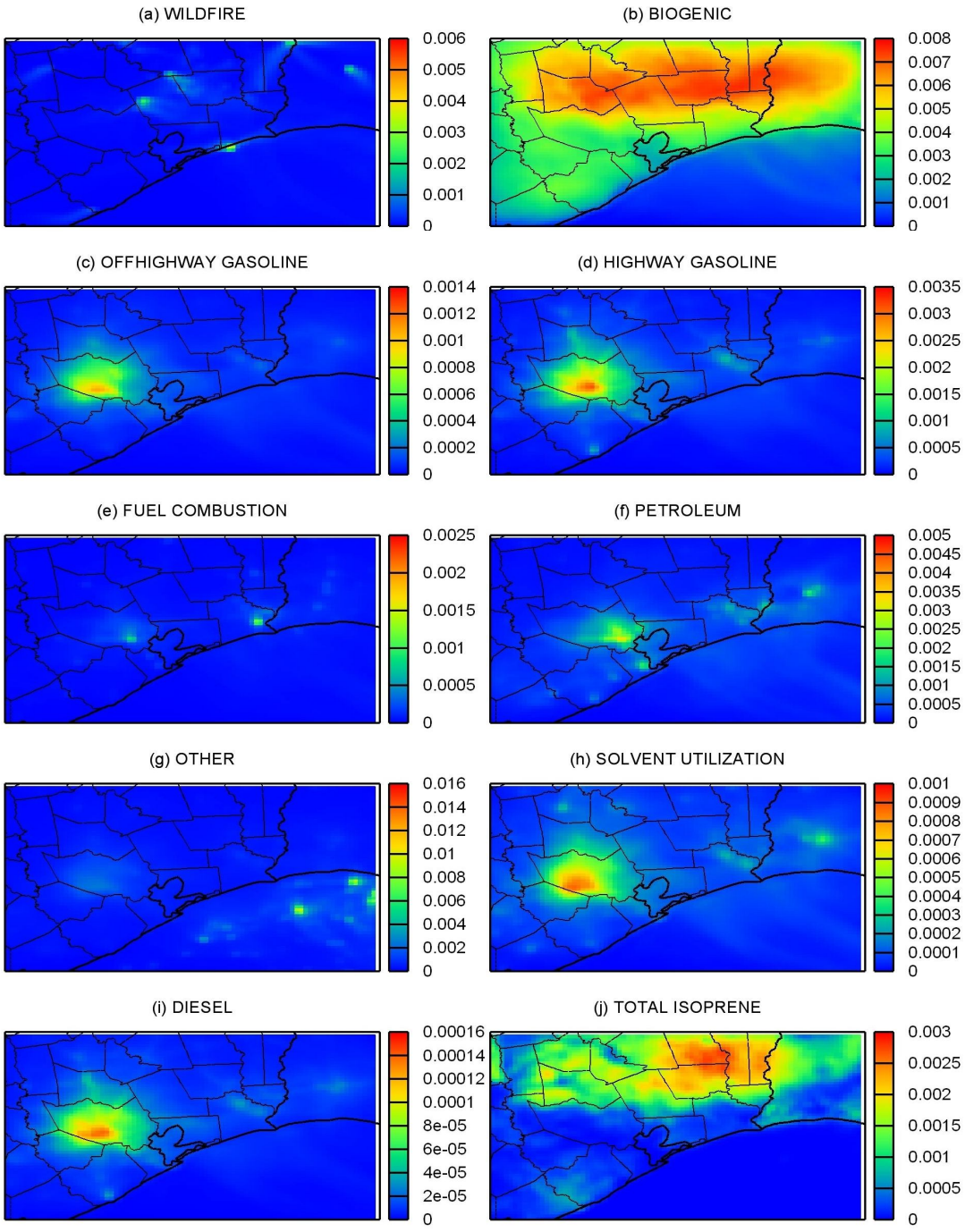

Figure 4.15 Regional distribution of column averaged CMAQ modeled VOC concentrations at CST 1200-1300 averaged over the entire model episode in the 4km HGB modeling domain. Units are ppm.

4.3.2 Source contributions to NO to NO_2 conversion

4.3.2.1 Relative source contributions to NO to NO_2 conversion

The total production of NO_2 has been found to be linearly proportional to the net ozone formation (see section 4.2). Therefore, by studying source contribution of NO to NO_2 conversion rate due to RO_2 and HO_2 radicals in each of the days in the study episode, we can estimate the source contributors to O_3 formation during that period.

The ozone formation rates and NO to NO_2 conversion rates near the ground might not represent the rates that prevail in the air above the ground where most of the tropospheric ozone is generated. On high convective summer days, the pollutants disperse rapidly within the mixing height, and the air above it does not significantly mix to affect the ground level ozone within the timescale of our analysis. Thus, a column-averaged NO to NO_2 conversion rate based on the thickness of each model layer below the mixing height is calculated according to equation 4.1 below. The mixing height information is provided by the meteorology model.

$$R_{NO_2,avg} = \frac{\sum_{i=1}^{n} H_i R_{NO_2,i}}{\sum_{i=1}^{n} H_i} \qquad (4.1)$$

where, R_{NO2avg} is the column-averaged conversion rate, H_i is the thickness of the i^{th} layer in the model below the mixing height and H_i is the conversion rate in layer i. n is the total number of model layers below the mixing height.

Figure 4.16 shows the daily source contributions to NO to NO_2 conversions due to RO_2/HO_2 radicals from different sources in the Houston urban areas in the 4km modeling domain. The Houston urban area is chosen in this analysis because the biogenic sources are more prominent

on a regional scale, and they are not the direct cause for Houston's non-attainment status for O_3. Calculating source contributions by averaging over the entire model domain would skew the results by unrealistically over-predicting the actual contributions of the biogenic sources to ozone exceedance events. In order to find a more accurate source contribution to NO to NO_2 conversion rates in the area of non-compliance, only a selected region of urban Houston is chosen.

The cell range chosen in the model domain for the source contribution calculation is (25,25)-(35,35), as illustrated by the red boxed area in Figure 4.1.

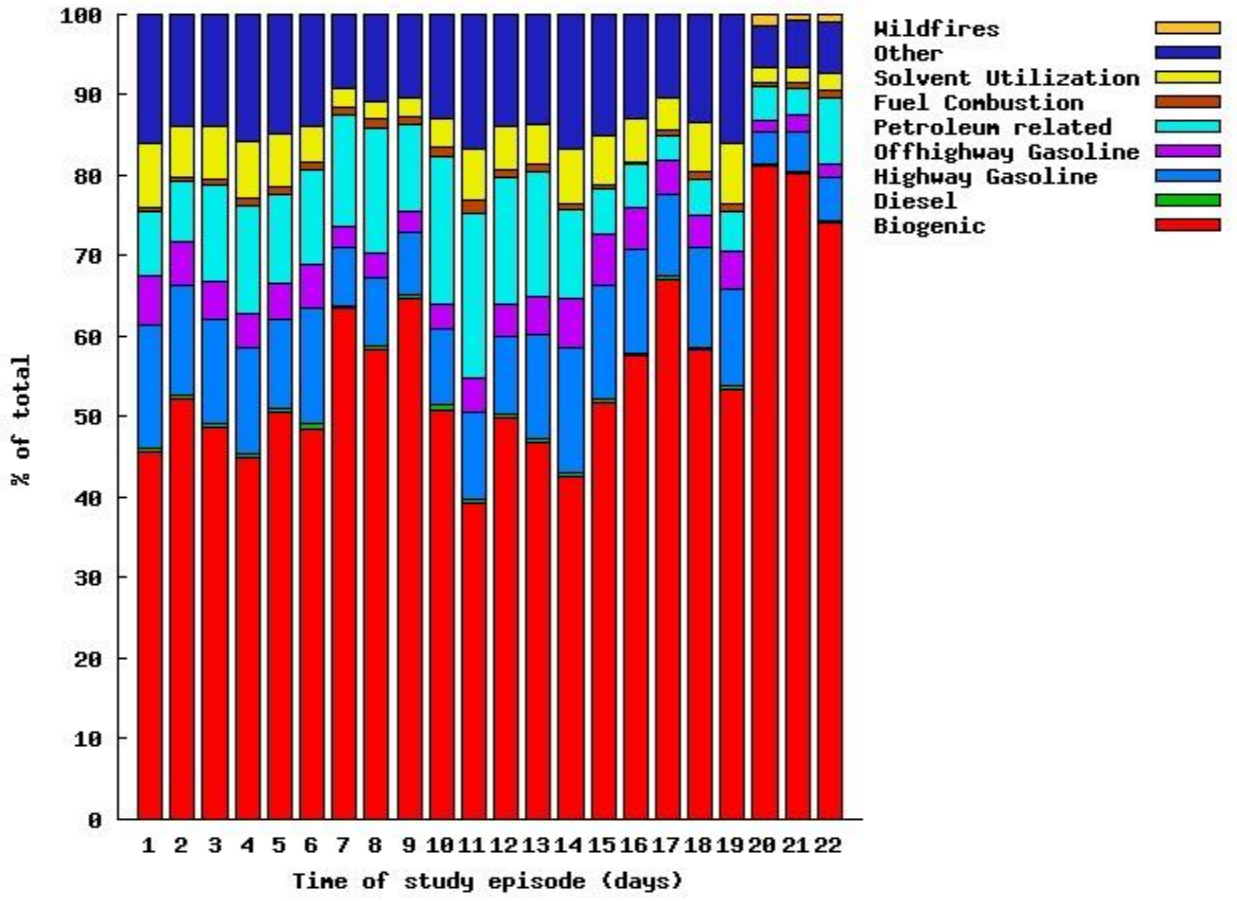

Figure 4.16 Daily variation of source contributions to NO to NO_2 conversion rates due to RO_2 and HO_2 radicals.

The results show that on all days of the study period, biogenic sources make a contribution of approximately 45% to total NO_2 production from NO due to RO_2/HO_2 radicals. The actual contributions to ozone concentrations in the downwind locations of major anthropogenic sources are much higher. In order to better illustrate the contributions due to anthropogenic sources, Figure 4.17 shows the contribution of all sources except biogenic sources, to NO to NO_2 conversion. Considering only anthropogenic sources, highest contributions come from "other" sources (30%), highway gasoline vehicles (28%) and petroleum related processes (15%), followed by solvent utilization (14%) and off-highway gasoline engines (11%). These contributions are approximate figures, as these values vary slightly day to day due to different meteorology conditions and varying emissions of O_3 precursors. While fuel combustion and diesel vehicles make up a small contribution of 2% and less than 1% respectively, wildfires differ with each day of the study period. Wildfires contributed as much as 10% of total NO to NO_2 conversion on September 4, 2000. In fact, significant contribution from wildfires was observed from September 2 onwards till September 6, 2000.

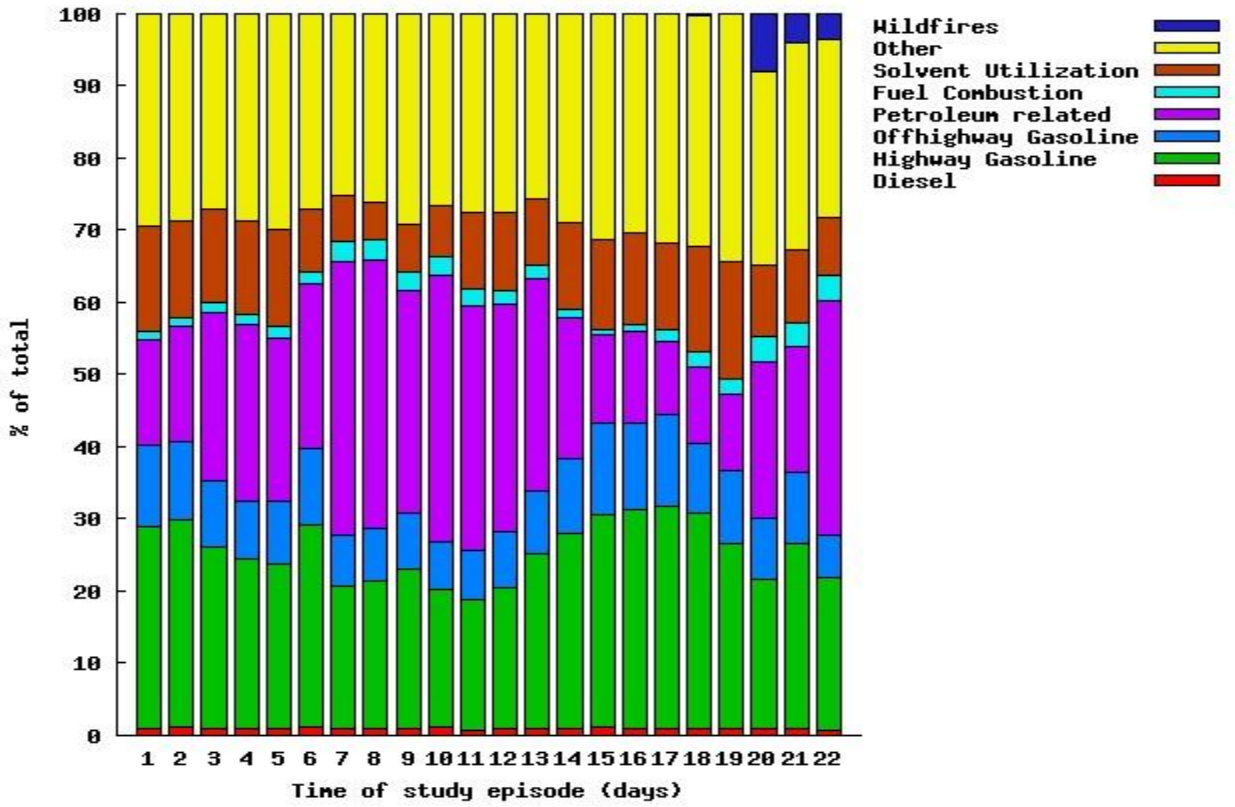

Figure 4.17 Relative source contributions to NO to NO_2 conversion rates due to RO_2 and HO_2 radicals due to anthropogenic sources.

4.3.2.2 Regional distribution of source contributions to NO to NO_2 conversion

Regional distributions of column-averaged NO_2 production at CST 1200-1300 due to RO_2/HO_2 from different sources are plotted of the modeling domain for three scenarios: episodic average of entire study episode, high ozone day (September 2, 2000) and low ozone day (August 27, 2000), as shown in Figures 4.18, 4.19 and 4.20 respectively.

The contribution from Biogenic sources towards NO to NO_2 conversion due to the RO_2 and HO_2 radical is spatially distributed throughout the HGB domain. The contributions from Highway gasoline, Off-highway gasoline and solvent utilization are concentrated near the urban areas, while that from petroleum-related processes contribute near the Houston Ship Channel, where there are many petro-chemical industries.

The difference in NO to NO_2 conversion rates differs from a high to low ozone day. This could be attributed to meteorology conditions favorable to the high ozone formation. Sudden releases of HRVOCs from industrial stacks can also increase the net O_3 formation downwind of the plume, through the conversion of NO to NO_2.

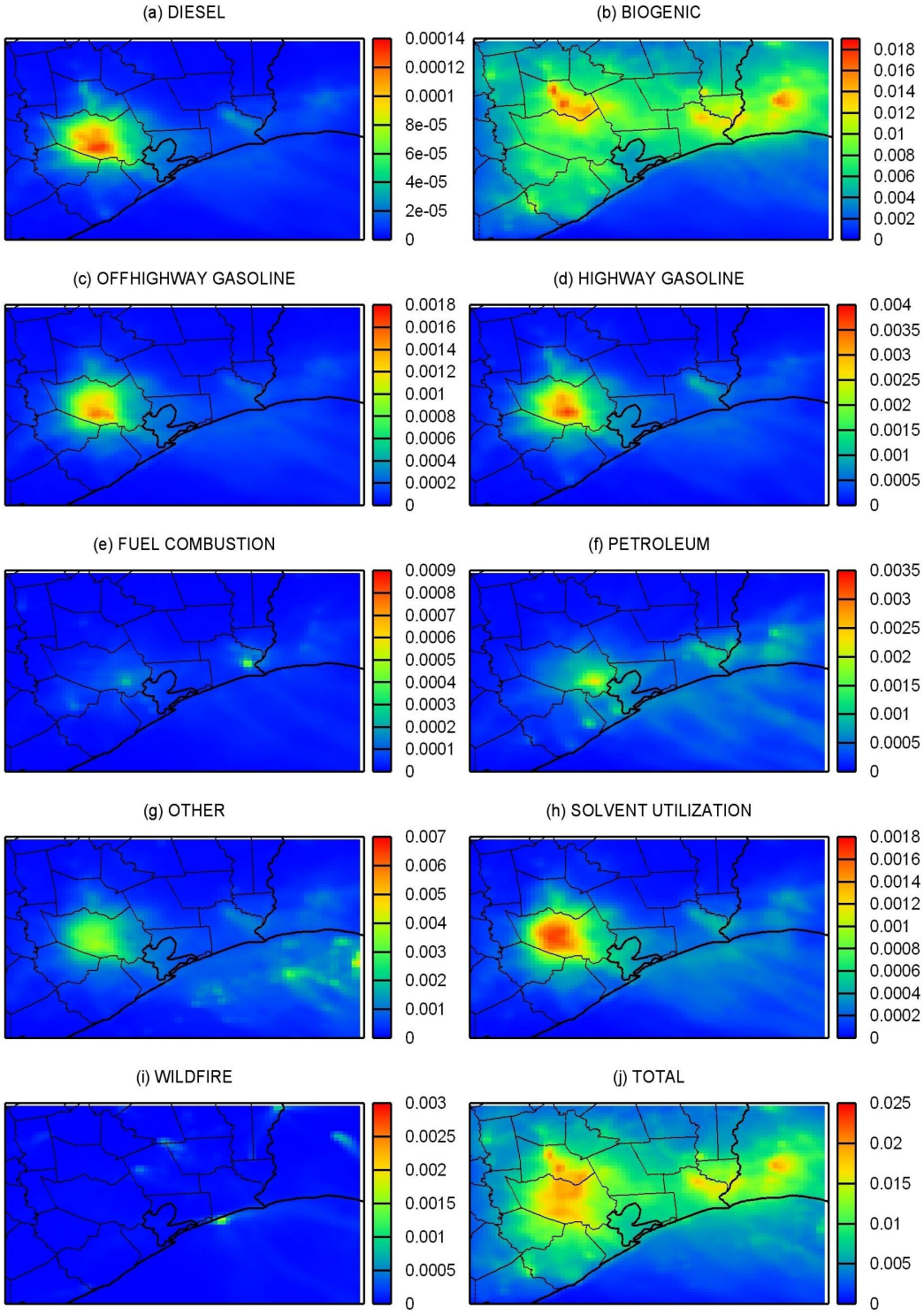

Figure 4.18 Regional distributions of column-averaged NO to NO_2 conversion rates due to RO_2 and HO_2 radicals at 1200-1300 CST averaged over the entire model episode for the 4 km HGB model domain. Units are ppm hr^{-1}.

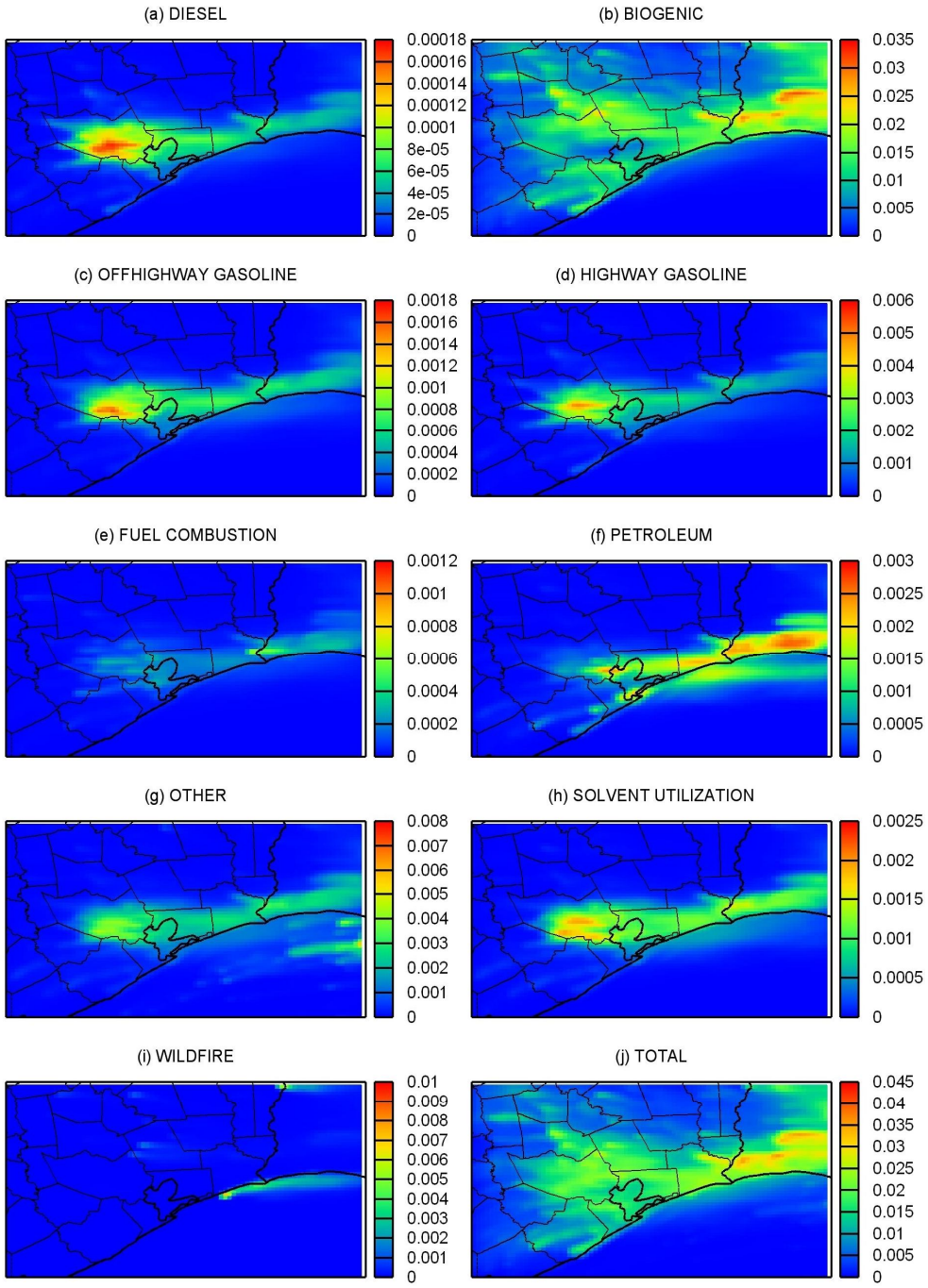

Figure 4.19 Regional distribution of column-averaged NO to NO_2 conversion rates due to RO_2 and HO_2 radicals at 1200-1300 CST on September 2, 2000 for the 4 km HGB model domain. Units are ppm hr^{-1}.

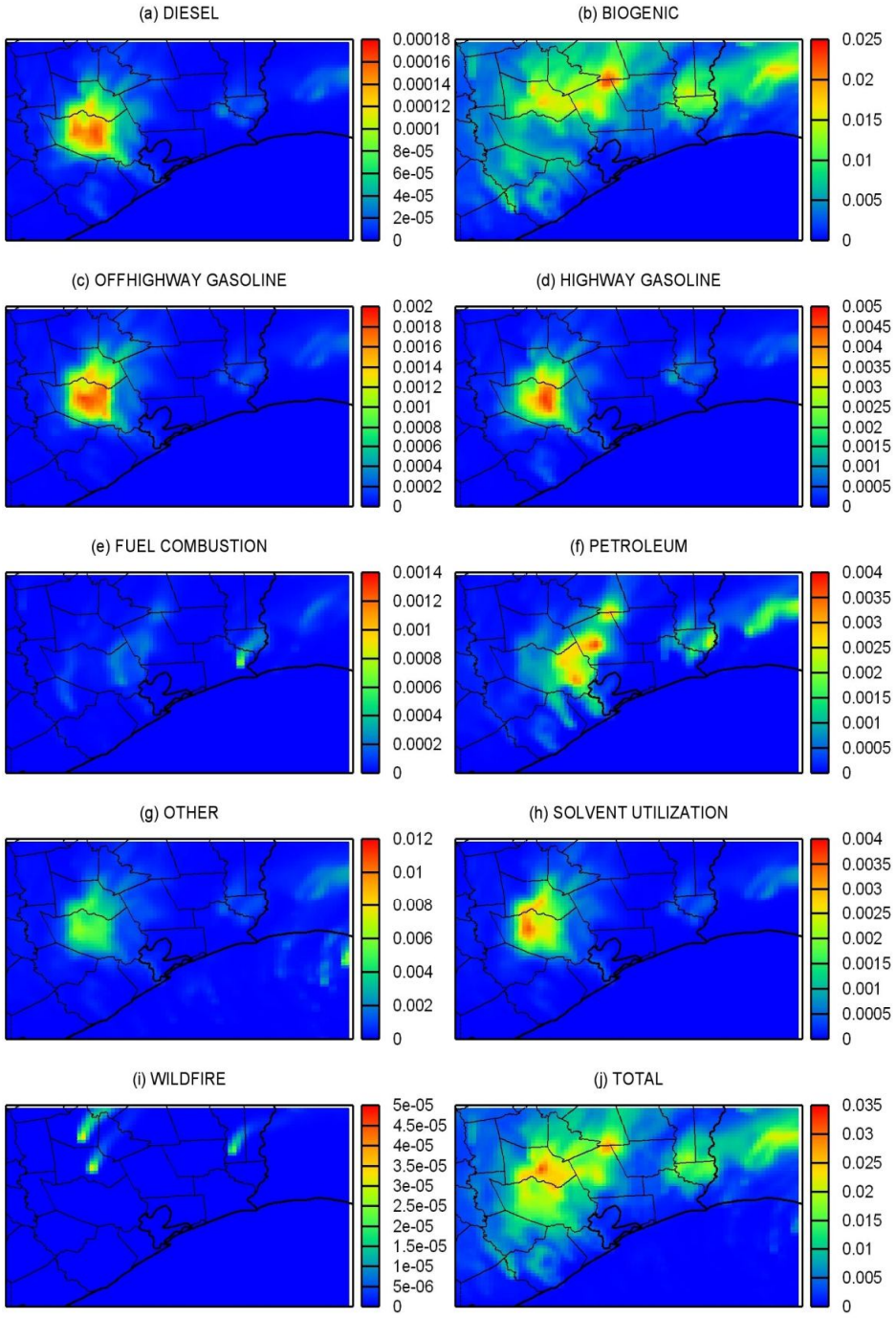

Figure 4.20 Regional distribution of column-averaged NO to NO_2 conversion rates due to RO_2 and HO_2 radicals at 1200-1300 CST on August 27, 2000 for the 4 km HGB model domain. Units are ppm hr^{-1}.

4.3.3 Source contribution to O_3 formation

An episodic average of the net O_3 formation in the modeling domain was done on an hourly basis. From Figure 4.21, it can be seen that the highest O_3 formation rate occurs at 1200-1300 CST (1800-1900 GMT) in the afternoon.

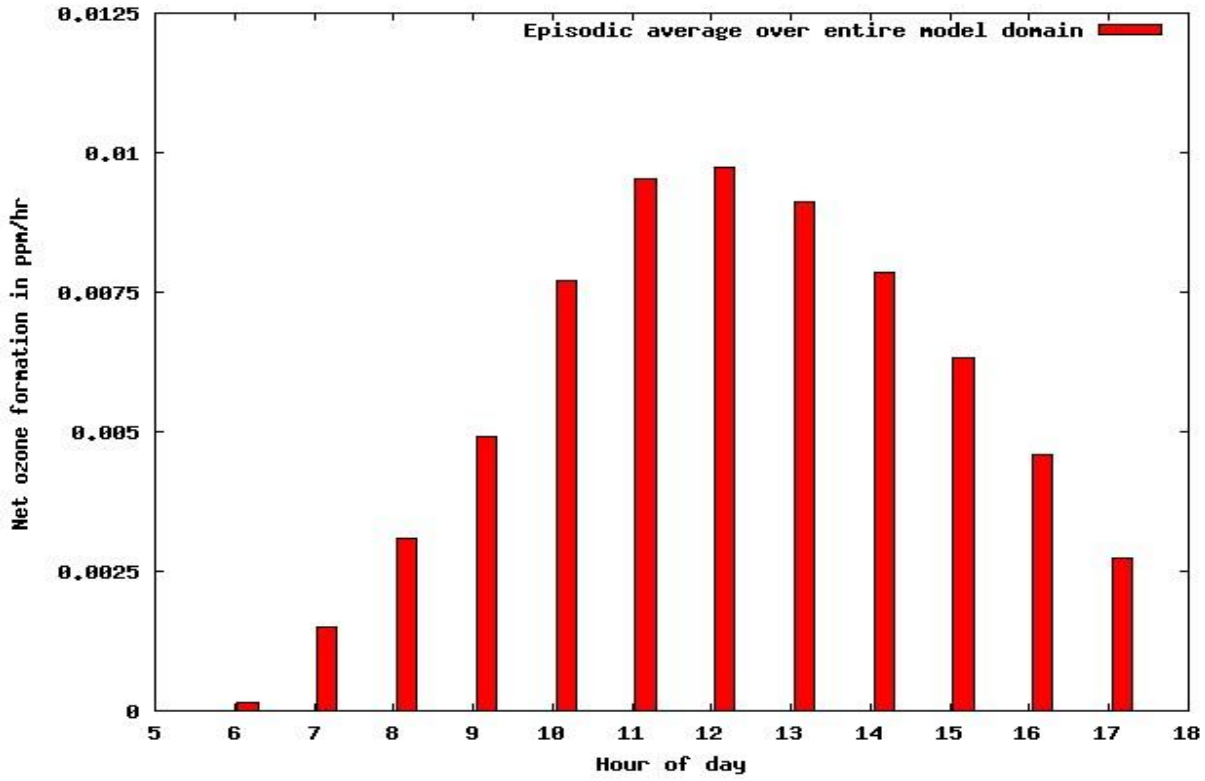

Figure 4.21 Episodic average of net O_3 formation for day time hours.

The contributions of VOC to O_3 formation can be estimated based on the linear relationship between the amount of NO to NO_2 conversion due to RO_2/HO_2 radicals and the amount of net O_3 formation, as shown in equations (4.2) and (4.3):

$$\Delta O_3^i = \Delta O_3 \,.\, f_i \qquad (4.2)$$

$$f_i = \frac{RNO_2^i}{\sum_{i=1}^{n} RNO_2^i} \tag{4.3}$$

where, ΔO_3^i is the net O_3 formed from source i, ΔO_3 is the overall net O_3 formed from all the sources combined and RNO_2 is the rate of NO to NO_2 conversion due to source i. When ΔO_3 is less than zero, its value is taken as zero. In other words, only positive net O_3 formation rates are included in the plot. Equations (4.2) and (4.3) are applied to O_3 formation in each model layer individually and then the column-averaged O_3 formation rate for each source is calculated using the source contributions calculated for each layer and the thickness of the layer (see Equation (4.1).

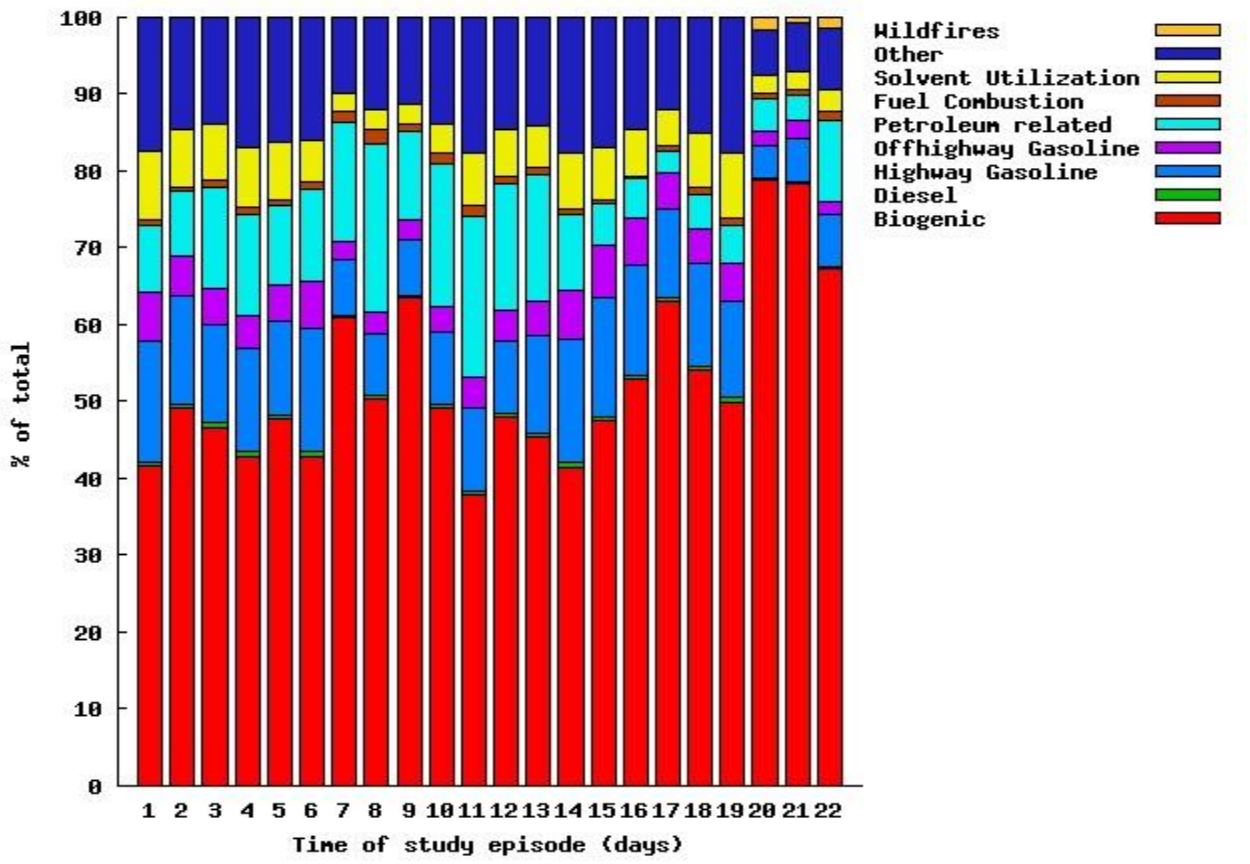

Figure 4.22 Relative source contributions to net O_3 Formation rates due to RO_2 and HO_2 radicals due to all sources.

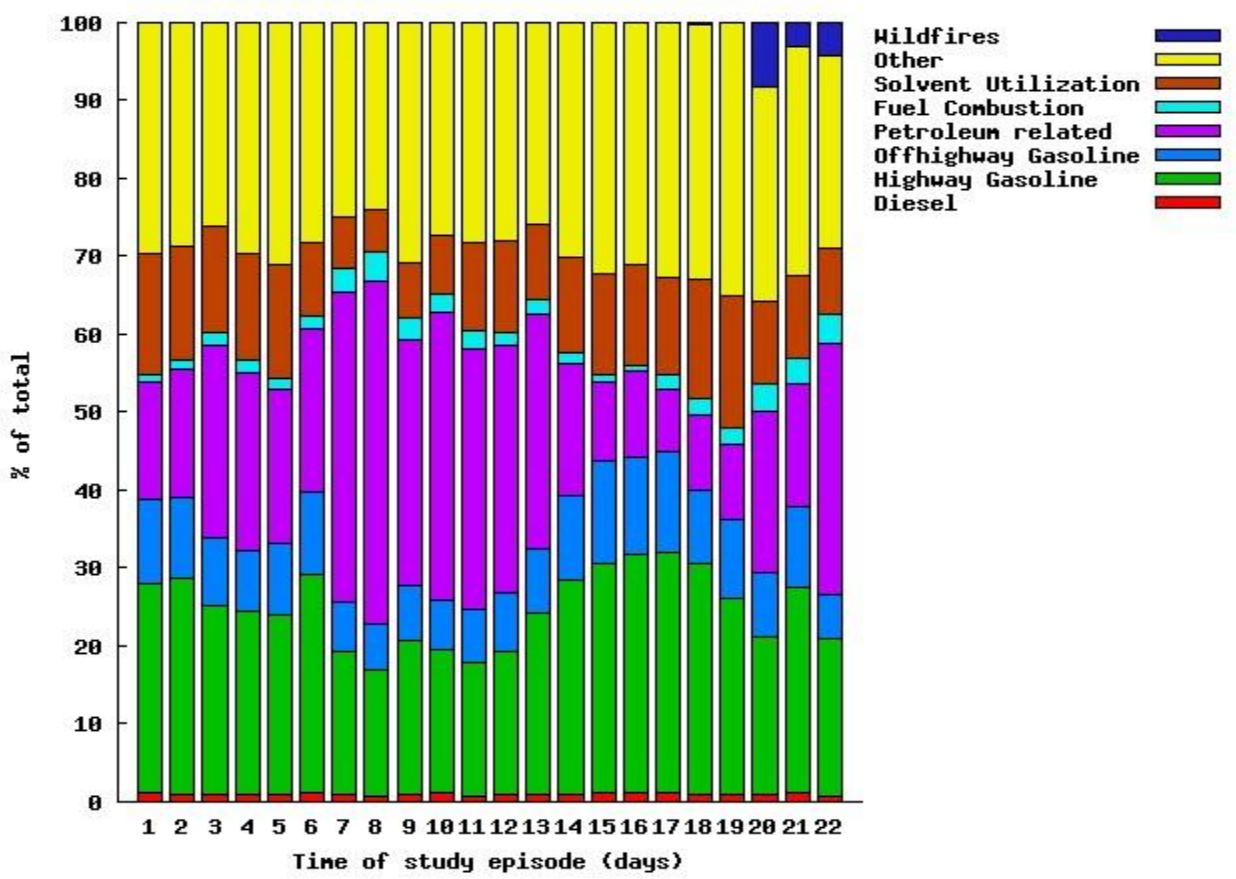

Figure 4.23 Relative source contributions to net O_3 formation rates due to RO_2 and HO_2 radicals due to anthropogenic sources.

The cell range chosen for the O_3 source contribution calculations is illustrated by the red boxed area in Figure 4.1. Figure 4.22 and 4.23 shows the daily-averaged column-weighted source contributions to net O_3 formation in the urban Houston areas of the domain. It is very similar to the pattern of source contribution to NO to NO_2 conversion due to RO_2 and HO_2 radical. Approximately 40% of the net O_3 formed comes from biogenic sources. Of the anthropogenic sources, highway gasoline vehicles and petroleum-related processes contribute approximately 27% and 15% to net O_3 formation in the domain. The industrial sources classified under "other" contribute to 30% of the net O_3 formation.

As shown in Figures 4.24, 4.25 and 4.26, the regional contributions to O_3 formation were studied by first choosing an episodic average, a high O_3 day and a low O_3 day, all at 1200-1300 CST. September 2, 2000 was considered a high O_3 day and August 27, 2000 was considered a low O_3 day. September 2, 2000 was chosen to represent a high ozone day due to its relatively more stagnant conditions during peak hour than the other high ozone days. A similar approach was used as done previously of calculating weighted average of concentrations for layers below the mixing height for the peak hour.

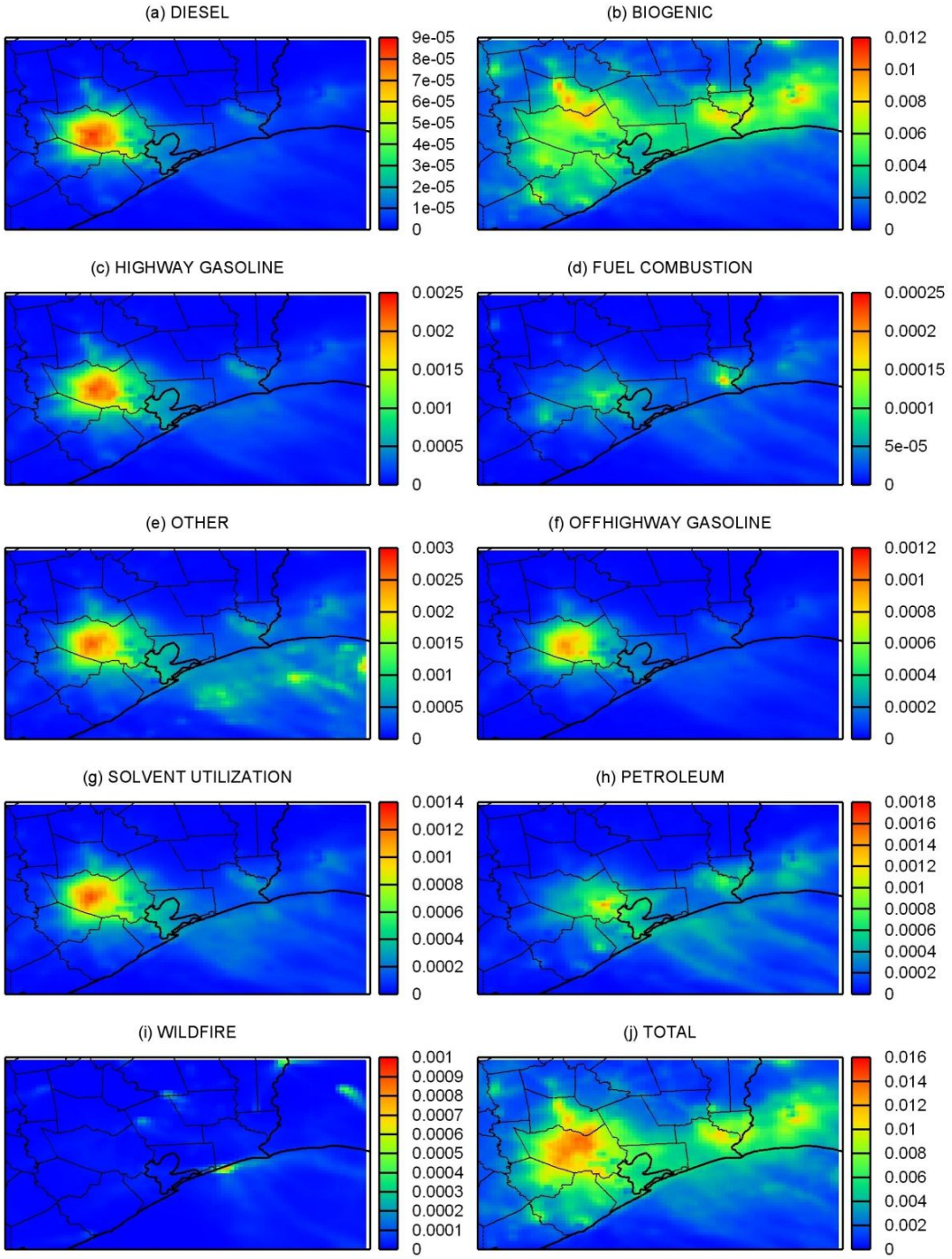

Figure 4.24 Regional distributions of column-averaged net O_3 formation rates due to RO_2 and HO_2 radicals at 1200-1300 CST averaged over the entire model episode for the 4 km HGB model domain. Units are ppm hr^{-1}.

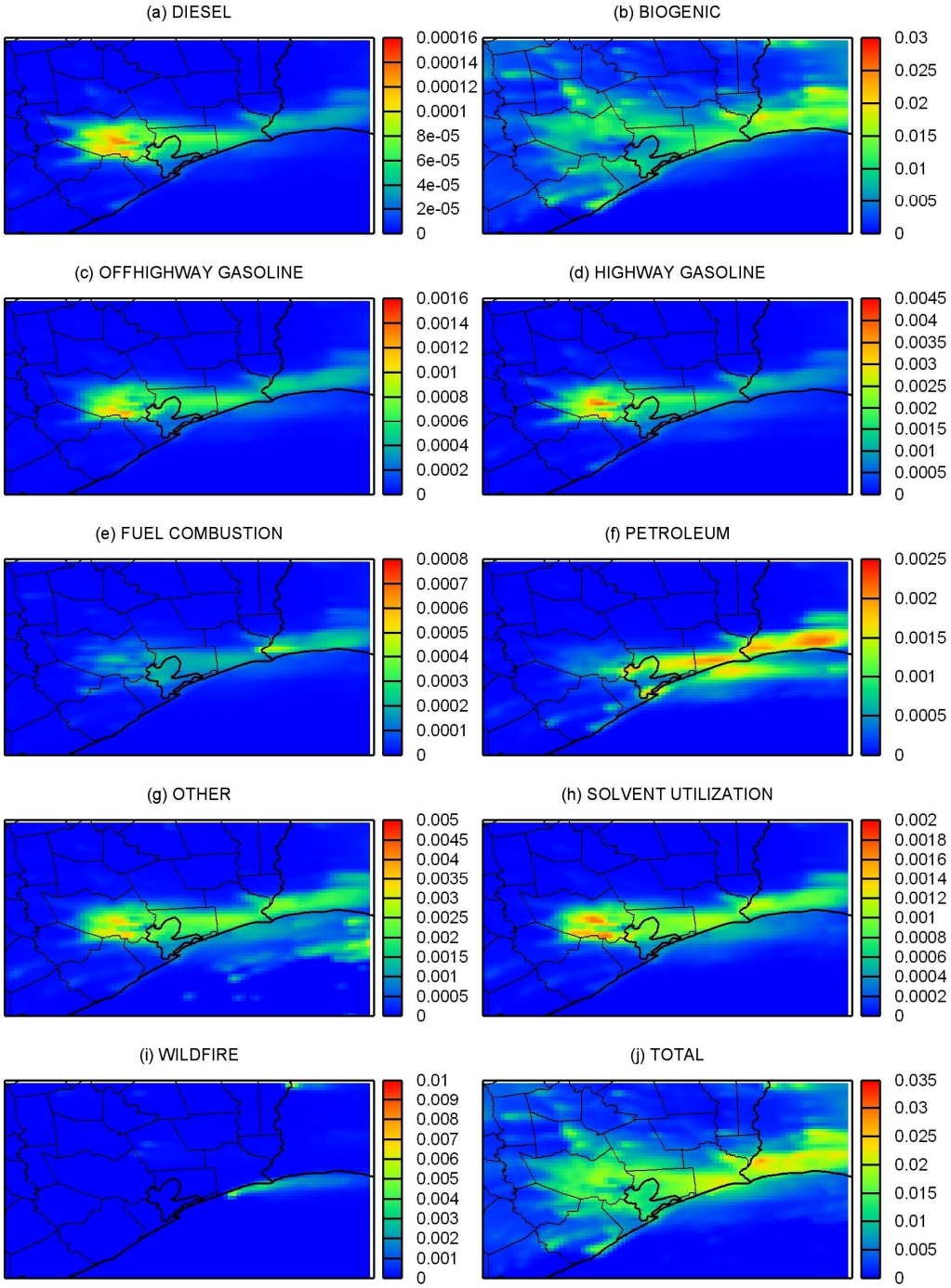

Figure 4.25 Regional distribution of column-averaged net O_3 formation rates due to RO_2 and HO_2 radicals at 1200-1300 CST on September 2, 2000 for the 4 km HGB model domain. Units are ppm hr^{-1}.

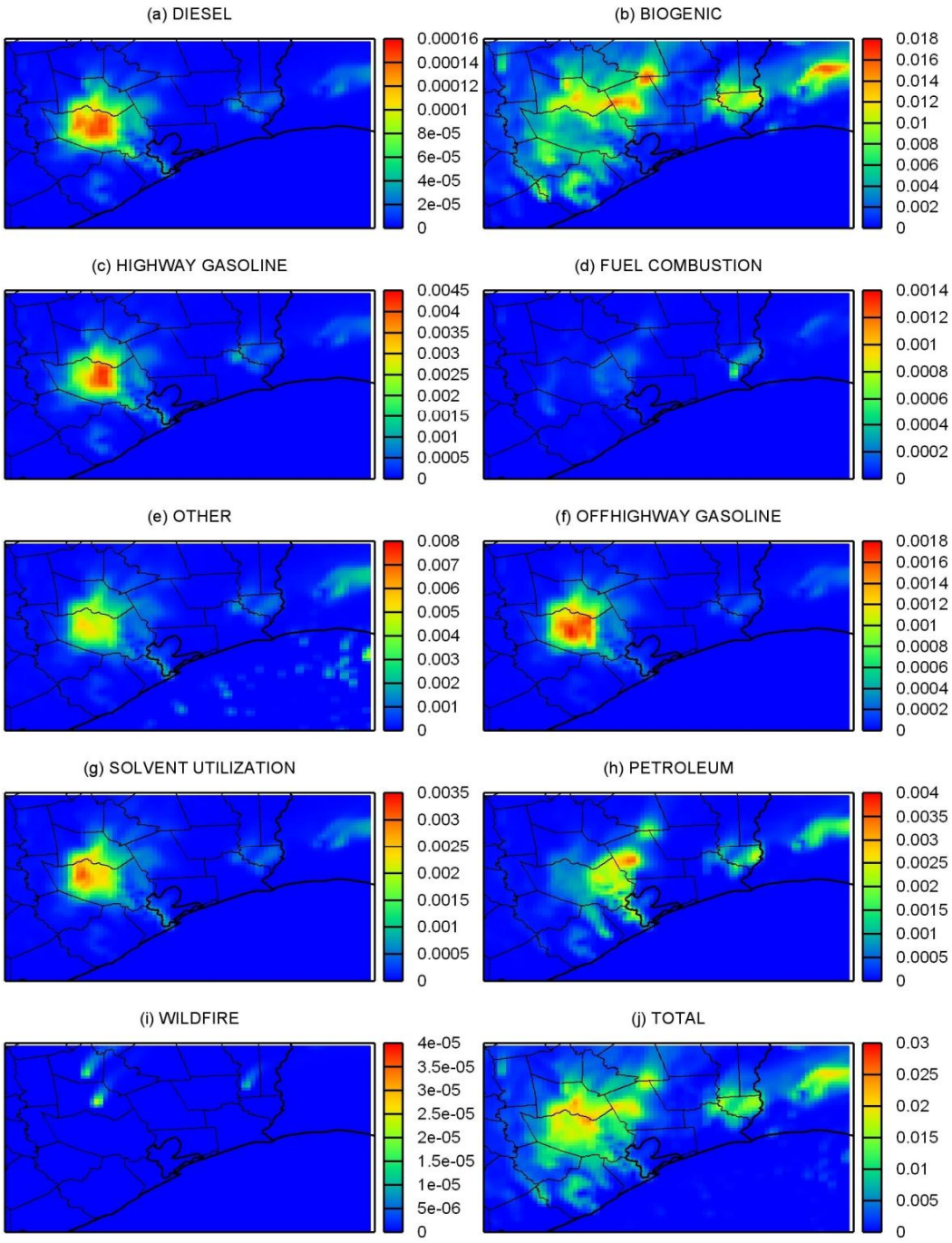

Figure 4.26 Regional distribution of column-averaged net O_3 formation rates due to RO_2 and HO_2 radicals at 1200-1300 CST on August 27, 2000 for the 4 km HGB model domain. Units are ppm hr^{-1}.

The model results show that biogenic emissions account for a significant amount of O_3 formation in the rural areas. The maximum ozone formation rate due to biogenic source can be as high as 0.03 ppm hr^{-1} on a high ozone day and averaging over all the days the highest formation rate is approximately 0.0122 ppm hr^{-1}. Both highway and off-highway vehicles contribute significantly to O_3 formation in the urban areas as well as downwind areas. The highest formation rates on a high ozone day are 0.0045 ppm hr^{-1} from highway vehicles and 0.0016 ppm hr^{-1} from off-highway vehicles. Fuel combustion makes a marginal contribution to O_3 formation, with a formation rate of 0.008 ppm hr^{-1} on a high ozone day. Diesel vehicles do not contribute significantly to O_3 formation (highest contribution is 0.0001 ppm hr^{-1} on a high ozone day) due to their low VOC emission rates. O_3 formation due to petroleum related emissions occurs primarily in areas downwind of the industrial regions. The O_3 formation rate due to this source is approximately 0.0025 ppm hr^{-1} on a high ozone day and 0.0018 ppm hr^{-1} averaged over the entire episode.

CHAPTER V

CONCLUSIONS

The time series comparisons between observed and predicted values along with the performance statistics for O_3 and PM2.5 indicated good model performance, thereby building confidence on the subsequent source-apportionment results. The basis of the ozone source apportionment is the linear relationship that was established between the amount of NO to NO_2 conversion due to RO_2 and HO_2 radical and the amount of net O_3 formation. The extent of linearity changes with the VOC/NO_x ratio and the time of day. It is visibly the highest for ratios from 5-15 and lowest for ratios less than 2. Net O_3 formation is seen to peak at mid-noon of the day, when photochemical activity is the highest in the troposphere. VOC/NO_x ratios are found to be critical to the net O_3 formation rates. Highest net O_3 formation is observed when the ratios are from 5-15, which was found to experience most linearity between total NO to NO_2 conversion and net O_3 formation. Net O_3 formation is the least for ratios less than 2 and greater than 15. Of the anthropogenic emission sources, petroleum and other industrial sources in the urban Houston region contribute to approximately 45% of the ozone formation in the HGB area. Further analysis revealed that the contributions from highway gasoline are approximately 28%. On days of high wildfire activity, wildfires contribute as much as 11%, which is as much as the contribution from off-highway gasoline. The regional distribution analysis for net O_3 formation shows that biogenic emissions account for a significant amount of O_3 formation in the rural areas. Both highway and off-highway vehicles contribute significantly to O_3 formation especially in the downwind region. Diesel vehicles do not contribute significantly to ozone formation due to their low VOC emissions.

REFERENCES

Abu-Allaban, M., Gertler, A.W., Lowenthal, D.H., 2002. A preliminary apportionment of the sources of ambient PM10, PM2.5, and VOCs in Cairo. Atmospheric Environment 36, 5549-5557.

Allen, D., Murphy, C., Kimura, Y., Vizuete, W., 2004. Variable industrial VOC emissions and their impact on ozone formation in the Houston-Galveston area, Houston Advanced Research Consortium (HARC). Final report. Texas Environmental Research Consortium Project H-13.

American Lung Association, 2008. State of the Air. Available online at: http://www.stateoftheair.org/2008/key-findings/

Banta, R., Senff, C., Nielsen-Gammon, J., Darby, L., Ryerson, T., Alvarez, R., Sandberg, S., Williams, E., Trainer, M., 2005. A bad air day in Houston. Bulletin of the American Meteorological Society 86, 657-669.

Bao, J.W., Michelson, S.A., McKeen, S.A., Grell, G.A., 2005. Meteorological evaluation of a weather-chemistry forecasting model using observations from the TEXAS AQS 2000 field experiment. Journal of Geophysical Research 110, 1-19.

Bascom R., Bromberg PA, Costa DA, Devlin R., Dockery DW, Frampton MW, Lambert W., Samet JM, Speizer FE, Utell M., 1996. Health effects of outdoor air pollution. American Journal of Respiratory and Critical Care Medicine 153, 3-50

Berkowitz, C.M., Spicer, C.W., Doskey, P.V., 2005. Hydrocarbon observations and ozone production rates in Western Houston during the Texas 2000 Air Quality Study. Atmospheric Environment 39, 3383-3396.

Boylan, J.W., Russell, A.G., 2006. PM and light extinction model performance metrics, goals, and criteria for three-dimensional air quality models. Atmospheric Environment 40, 4946-4959.

Buzcu, B., Fraser, M.P., 2006. Source identification and apportionment of volatile organic compounds in Houston, TX. Atmospheric Environment 40, 2385-2400.

Byun, D., Schere, K., 2006. Review of the governing equations, computational algorithms, and other components of the Models-3 Community Multiscale Air Quality (CMAQ) modeling system. Applied Mechanics Reviews 59, 51.

Byun, D.W., Kim, S.-T., Kim, S.B., 2007. Evaluation of air quality models for the simulation of a high ozone episode in the Houston metropolitan area. Atmospheric Environment 41, 837-853.

Byun, D.W., Kim, S., Czader, B., Nowak, D., Stetson, S., Estes, M., 2005. Estimation of biogenic emissions with satellite-derived land use and land cover data for air quality modeling of Houston-Galveston ozone nonattainment area. Journal of Environmental Management 75, 285-301.

Camalier, L., Cox, W., Dolwick, P., 2007. The effects of meteorology on ozone in urban areas and their use in assessing ozone trends. Atmospheric Environment 41, 7127-7137.

Carter, W.P.L., 2000. Documentation of the SAPRC-99 chemical mechanism for VOC reactivity assessment, Air Pollution Research Center and College of Engineering, Center for Environmental Research and Technology, University of California at Riverside, CA.

Chang, C.C., Wang, J.L., Candice Lung, S.C., Liu, S.C., Shiu, C.J., 2009. Source characterization of ozone precursors by complementary approaches of vehicular indicator and principal component analysis. Atmospheric Environment 43, 1771-1778.

Chang, S., Allen, D.T., 2005. Atmospheric chlorine chemistry in Southeast Texas: Impacts on ozone formation and control. Environmental Science and Technology 40, 251-262.

CMAS Center, 2009a. Community Multi-Scale Air Quality Model features. Available online at: http://www.cmaq-model.org/

CMAS Center, 2009b. Sparse Matrix Operator Kernel Emissions (SMOKE) Model features. Available online at: http://www.smoke-model.org/version2.6/html/ch01s03.html

CMAS Center, 2009c. Sparse Matrix Operator Kernel Emissions Model, SMOKE. Available online at: http://www.smoke-model.org/index.cfm

Czader, B.H., Byun, D.W., Kim, S.T., Carter, W.P.L., 2008. A study of VOC reactivity in the Houston-Galveston air mixture utilizing an extended version of SAPRC-99 chemical mechanism. Atmospheric Environment 42, 5733-5742.

Daum, P.H., L. I. Kleinman, S. R. Springston, L. J. Nunnermacker, Y.N. Lee, J. Weinstein-Lloyd, J. Zheng, C. M. Berkowitz, 2003. A comparative study of O_3 formation in the Houston urban and industrial plumes during the 2000 Texas Air Quality Study. Journal of Geophysical Research 108(D23), 1-18.

Daum, P.H., L. I. Kleinman, S. R. Springston, L. J. Nunnermacker, Y.N. Lee, J. Weinstein-Lloyd, J. Zheng, C. M. Berkowitz, 2004. Origin and properties of plumes of high ozone observed during the Texas 2000 Air Quality Study (TexAQS 2000). Journal of Geophysical Research 109, 1-16.

Davis, J.M., Eder, B.K., Nychka, D., Yang, Q., 1998. Modeling the effects of meteorology on ozone in Houston using cluster analysis and generalized additive models. Atmospheric Environment 32, 2505-2520.

Elbir, T., Cetin, B., Cetin, E., Bayram, A., Odabasi, M., 2007. Characterization of volatile organic compounds (VOCs) and their sources in the air of Izmir, Turkey. Environmental Monitoring and Assessment 133, 149-160.

EPA, U.S, 1991. Guidance for Regulatory Application of the Urban Airshed Model (UAM), US Environmental Protection Agency, Office of Air Quality Planning and Standards, Research Triangle Park, NC.

EPA, U.S. 2010. Clean Air Interstate Rule (CAIR) Emissions Inventory. Available online at: http://cfpub.epa.gov/si/si_public_record_Report.cfm?dirEntryID=73960

Fujita, E., 2001. Hydrocarbon source apportionment for the 1996 Paso del Norte Ozone Study. Science of the Total Environment 276, 171-184.

Gilman, J., Kuster, W., Goldan, P., Herndon, S., Zahniser, M., Tucker, S., Brewer, W., Lerner, B., Williams, E., Harley, R., 2009. Measurements of volatile organic compounds during the 2006 TexAQS/GoMACCS campaign: Industrial influences, regional characteristics, and diurnal dependencies of the OH reactivity. Journal of Geophysical Research -Atmospheres 114, 1-17.

Grell, G.A., Dudhia, J., Stauffer, D.R., 1994. A description of the fifth-generation Penn State/NCAR mesoscale model. NCAR Technical Note NCAR/TN-398+STR, 122-125.

Houyoux, M.R., Vukovich, J.M., Coats Jr., C.J., Wheeler, N.W., Kasibhatla, P.S., 2000. Emission inventory development and processing for the Seasonal Model for Regional Air Quality (SMRAQ) project. Journal of Geophysical Research 105, 9079–9090.

Jiang, G., Fast, J.D., 2004. Modeling the effects of VOC and NOX emission sources on ozone formation in Houston during the TexAQS 2000 field campaign. Atmospheric Environment 38, 5071-5085.

Jobson B.T., Berkowitz C.M., Kuster W.C., Goldan P. D., Williams E. J., Fesenfeld F. C., Apel E. C., Karl T., Lonneman W. A., Riemer D., 2004. Hydrocarbon source signatures in Houston, Texas: Influence of the petrochemical industry. Journal of Geophysical Research -Atmospheres 109(D24), 1-24.

Junquera, V., 2004. Inventory of emissions of gaseous compounds and particulate matter from wildfires in east Texas in August and September 2000 and comparison with aircraft measurements. Masters Thesis, University of Texas, Austin.

Junquera, V., Russell, M.M., Vizuete, W., Kimura, Y., Allen, D., 2005. Wildfires in eastern Texas in August and September 2000: Emissions, aircraft measurements, and impact on photochemistry. Atmospheric Environment 39, 4983-4996.

Kemball-Cook, S., Parrish, D., Ryerson, T., Nopmongcol, U., Johnson, J., Tai, E., Yarwood, G., 2009. Contributions of regional transport and local sources to ozone exceedances in Houston and Dallas: Comparison of results from a photochemical grid model to aircraft and surface measurements. Journal of Geophysical Research -Atmospheres 114, 1-14.

Kleeman, M., Cass, G., 2001. A 3D Eulerian source-oriented model for an externally mixed aerosol. Environmental Science and Technology 35, 4834-4848.

Kleinman, L.I., Daum, P.H., Imre, D., Lee, Y.N., Nunnermacker, L.J., Springston, S.R., Weinstein-Lloyd, J., Rudolph, J., 2002. Ozone production rate and hydrocarbon reactivity in 5 urban areas: A cause of high ozone concentration in Houston. Geophysical Research Letters 29, 1-4.

Langford, A.O., Senff, C.J., Banta, R.M., Hardesty, R.M., Alvarez, R.J., II, Sandberg, S.P., Darby, L.S., 2009. Regional and local background ozone in Houston during Texas Air Quality Study 2006. Journal of Geophysical Research 114, 1467-1470.

Lei, W., Zhang, R., Tie, X., Hess, P., 2004. Chemical characterization of ozone formation in the Houston-Galveston area: A chemical transport model study. Journal of Geophysical Research 109, 1-15.

Lin, C.H., Chang, L.F.W., 2002. Relative source contribution analysis using an air trajectory statistical approach. Journal of Geophysical Research 107, 1-10.

Lin, C.J., Ho, T.C., Chu, H., Yang, H., Chandru, S., Krishnarajanagar, N., Chiou, P., Hopper, J.R., 2005. Sensitivity analysis of ground-level ozone concentration to emission changes in two urban regions of southeast Texas. Journal of Environmental Management 75, 315-323.

Lippmann, M., 1993. Health effects of tropospheric ozone: review of recent research findings and their implications to ambient air quality standards. Journal of Exposure Analysis and Environmental Epidemiology 3, 103-129.

Miller, S.L., Anderson, M.J., Daly, E.P., Milford, J.B., 2002. Source apportionment of exposures to volatile organic compounds. I. Evaluation of receptor models using simulated exposure data. Atmospheric Environment 36, 3629-3641.

Murphy, C.F., Allen, D.T., 2005. Hydrocarbon emissions from industrial release events in the Houston-Galveston area and their impact on ozone formation. Atmospheric Environment 39, 3785-3798.

Nam, J., Kimura, Y., Vizuete, W., Murphy, C., Allen, D.T., 2006. Modeling the impacts of emission events on ozone formation in Houston, Texas. Atmospheric Environment 40, 5329-5341.

Paatero, P., Tapper, U., 1994. Positive matrix factorization: a non-negative factor model with optimal utilization of error estimates of data values. Environmetrics 5, 111-126.

Parrish, D.D., Allen, D.T., Bates T.S., Estes M., Fehsenfeld, F.H., Feingold, G., Ferrare, R., Hardesty R.M., Meagher J.F., Nielsen-Gammon J.W., Pierce R.B., Ryerson T.B., Seinfeld J.H., Williams E.J., 2009. Overview of the Second Texas Air Quality Study (TexAQS II) and the Gulf of Mexico Atmospheric Composition and Climate Study (GoMACCS). Journal of Geophysical Research 114, 1-28.

Pennsylvania State University/National Center for Atmospheric Research, 2008. National Center for Atmospheric Research Mesoscale Model (MM5) Features. Available online at: http://www.mmm.ucar.edu/mm5/

Phillips, L.F., Finlayson-Pitts B.J., Pitts J.N., 2001. Chemistry of the upper and lower atmosphere. Journal of Atmospheric Chemistry 39, 327-328.

Ryerson, T.B., Trainer, M., Angevine, W.M., Brock, C.A., Dissly, R.W., Fehsenfeld, F.C., Frost, G.J., Goldan, P.D., Holloway, J.S., Hübler, G., Jakoubek, R.O., Kuster, W.C., Neuman, J.A., Nicks, D.K., Jr., Parrish, D.D., Roberts, J.M., Sueper, D.T., Atlas, E.L., Donnelly, S.G., Flocke, F., Fried, A., Potter, W.T., Schauffler, S., Stroud, V., Weinheimer, A.J., Wert, B.P., Wiedinmyer, C., Alvarez, R.J., Banta, R.M., Darby, L.S., Senff, C.J., 2003. Effect of petrochemical industrial emissions of reactive alkenes and NOx on tropospheric ozone formation in Houston, Texas. Journal of Geophysical Research 108, 1-24.

Seinfeld J. H., Pandis S. N. (1998) Atmospheric Chemistry and Physics: From Air Pollution to Climate Change, J. Wiley, New York.

Shi, C., Fernando, H.J.S., Yang, J., 2009. Contributors to ozone episodes in three U.S./Mexico border twin-cities. Science of the Total Environment 407, 5128-5138.

Shrestha, K.L., Kondo, A., Kaga, A., Inoue, Y., 2009. High-resolution modeling and evaluation of ozone air quality of Osaka using MM5-CMAQ system. Journal of Environmental Sciences 21, 782-789.

Sillman, S., 1999. The relation between ozone, NOx and hydrocarbons in urban and polluted rural environments. Atmospheric Environment 33, 1821-1845.

Sillman, S., 2003. Tropospheric ozone and photochemical smog. Treatise on Geochemistry 9, 407-431.

Simon, H., Kimura, Y., McGaughey, G., Allen, D.T., Brown, S.S., Osthoff, H.D., Roberts, J.M., Byun, D., Lee, D., 2009. Modeling the impact of ClNO2 on ozone formation in the Houston area. Journal of Geophysical Research 114, 1-17.

Song, J., Vizuete, W., Chang, S., Allen, D., Kimura, Y., Kemball-Cook, S., Yarwood, G., Kioumourtzoglou, M.A., Atlas, E., Hansel, A., Wisthaler, A., McDonald-Buller, E., 2008. Comparisons of modeled and observed isoprene concentrations in southeast Texas. Atmospheric Environment 42, 1922-1940.

U.S. EPA, 1999. Science Algorithms of the EPA Models-3 Community Multiscale Air Quality (CMAQ) Modeling System, CMAQ Science Documentation. Available online at: http://www.epa.gov/AMD/CMAQ/CMAQscienceDoc.html

U.S. EPA, 2009. Air Releases Data(AIRS/AFS). Available online at: http://www.epa.gov/enviro/html/airs/index.html

Vizuete, W., Kim, B., Jeffries, H., Kimura, Y., Allen, D., Kioumourtzoglou, M., Biton, L., Henderson, B., 2008. Modeling ozone formation from industrial emission events in Houston, Texas. Atmospheric Environment 42, 7641-7650.

Watson, J., Probert, J., Picot, S., 1991. Global inventory of volatile organic compound emissions from anthropogenic sources. Journal of Geophysical Research, 97(D9), 9897–9912.

Watson, J.G., Robinson, N.F., Chow, J.C., Henry, R.C., Kim, B.M., Nguyen, Q., Meyer, E.L., Pace, T.G., 1990. Receptor Model Technical series, Vol. III, CMB7 User's Manual, in U.S EPA, Report No. EPA-450/4-90-004.

Wert, B.P., Trainer, M., Fried, A., Ryerson, T.B., Henry, B., Potter, W., Angevine, W.M., Atlas, E., Donnelly, S.G., Fehsenfeld, F.C., Frost, G.J., Goldan, P.D., Hansel, A., Holloway, J.S., Hubler, G., Kuster, W.C., Nicks, D.K., Jr., Neuman, J.A., Parrish, D.D., Schauffler, S., Stutz, J., Sueper, D.T., Wiedinmyer, C., Wisthaler, A., 2003. Signatures of terminal alkene oxidation in airborne formaldehyde measurements during TexAQS 2000. Journal of Geophysical Research 108, 1-9.

Wittig, A.E., Allen, D.T., 2008. Improvement of the chemical mass balance model for apportioning--sources of non-methane hydrocarbons using composite aged source profiles. Atmospheric Environment 42, 1319-1337.

Ying, Q., Fraser, M.P., Griffin, R.J., Chen, J., Kleeman, M.J., 2007. Verification of a source-oriented externally mixed air quality model during a severe photochemical smog episode. Atmospheric Environment 41, 1521-1538.

Ying, Q., Kleeman, M., 2006. Source contributions to the regional distribution of secondary particulate matter in California. Atmospheric Environment 40, 736-752.

Yuan, Z., Lau, A.K.H., Shao, M., Louie, P.K.K., Liu, S.C., Zhu, T., 2009. Source analysis of volatile organic compounds by positive matrix factorization in urban and rural environments in Beijing. Journal of Geophysical Research 114, 1-14.

Zhang, F., Bei, N., Nielsen-Gammon, J., Li, G., Zhang, R., Stuart, A., Aksoy, A., 2007. Impacts of meteorological uncertainties on ozone pollution predictability estimated through meteorological and photochemical ensemble forecasts. Journal of Geophysical Research 112, 1-14.

Zhao, W., Hopke, P., Karl, T., 2004. Source identification of volatile organic compounds in Houston, Texas. Environmental Science and Technology 38, 1338-1347.

APPENDIX A

Statistical Analysis Code

```
c     To do stat analysis for all the model prediction results

      character*8 date
      real obs(13,24),pre(13,24)
      real maxobs_pre(24),maxpre_obs(24)
      real maxobs(24),maxpre(24),app(24)
      integer i,j,s
      real obsd, pred, aup(24),aaup(24),aapp(24)

      open (1,file='CONRplot_o3.txt.ext2'
     +,status='old')

c     Store values in arrays

      do i=1,13
            do j=1,24
                  read (1,*,end=200)date,obsd,pred
                  obs(i,j)=obsd
                  pre(i,j)=pred
            enddo
      enddo

      do i=1,13
            maxobs(i)=0.
            maxpre(i)=0.
            do j=1,24
               if (obs(i,j).ge.maxobs(i))then
               maxobs(i)=obs(i,j)
               maxobs_pre(i)=pre(i,j)
               endif
               if (pre(i,j).ge.maxpre(i))then
               maxpre(i)=pre(i,j)
               maxpre_obs(i)=obs(i,j)
               endif
            enddo

            if (maxobs(i).le.0.06)then
            app(i)=0.
            aup(i)=0.
            aapp(i)=0.
            aaup(i)=0.

            else
            app(i)=((maxobs_pre(i)-maxobs(i)))/maxobs(i)

            aup(i)=(maxpre(i)-maxobs(i))/maxpre_obs(i)

            aapp(i)=abs(((maxobs_pre(i)-maxobs(i)))/maxobs(i))

            aaup(i)=abs((maxpre(i)-maxobs(i))/maxpre_obs(i))
```

```
            endif
      enddo

c     APP calculation

      app_f=0.
      s=1
      do i=1,13
            app_f=app_f+app(i)
            if (app(i).ne.o)then
            s=s+1
            endif
      enddo

      C_APP=app_f/s

c     AUP calculation

      aup_f=0.
      s=1
      do i=1,13
            aup_f=aup_f+aup(i)
            if (aup(i).ne.o)then
            s=s+1
            endif
      enddo

      C_AUP=aup_f/s

c     AAUP calculation

      aaup_f=0.
      s=1
      do i=1,13
            aaup_f=aaup_f+aaup(i)
            if (aaup(i).ne.o)then
            s=s+1
            endif
      enddo

      C_AAUP=aaup_f/s

c     AAPP calculation

      aapp_f=0.
      s=1
      do i=1,13
            aapp_f=aapp_f+aapp(i)
            if (aapp(i).ne.o)then
            s=s+1
            endif
      enddo

      C_AAPP=aapp_f/s


      print*,"APP=", C_APP
```

```
      print*,"AUP=", C_AUP
      print*,"AAUP=", C_AAUP
      print*,"AAPP=", C_AAPP


c     Print results

c      print*,"APP=", app_f, "AUP=", aup_f

c      print*, "AAPP=", aapp_f,"AAUP=", aaup_f

200   continue

      end
```

APPENDIX B

SAPRC-99 CHEMICAL MECHANISM

```
REACTIONS[CM] =
<1> NO2 = NO + O3P # 1.0/<NO2_SAPRC99>;
<2> O3P + O2 + M = O3 # 5.68e-34^-2.80;
<3> O3P + O3 =  # 8.00e-12@2060;
<4> O3P + NO + M = NO2 # 1.00e-31^-1.60;
<5> O3P + NO2 = NO # 6.50e-12@-120;
<6> O3P + NO2 = NO3 # 9.00e-32^-2.00&2.20e-11&0.80&1.0;
<8> O3 + NO = NO2 # 1.80e-12@1370;
<9> O3 + NO2 = NO3 # 1.40e-13@2470;
<10> NO + NO3 = 2*NO2 # 1.80e-11@-110;
<11> NO + NO + O2 = 2*NO2 # 3.30e-39@-530;
<12> NO2 + NO3 = N2O5 # 2.80e-30^-3.50&2.00e-12^0.20&0.45&1.0;
<13> N2O5 = NO2 + NO3 # 1.00e-03^-3.50@11000&9.70e+14^0.10@11080&0.45&1.0;
<14> N2O5 + H2O = 2*HNO3 # 2.60e-22;
<17> NO2 + NO3 = NO + NO2 # 4.50e-14@1260;
<18> NO3 = NO # 1.0/<NO3NO_SAPRC99>;
<19> NO3 = NO2 + O3P # 1.0/<NO3NO2_SAPRC99>;
<20> O3 = O3P # 1.0/<O3O3P_SAPRC99>;
<21> O3 = O1D2 # 1.0/<O3O1D_SAPRC99>;
<22> O1D2 + H2O = 2*HO # 2.20e-10;
<23> O1D2 + M = O3P # 2.09e-11@-95;
<24> HO + NO = HONO # 7.00e-31^-2.60&3.60e-11^-0.10&0.60&1.0;
<25> HONO = HO + NO # 1.0/<HONO_NO_SAPRC99>;
<26> HONO = HO2 + NO2 # 1.0/<HONO_NO2_SAPRC99>;
<27> HO + HONO = NO2 # 2.70e-12@-260;
<28> HO + NO2 = HNO3 # 2.43e-30^-3.10&1.67e-11^-2.10&0.60&1.0;
<29> HO + NO3 = HO2 + NO2 # 2.00e-11;
<30> HO + HNO3 = NO3 %2 # 7.20e-15@-785&4.10e-16@-1440&1.90e-33@-725;
<31> HNO3 = HO + NO2 # 1.0/<HNO3_SAPRC99>;
<32> HO + CO = HO2 %3 # 1.30e-13@0.0&3.19e-33@0.0;
<33> HO + O3 = HO2 # 1.90e-12@1000;
<34> HO2 + NO = HO + NO2 # 3.40e-12@-270;
<35> HO2 + NO2 = HNO4 # 1.80e-31^-3.20&4.70e-12&0.60&1.0;
<36> HNO4 = HO2 + NO2 # 4.10e-05@10650&5.70e+15@11170&0.50&1.0;
<37> HNO4 = 0.61*HO2 + 0.61*NO2 + 0.39*HO + 0.39*NO3 # 1.0/<HO2NO2_SAPRC99>;
<38> HNO4 + HO = NO2 # 1.50e-12@-360;
<39> HO2 + O3 = HO # 1.40e-14@600;
<40A> HO2 + HO2 = HO2H %3 # 2.20e-13@-600&1.85e-33@-980;
<40B> HO2 + HO2 + H2O = HO2H %3 # 3.08e-34@-2800&2.59e-54@-3180;
<41> NO3 + HO2 = 0.8*HO + 0.8*NO2 + 0.2*HNO3 # 4.00e-12;
<42> NO3 + NO3 = 2*NO2 # 8.50e-13@2450;
<43> HO2H = 2*HO # 1.0/<H2O2_SAPRC99>;
<44> HO2H + HO = HO2 # 2.90e-12@160;
<45> HO + HO2 =  # 4.80e-11@-250;
<S2OH> HO + SO2 = HO2 + SULF # 4.00e-31^-3.30&2.00e-12&0.45&1.0;
<H2OH> HO + H2 = HO2 # 7.70e-12@2100;
<MER1> C_O2 + NO = NO2 + HCHO + HO2 # 2.80e-12@-285;
<MER4> C_O2 + HO2 = COOH # 3.80e-13@-780;
<MEN3> C_O2 + NO3 = HCHO + HO2 + NO2 # 1.30e-12;
<MER5> C_O2 + C_O2 = MEOH + HCHO # 2.45e-14@-710;
<MER6> C_O2 + C_O2 = 2*HCHO + 2*HO2 # 5.90e-13@509;
<RRNO> RO2_R + NO = NO2 + HO2 # 2.70e-12@-360;
```

```
<RRH2> RO2_R + HO2 = ROOH # 1.90e-13@-1300;
<RRN3> RO2_R + NO3 = NO2 + HO2 # 2.30e-12;
<RRME> RO2_R + C_O2 = HO2 + 0.75*HCHO + 0.25*MEOH # 2.00e-13;
<RRR2> RO2_R + RO2_R = HO2 # 3.50e-14;
<R2NO> R2O2 + NO = NO2 # 1.0*K<RRNO>;
<R2H2> R2O2 + HO2 = HO2 # 1.0*K<RRH2>;
<R2N3> R2O2 + NO3 = NO2 # 1.0*K<RRN3>;
<R2ME> R2O2 + C_O2 = C_O2 # 1.0*K<RRME>;
<R2RR> R2O2 + RO2_R = RO2_R # 1.0*K<RRR2>;
<R2R3> R2O2 + R2O2 =  # 1.0*K<RRR2>;
<RNNO> RO2_N + NO = RNO3 # 1.0*K<RRNO>;
<RNH2> RO2_N + HO2 = ROOH # 1.0*K<RRH2>;
<RNME> RO2_N + C_O2 = HO2 + 0.25*MEOH + 0.5*MEK + 0.5*PROD2 + 0.75*HCHO
       # 1.0*K<RRME>;
<RNN3> RO2_N + NO3 = NO2 + HO2 + MEK # 1.0*K<RRN3>;
<RNRR> RO2_N + RO2_R = HO2 + 0.5*MEK + 0.5*PROD2 # 1.0*K<RRR2>;
<RNR2> RO2_N + R2O2 = RO2_N # 1.0*K<RRR2>;
<RNRN> RO2_N + RO2_N = MEK + HO2 + PROD2 # 1.0*K<RRR2>;
<APN2> CCO_O2 + NO2 = PAN # 2.70e-28^-7.10&1.20e-11^-0.90&0.30&1.0;
<DPAN> PAN = CCO_O2 + NO2 # 4.90e-03@12100&4.00e+16@13600&0.30&1.0;
<APNO> CCO_O2 + NO = C_O2 + NO2 # 7.80e-12@-300;
<APH2> CCO_O2 + HO2 = 0.75*CCO_OOH + 0.25*CCO_OH + 0.25*O3 # 4.30e-13@-1040;
<APN3> CCO_O2 + NO3 = C_O2 + NO2 # 4.00e-12;
<APME> CCO_O2 + C_O2 = CCO_OH + HCHO # 1.80e-12@-500;
<APRR> CCO_O2 + RO2_R = CCO_OH # 7.50e-12;
<APR2> CCO_O2 + R2O2 = CCO_O2 # 1.0*K<APRR>;
<APRN> CCO_O2 + RO2_N = CCO_OH + PROD2 # 1.0*K<APRR>;
<APAP> CCO_O2 + CCO_O2 = 2*C_O2 # 2.90e-12@-500;
<PPN2> RCO_O2 + NO2 = PAN2 # 1.20e-11^-0.90;
<PAN2> PAN2 = RCO_O2 + NO2 # 2.00e+15@12800;
<PPNO> RCO_O2 + NO = NO2 + CCHO + RO2_R # 1.25e-11@-240;
<PPH2> RCO_O2 + HO2 = 0.75*RCO_OOH + 0.25*RCO_OH + 0.25*O3 # 1.0*K<APH2>;
<PPN3> RCO_O2 + NO3 = NO2 + CCHO + RO2_R # 1.0*K<APN3>;
<PPME> RCO_O2 + C_O2 = RCO_OH + HCHO # 1.0*K<APME>;
<PPRR> RCO_O2 + RO2_R = RCO_OH # 1.0*K<APRR>;
<PPR2> RCO_O2 + R2O2 = RCO_O2 # 1.0*K<APRR>;
<PPRN> RCO_O2 + RO2_N = RCO_OH + PROD2 # 1.0*K<APRR>;
<PPAP> RCO_O2 + CCO_O2 = C_O2 + CCHO + RO2_R # 1.0*K<APAP>;
<PPPP> RCO_O2 + RCO_O2 = 2*CCHO + 2*RO2_R # 1.0*K<APAP>;
<BPN2> BZCO_O2 + NO2 = PBZN # 1.37e-11;
<BPAN> PBZN = BZCO_O2 + NO2 # 7.90e+16@14000;
<BPNO> BZCO_O2 + NO = NO2 + BZ_O + R2O2 # 1.0*K<PPNO>;
<BPH2> BZCO_O2 + HO2 = 0.75*RCO_OOH + 0.25*RCO_OH + 0.25*O3 # 1.0*K<APH2>;
<BPN3> BZCO_O2 + NO3 = NO2 + BZ_O + R2O2 # 1.0*K<APN3>;
<BPME> BZCO_O2 + C_O2 = RCO_OH + HCHO # 1.0*K<APME>;
<BPRR> BZCO_O2 + RO2_R = RCO_OH # 1.0*K<APRR>;
<BPR2> BZCO_O2 + R2O2 = BZCO_O2 # 1.0*K<APRR>;
<BPRN> BZCO_O2 + RO2_N = RCO_OH + PROD2 # 1.0*K<APRR>;
<BPAP> BZCO_O2 + CCO_O2 = C_O2 + BZ_O + R2O2 # 1.0*K<APAP>;
<BPPP> BZCO_O2 + RCO_O2 = CCHO + RO2_R + BZ_O + R2O2 # 1.0*K<APAP>;
<BPBP> BZCO_O2 + BZCO_O2 = 2*BZ_O + 2*R2O2 # 1.0*K<APAP>;
<MPN2> MA_RCO3 + NO2 = MA_PAN # 1.0*K<PPN2>;
<MPPN> MA_PAN = MA_RCO3 + NO2 # 1.60e+16@13486;
<MPNO> MA_RCO3 + NO = NO2 + HCHO + CCO_O2 # 1.0*K<PPNO>;
<MPH2> MA_RCO3 + HO2 = 0.75*RCO_OOH + 0.25*RCO_OH + 0.25*O3 # 1.0*K<APH2>;
<MPN3> MA_RCO3 + NO3 = NO2 + HCHO + CCO_O2 # 1.0*K<APN3>;
<MPME> MA_RCO3 + C_O2 = RCO_OH + HCHO # 1.0*K<APME>;
```

```
<MPRR> MA_RCO3 + RO2_R = RCO_OH # 1.0*K<APRR>;
<MPR2> MA_RCO3 + R2O2 = MA_RCO3 # 1.0*K<APRR>;
<MPRN> MA_RCO3 + RO2_N = 2*RCO_OH # 1.0*K<APRR>;
<MPAP> MA_RCO3 + CCO_O2 = C_O2 + HCHO + CCO_O2 # 1.0*K<APAP>;
<MPPP> MA_RCO3 + RCO_O2 = HCHO + CCO_O2 + CCHO + RO2_R # 1.0*K<APAP>;
<MPBP> MA_RCO3 + BZCO_O2 = HCHO + CCO_O2 + BZ_O + R2O2 # 1.0*K<APAP>;
<MPMP> MA_RCO3 + MA_RCO3 = 2*HCHO + 2*CCO_O2 # 1.0*K<APAP>;
<TBON> TBU_O + NO2 = RNO3 # 2.40e-11;
<TBOD> TBU_O = ACET + C_O2 # 7.50e+14@8152;
<BRN2> BZ_O + NO2 = NPHE # 2.30e-11@-150;
<BRH2> BZ_O + HO2 = PHEN # 1.0*K<RRH2>;
<BRXX> BZ_O = PHEN # 1.00e-03;
<BNN2> BZNO2_O + NO2 =  # 1.0*K<BRN2>;
<BNH2> BZNO2_O + HO2 = NPHE # 1.0*K<RRH2>;
<BNXX> BZNO2_O = NPHE # 1.0*K<BRXX>;
<FAHV> HCHO = 2*HO2 + CO # 1.0/<HCHO_R_SAPRC99>;
<FAVS> HCHO = CO # 1.0/<HCHO_M_SAPRC99>;
<FAOH> HCHO + HO = HO2 + CO # 8.60e-12@-20;
<FAH2> HCHO + HO2 = HOCOO # 9.70e-15@-625;
<FAHR> HOCOO = HO2 + HCHO # 2.40e+12@7000;
<FAHN> HOCOO + NO = HCOOH + NO2 + HO2 # 1.0*K<MER1>;
<FAN3> HCHO + NO3 = HNO3 + HO2 + CO # 2.00e-12@2431;
<AAOH> CCHO + HO = CCO_O2 # 5.60e-12@-310;
<AAHV> CCHO = CO + HO2 + C_O2 # 1.0/<CCHO_R_SAPRC99>;
<AAN3> CCHO + NO3 = HNO3 + CCO_O2 # 1.40e-12@1860;
<PAOH> RCHO + HO = 0.034*RO2_R + 0.001*RO2_N + 0.965*RCO_O2 + 0.034*CO +
         0.034*CCHO # 2.00e-11;
<PAHV> RCHO = CCHO + RO2_R + CO + HO2 # 1.0/<C2CHO_SAPRC99>;
<PAN3> RCHO + NO3 = HNO3 + RCO_O2 # 1.40e-12@1771;
<K3OH> ACET + HO = HCHO + CCO_O2 + R2O2 # 1.10e-12@520;
<K3HV> ACET = CCO_O2 + C_O2 # 1.0/<ACETONE_SAPRC99>;
<K4OH> MEK + HO = 0.37*RO2_R + 0.042*RO2_N + 0.616*R2O2 + 0.492*CCO_O2 +
         0.096*RCO_O2 + 0.115*HCHO + 0.482*CCHO + 0.37*RCHO # 1.30e-
12^2.00@25;
<K4HV> MEK = CCO_O2 + CCHO + RO2_R # 1.50e-1/<KETONE_SAPRC99>;
<MeOH> MEOH + HO = HCHO + HO2 # 3.10e-12^2.00@360;
<MER9> COOH + HO = 0.35*HCHO + 0.35*HO + 0.65*C_O2 # 2.90e-12@-190;
<MERA> COOH = HCHO + HO2 + HO # 1.0/<COOH_SAPRC99>;
<LPR9> ROOH + HO = RCHO + 0.34*RO2_R + 0.66*HO # 1.10e-11;
<LPRA> ROOH = RCHO + HO2 + HO # 1.0/<COOH_SAPRC99>;
<GLHV> GLY = 2*CO + 2*HO2 # 1.0/<GLY_R_SAPRC99>;
<GLVM> GLY = HCHO + CO # 6.00e-3/<GLY_ABS_SAPRC99>;
<GLOH> GLY + HO = 0.63*HO2 + 1.26*CO + 0.37*RCO_O2 # 1.10e-11;
<GLN3> GLY + NO3 = HNO3 + 0.63*HO2 + 1.26*CO + 0.37*RCO_O2 # 2.80e-12@2376;
<MGHV> MGLY = HO2 + CO + CCO_O2 # 1.0/<MGLY_ADJ_SAPRC99>;
<MGOH> MGLY + HO = CO + CCO_O2 # 1.50e-11;
<MGN3> MGLY + NO3 = HNO3 + CO + CCO_O2 # 1.40e-12@1895;
<BAHV> BACL = 2*CCO_O2 # 1.0/<BACL_ADJ_SAPRC99>;
<PHOH> PHEN + HO = 0.24*BZ_O + 0.76*RO2_R + 0.23*GLY # 2.63e-11;
<PHN3> PHEN + NO3 = HNO3 + BZ_O # 3.78e-12;
<CROH> CRES + HO = 0.24*BZ_O + 0.76*RO2_R + 0.23*MGLY # 4.20e-11;
<CRN3> CRES + NO3 = HNO3 + BZ_O # 1.37e-11;
<NPN3> NPHE + NO3 = HNO3 + BZNO2_O # 1.0*K<PHN3>;
<BZOH> BALD + HO = BZCO_O2 # 1.29e-11;
<BZHV> BALD =  # 5.00e-2/<BZCHO_SAPRC99>;
<BZNT> BALD + NO3 = HNO3 + BZCO_O2 # 1.40e-12@1872;
<MAOH> METHACRO + HO = 0.5*RO2_R + 0.416*CO + 0.084*HCHO + 0.416*MEK +
```

```
         0.084*MGLY + 0.5*MA_RCO3 # 1.86e-11@-176;
<MAO3> METHACRO + O3 = 0.008*HO2 + 0.1*RO2_R + 0.208*HO + 0.1*RCO_O2 +
0.45*CO +
         0.2*HCHO + 0.9*MGLY + 0.333*HCOOH # 1.36e-15@2114;
<MAN3> METHACRO + NO3 = 0.5*HNO3 + 0.5*RO2_R + 0.5*CO + 0.5*MA_RCO3
        # 1.50e-12@1726;
<MAOP> METHACRO + O3P = RCHO # 6.34e-12;
<MAHV> METHACRO = 0.34*HO2 + 0.33*RO2_R + 0.33*HO + 0.67*CCO_O2 + 0.67*CO +
         0.67*HCHO + 0.33*MA_RCO3 # 4.10e-3/<ACROLEIN_SAPRC99>;
<MVOH> MVK + HO = 0.3*RO2_R + 0.025*RO2_N + 0.675*R2O2 + 0.675*CCO_O2 +
         0.3*HCHO + 0.675*RCHO + 0.3*MGLY # 4.14e-12@-453;
<MVO3> MVK + O3 = 0.064*HO2 + 0.05*RO2_R + 0.164*HO + 0.05*RCO_O2 + 0.475*CO
+
         0.1*HCHO + 0.95*MGLY + 0.351*HCOOH # 7.51e-16@1520;
<MVOP> MVK + O3P = 0.45*RCHO + 0.55*MEK # 4.32e-12;
<MVHV> MVK = 0.3*C_O2 + 0.7*CO + 0.7*PROD2 + 0.3*MA_RCO3
             # 2.10e-3/<ACROLEIN_SAPRC99>;
<IPOH> ISOPROD + HO = 0.67*RO2_R + 0.041*RO2_N + 0.289*MA_RCO3 + 0.336*CO +
         0.055*HCHO + 0.129*CCHO + 0.013*RCHO + 0.15*MEK + 0.332*PROD2 +
         0.15*GLY + 0.174*MGLY # 6.19e-11;
<IPO3> ISOPROD + O3 = 0.4*HO2 + 0.048*RO2_R + 0.048*RCO_O2 + 0.285*HO +
         0.498*CO + 0.125*HCHO + 0.047*CCHO + 0.21*MEK + 0.023*GLY +
         0.742*MGLY + 0.1*HCOOH + 0.372*RCO_OH # 4.18e-18;
<IPN3> ISOPROD + NO3 = 0.799*RO2_R + 0.051*RO2_N + 0.15*MA_RCO3 + 0.572*CO +
         0.15*HNO3 + 0.227*HCHO + 0.218*RCHO + 0.008*MGLY + 0.572*RNO3
        # 1.00e-13;
<IPHV> ISOPROD = 1.233*HO2 + 0.467*CCO_O2 + 0.3*RCO_O2 + 1.233*CO + 0.3*HCHO
+
         0.467*CCHO + 0.233*MEK # 4.10e-3/<ACROLEIN_SAPRC99>;
<K6OH> PROD2 + HO = 0.379*HO2 + 0.473*RO2_R + 0.07*RO2_N + 0.029*CCO_O2 +
         0.049*RCO_O2 + 0.213*HCHO + 0.084*CCHO + 0.558*RCHO + 0.115*MEK +
         0.329*PROD2 # 1.50e-11;
<K6HV> PROD2 = 0.96*RO2_R + 0.04*RO2_N + 0.515*R2O2 + 0.667*CCO_O2 +
         0.333*RCO_O2 + 0.506*HCHO + 0.246*CCHO + 0.71*RCHO
         # 2.00e-2/<KETONE_SAPRC99>;
<RNOH> RNO3 + HO = 0.338*NO2 + 0.113*HO2 + 0.376*RO2_R + 0.173*RO2_N +
         0.596*R2O2 + 0.01*HCHO + 0.439*CCHO + 0.213*RCHO + 0.006*ACET +
         0.177*MEK + 0.048*PROD2 + 0.31*RNO3 # 7.80e-12;
<RNHV> RNO3 = NO2 + 0.341*HO2 + 0.564*RO2_R + 0.095*RO2_N + 0.152*R2O2 +
         0.134*HCHO + 0.431*CCHO + 0.147*RCHO + 0.02*ACET + 0.243*MEK +
         0.435*PROD2 # 1.0/<IC3ONO2_SAPRC99>;
<D1OH> DCB1 + HO = RCHO + RO2_R + CO # 5.00e-11;
<D1O3> DCB1 + O3 = 1.5*HO2 + 0.5*HO + 1.5*CO + GLY # 2.00e-18;
<D2OH> DCB2 + HO = R2O2 + RCHO + CCO_O2 # 5.00e-11;
<D2HV> DCB2 = RO2_R + 0.5*CCO_O2 + 0.5*HO2 + CO + R2O2 + 0.5*GLY + 0.5*MGLY
        # 3.65e-1/<MGLY_ABS_SAPRC99>;
<D3OH> DCB3 + HO = R2O2 + RCHO + CCO_O2 # 5.00e-11;
<D3HV> DCB3 = RO2_R + 0.5*CCO_O2 + 0.5*HO2 + CO + R2O2 + 0.5*GLY + 0.5*MGLY
        # 7.28e+0/<ACROLEIN_SAPRC99>;
<c1OH> CH4 + HO = C_O2 # 2.15e-12@1735;
<etOH> ETHENE + HO = RO2_R + 1.61*HCHO + 0.195*CCHO # 1.96e-12@-438;
<etO3> ETHENE + O3 = 0.12*HO + 0.12*HO2 + 0.5*CO + HCHO + 0.37*HCOOH
        # 9.14e-15@2580;
<etN3> ETHENE + NO3 = RO2_R + RCHO # 4.39e-13^2.00@2282;
<etOA> ETHENE + O3P = 0.5*HO2 + 0.2*RO2_R + 0.3*C_O2 + 0.491*CO + 0.191*HCHO
+
         0.25*CCHO + 0.009*GLY # 1.04e-11@792;
```

```
<isOH> ISOPRENE + HO = 0.907*RO2_R + 0.093*RO2_N + 0.079*R2O2 + 0.624*HCHO +
         0.23*METHACRO + 0.32*MVK + 0.357*ISOPROD # 2.50e-11@-408;
<isO3> ISOPRENE + O3 = 0.266*HO + 0.066*RO2_R + 0.008*RO2_N + 0.126*R2O2 +
         0.192*MA_RCO3 + 0.275*CO + 0.592*HCHO + 0.1*PROD2 + 0.39*METHACRO +
         0.16*MVK + 0.204*HCOOH + 0.15*RCO_OH # 7.86e-15@1912;
<isN3> ISOPRENE + NO3 = 0.187*NO2 + 0.749*RO2_R + 0.064*RO2_N + 0.187*R2O2 +
         0.936*ISOPROD # 3.03e-12@448;
<isOP> ISOPRENE + O3P = 0.01*RO2_N + 0.24*R2O2 + 0.25*C_O2 + 0.24*MA_RCO3 +
         0.24*HCHO + 0.75*PROD2 # 3.60e-11;
<t1OH> TRP1 + HO = 0.75*RO2_R + 0.25*RO2_N + 0.5*R2O2 + 0.276*HCHO +
         0.474*RCHO + 0.276*PROD2 # 1.83e-11@-449;
<t1O3> TRP1 + O3 = 0.567*HO + 0.033*HO2 + 0.031*RO2_R + 0.18*RO2_N +
         0.729*R2O2 + 0.123*CCO_O2 + 0.201*RCO_O2 + 0.157*CO + 0.235*HCHO +
         0.205*RCHO + 0.13*ACET + 0.276*PROD2 + 0.001*GLY + 0.031*BACL +
         0.103*HCOOH + 0.189*RCO_OH # 1.08e-15@821;
<t1N3> TRP1 + NO3 = 0.474*NO2 + 0.276*RO2_R + 0.25*RO2_N + 0.75*R2O2 +
         0.474*RCHO + 0.276*RNO3 # 3.66e-12@-175;
<t1OP> TRP1 + O3P = 0.147*RCHO + 0.853*PROD2 # 3.27e-11;
<a1OH> ALK1 + HO = RO2_R + CCHO # 1.37e-12^2.00@498;
<a2OH> ALK2 + HO = 0.246*HO + 0.121*HO2 + 0.612*RO2_R + 0.021*RO2_N + 0.16*CO
+
         0.039*HCHO + 0.155*RCHO + 0.417*ACET + 0.248*GLY + 0.121*HCOOH
        # 9.87e-12@671;
<a3OH> ALK3 + HO = 0.695*RO2_R + 0.07*RO2_N + 0.559*R2O2 + 0.236*TBU_O +
         0.026*HCHO + 0.445*CCHO + 0.122*RCHO + 0.024*ACET + 0.332*MEK
        # 1.02e-11@434;
<a4OH> ALK4 + HO = 0.835*RO2_R + 0.143*RO2_N + 0.936*R2O2 + 0.011*C_O2 +
         0.011*CCO_O2 + 0.002*CO + 0.024*HCHO + 0.455*CCHO + 0.244*RCHO +
         0.452*ACET + 0.11*MEK + 0.125*PROD2 # 5.95e-12@91;
<a5OH> ALK5 + HO = 0.653*RO2_R + 0.347*RO2_N + 0.948*R2O2 + 0.026*HCHO +
         0.099*CCHO + 0.204*RCHO + 0.072*ACET + 0.089*MEK + 0.417*PROD2
        # 1.11e-11@52;
<b1OH> ARO1 + HO = 0.224*HO2 + 0.765*RO2_R + 0.011*RO2_N + 0.055*PROD2 +
         0.118*GLY + 0.119*MGLY + 0.017*PHEN + 0.207*CRES + 0.059*BALD +
         0.491*DCB1 + 0.108*DCB2 + 0.051*DCB3 # 1.81e-12@-355;
<b2OH> ARO2 + HO = 0.187*HO2 + 0.804*RO2_R + 0.009*RO2_N + 0.097*GLY +
         0.287*MGLY + 0.087*BACL + 0.187*CRES + 0.05*BALD + 0.561*DCB1 +
         0.099*DCB2 + 0.093*DCB3 # 2.64e-11;
<o1OH> OLE1 + HO = 0.91*RO2_R + 0.09*RO2_N + 0.205*R2O2 + 0.732*HCHO +
         0.294*CCHO + 0.497*RCHO + 0.005*ACET + 0.119*PROD2 # 7.10e-12@-451;
<o1O3> OLE1 + O3 = 0.155*HO + 0.056*HO2 + 0.022*RO2_R + 0.001*RO2_N +
         0.076*C_O2 + 0.345*CO + 0.5*HCHO + 0.154*CCHO + 0.363*RCHO +
         0.001*ACET + 0.215*PROD2 + 0.185*HCOOH + 0.05*CCO_OH + 0.119*RCO_OH
        # 2.62e-15@1640;
<o1N3> OLE1 + NO3 = 0.824*RO2_R + 0.176*RO2_N + 0.488*R2O2 + 0.009*CCHO +
         0.037*RCHO + 0.024*ACET + 0.511*RNO3 # 4.45e-14@376;
<o1OP> OLE1 + O3P = 0.45*RCHO + 0.437*MEK + 0.113*PROD2 # 1.07e-11@234;
<o2OH> OLE2 + HO = 0.918*RO2_R + 0.082*RO2_N + 0.001*R2O2 + 0.244*HCHO +
         0.732*CCHO + 0.511*RCHO + 0.127*ACET + 0.072*MEK + 0.061*BALD +
         0.025*METHACRO + 0.025*ISOPROD # 1.74e-11@-384;
<o2O3> OLE2 + O3 = 0.378*HO + 0.003*HO2 + 0.033*RO2_R + 0.002*RO2_N +
         0.137*R2O2 + 0.197*C_O2 + 0.137*CCO_O2 + 0.006*RCO_O2 + 0.265*CO +
         0.269*HCHO + 0.456*CCHO + 0.305*RCHO + 0.045*ACET + 0.026*MEK +
         0.006*PROD2 + 0.042*BALD + 0.026*METHACRO + 0.073*HCOOH +
         0.129*CCO_OH + 0.303*RCO_OH # 5.02e-16@461;
<o2N3> OLE2 + NO3 = 0.391*NO2 + 0.442*RO2_R + 0.136*RO2_N + 0.711*R2O2 +
         0.03*C_O2 + 0.079*HCHO + 0.507*CCHO + 0.151*RCHO + 0.102*ACET +
```

```
         0.001*MEK + 0.015*BALD + 0.048*MVK + 0.321*RNO3 # 7.26e-13;
<o2OP> OLE2 + O3P = 0.013*HO2 + 0.012*RO2_R + 0.001*RO2_N + 0.012*CO +
         0.069*RCHO + 0.659*MEK + 0.259*PROD2 + 0.012*METHACRO # 2.09e-11;
<c1OH> HCOOH + HO = HO2 # 4.5E-13;
<c2OH> CCO_OH + HO = 0.13*RO2_R + 0.87*C_O2 + 0.13*MGLY # 8.00E-13;
<c3OH> RCO_OH + HO = RO2_R + 0.605*CCHO + 0.21*RCHO + 0.185*BACL # 1.16E-12;
endmech
```

VITA

Name:	Anupama Krishnan
Permanent Address:	Department of Civil Engineering Texas A&M University 3136 TAMU College Station, Texas 77843-3136
Education:	B.E. Civil Engineering Anna University, Chennai, India 2007 M.S. Civil Engineering Texas A&M University, College Station 2010
Member:	American Society of Civil Engineers American Water Works Association
Email Address:	anupama272@gmail.com